Master's thesis

NTNU
Norwegian University of Science and Technology
Faculty of Medicine and Health Sciences
Department of Neuromedicine and Movement Science

Sondre Valentin Jordbræk

# Self-organized Criticality in engineered in vitro networks; A balance of excitation and inhibition

Master's thesis in Neuroscience
Supervisor: Axel Sandvig, Ioanna Sandvig
Co-supervisor: Nicholas Christiansen, Vegard Fiskum
October 2020

NTNU
Norwegian University of Science and Technology

Sondre Valentin Jordbræk

# Self-organized Criticality in engineered in vitro networks; A balance of excitation and inhibition

Master's thesis in Neuroscience
Supervisor: Axel Sandvig, Ioanna Sandvig
Co-supervisor: Nicholas Christiansen, Vegard Fiskum
October 2020

Norwegian University of Science and Technology
Faculty of Medicine and Health Sciences
Department of Neuromedicine and Movement Science

NTNU
Norwegian University of
Science and Technology

# Abstract

Criticality in the brain is considered by many to be one of the underlying activity dynamics for healthy neural networks, and thereby important for optimal information processing and computational capacity. Furthermore, the emergence of critical dynamics has been associated with the balance of excitation to inhibition (E/I). The aim of this thesis was to explore the relationship of E/I balance with emergence of critical dynamics, stability of critical dynamics and critical resilience. This was examined by creating an *in silico* model predicting which ratios of excitatory to inhibitory neurons supported critical emergence, and then culturing biological neural networks based on the modeled data. These networks consisted of 8%, 15% and 24% inhibitory neurons. Electrophysiological data were obtained from the networks, then the topology was analyzed with graph theory, critical dynamics were assessed, and network resilience was tested with GABA and NMDA perturbation. Finally, the topology, bursting activity, synchrony, and the effects of cell culture media change were studied with regard to critical dynamics. Our *in vitro* data suggests that neural networks consisting of 24% inhibitory neurons, compared to networks with inhibitory populations of 8% and 15%, tend to have better critical resilience and critical emergence. Our data also suggests that networks with 24% and 15% inhibitory populations stay active over longer periods than the lower inhibitory population networks and that graph theory parameters clustering, mean degree and small-worldness seem to change with increased inhibitory populations. Network bursts and synchronous activity tended to increase with inhibitory populations, however, out of the two, only evidence for synchronous activity's association to critical dynamics was found.

# Preface

## Acknowledgement

This thesis could not have been done without the help of many people. I would like to thank my supervisors and group leaders Ioanna and Axel Sandvig for giving me this opportunity, and for guiding and overseeing my thesis. Additionally, would I like to thank NTNU for everything this master's course in neuroscience has given me.

A special thank my Co-supervisor Nicholas Christiansen and Vegard Fiskum for helping me with the computational and biological parts of my project respectfully. Without their guidance would this thesis not have been possible, helping me create the critical analysis script and for supplying me with analysis scrips for the electrophysiological data. Through them have I learned valuable new techniques and skills which will help me in my education going forward.

A would also like to extend my gratitude to Ola Hause Ramstad for supplying me with the code for the adjacency matrix, and for coming with valuable insight on the topic of graph theory.

And last but not least everyone at the Sandvig group for continued support and help.

## Permits

# Table of Contents

# List of Figures

# List of Tables

# Abbreviations

| | |
|---|---|
| ALDH1L1 | 10-formyltetrahydrofolate dehydrogenase |
| CA | Cellular Automata |
| DAPI | 4′,6-diamidino-2-phenylindole |
| DMEM | Dulbecco's modified Eagle's medium |
| E/I | Excitation to Inhibition |
| ECOG | Eastern Cooperative Oncology Group |
| EGG | Electroencephalography |
| fMRI | Functional magnetic resonance imaging |
| GABA | Gamma-Aminobutyric acid |
| GFAP | Glial fibrillary acidic protein |
| GFP | Green fluorescent protein |
| GS | Goat Serum |
| HEPES | 4-(2-hydroxyethyl)-1-piperazineethanesulfonic acid |
| IgG | Immunoglobulin G |
| ICC | Immunocytochemistry |
| IPSC | Induced pluripotent stem cell |
| ISI | Interspike interval |
| LFP | Local field potential |
| MEA | Microelectrode array |
| MEG | Magnetoencephalography |
| MI | Mutual Information |
| NB | Network burst |
| NB/S | Network burst to synchrony |
| NeuN | Fox-3, Rbfox3, or Hexaribonucleotide Binding Protein-3 |
| nLFP | Negative Local field potential |
| NMDAR | N-methyl-D-aspartate receptor |
| PBS | Phosphate-buffered saline |
| PEDOT | Poly(3,4-ethylenedioxythiophene) |
| PEI | Polyethylenimine |
| pH | 'potential of hydrogen' or 'power of hydrogen |
| SD | Standard deviation |
| SOC | Self-organizing Criticality |
| SW | Small-world |
| Tuj | β-Tubulin 3 |

# 1. Introduction

Criticality in the brain is considered by many to be one of the underlying activity dynamics for healthy neural networks and this dynamic is accompanied by a signaling behavior named neuronal avalanches following distinct size distributions. This dynamic emerges spontaneously both *in vivo* and *in vitro* through self-organization and was subsequently named self-organized criticality (SOC).

This mode of activity is proposed to be one that maximizes information transfer and capacity (1) and it has indicated relevance to disease and information integration mechanisms (1-5). Through self-organization, the dynamic also encompasses more researched topics like attractor dynamics, albeit in a different kind of attractor state then the ones previously studied in hippocampal cells. The research of this topic might not only be of clinical interest, but also as a new puzzle-piece in understanding information processing and homeostatic brain mechanisms.

## 1.1 Definitions

Neural dynamics: The collective signaling behavior of neurons in a network. Neural dynamics are a specific way neurons communicate and interact with each other, both in a temporal and spatial manner.

Phases/states: Phase or state are specific configuration of a system. These configurations are associated with distinct dynamics and features (6, 7). A state in regard to neural networks is defined as distinct dynamical regimes, displaying different modes of activity and processing properties.

Phase transitions: A phase transition is the process of change from one phase of a system to another, altering the dynamics or features the systems displays (7). Concerning the brain, phase transitions regards changes in firing dynamics, changing from one activity state to another (8). An example of such a phase transition may be the change form asynchronous to synchronous activity.

Critical point: The critical point is characterized as a phenomenon that emerges between phase transitions through precise tuning of tuning parameters. In the critical point the transitions between phases are continuous and the two phases at both sides of the critical point coexists with no clear differences in phases between the transition, giving unique properties to systems. This stands in contrast to standard phase transition behavior, where a system only exists in one state at any given time. Some of the defining features of critical emergence are

that critical dynamics are found to be independent of quantity (i.e. independent of the systems size and scale) and are found to only be dependent on specific adjustment of tuning-parameters (7). Systems which have reached the critical point are here referred to as being in a critical state.

Criticality: Criticality is a synonym for critical state dynamics. The states concerning critical dynamics are divided into the states sub-critical, critical, and super-critical. These states are the states of a system which occur prior to a critical state, during a critical state, and the state past the critical state in respect to a specific tuning factor (7, 9).

Criticality in the brain: Criticality in the brain is observed though changes in firing dynamics. In the brain, the sub-critical, critical and super-critical states are abstract descriptions for different states of activity with different neural firing dynamics. (2, 10). Criticality in the brain can be measured though many means, but the most common is through the behavior of signaling cascades in regard to the branching ratio.

Branching ratio: The branching ratio is a measurement of the average number of downstream neural firings each up stream firing elicits. Signal branching is categorized by branching $< 1$, where signals die out quickly without spreading, branching $= 1$ where signals propagate normally, and branching $> 1$, where each firing may cause widespread activity.

Power Law: A power law is a type of data distribution which describes scale invariant functional relationships where one quantity varies as power of a scalar (11).

Scale invariant: When a system is scale invariant then the behavior of the system is the same no matter which size or scale the system is observed from.

Neural avalanches: Neural avalanches are a type of neural activity in the form of continuous cascading bursts of neural signaling. Each avalanche is separated by periods of inactivity, and the size distribution of avalanches can be approximated by power laws, meaning that this signaling activity is scale invariant. The power law exponent of avalanches is dependent on the branching ratio as high branching numbers favors heavy tailed distributions (power law-like distributions) while low branching favors no heavy tail and branching approximately equal to 1 facilitates size distributions closest approximated by power laws. Additionally, the spatio-temporal patterns avalanches occur in are shown to be different than pure random patterns (9, 12-14).

Sub-critical behavior in the brain: Sub-critical behavior in the brain is associated with depressed activity. Branching < 1 and power law exponents > -3/2 for size distributions.

Super-critical behavior in the brain: Super-critical behavior in the brain is associated with network-wide activity. Branching > 1 and power law exponents < -3/2 for size distributions.

Critical behavior in the brain: Critical behavior in the brain is associated with varied and balanced activity (1, 4, 9, 15). The dynamics in the critical state is observed to be scale invariant, and in this state neural avalanches are observed with specific size distributions and branching ratios. Additionally, in the critical state does networks gain attributes beneficial for information processing; neural signals are sent over longer distances, increase dynamic range for amplitude integration, maximized mutual information and intermediary entropy (13, 14, 16, 17). In neural avalanches following critical dynamics, the size distributions of propagating signals are expected to have a power law distribution with an exponent of -3/2 and an average branching parameter of 1. How well size duration distributions conform to power laws are used as a measure of critical dynamics (9, 13, 14). Features associated with critical dynamics are illustrated in figure 1.

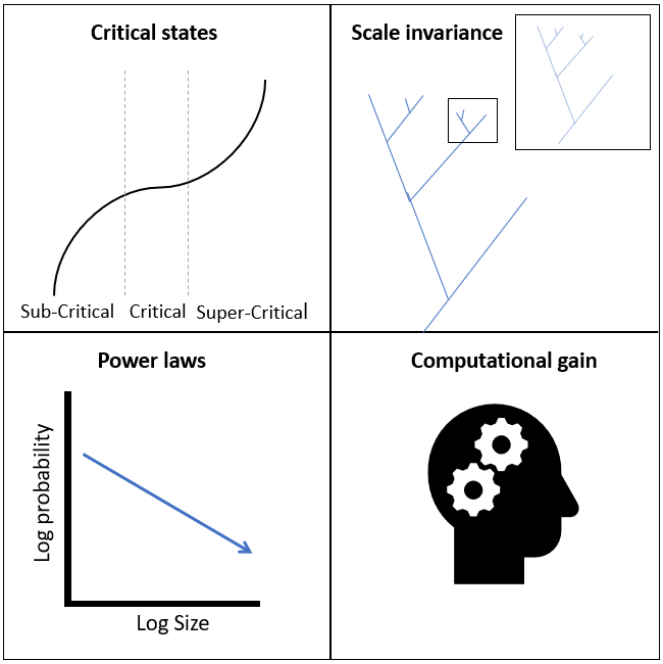


**Figure 1:** *Predicted features of critical dynamics in the brain. This figure depicts the three critical states, scale invariance, power law distributed avalanche data and computational gain.*

Attractor dynamics: Attractor dynamics are a type of dynamical network behavior in which a system evolves towards a specific state. The state which the system evolves towards is called an attractor state, and the system evolves towards the attractor state without the help of tuning parameters. This attraction only works if the system is within the attractor zone; a limit to deviations in which the system is able to stabilize back into its attractor state. If the system is pushed past this attractor zone, the system will not stabilize back into the attractor state

without additional influence (18, 19). A conceptual illustration of point attractor dynamics is shown in Figure 2.

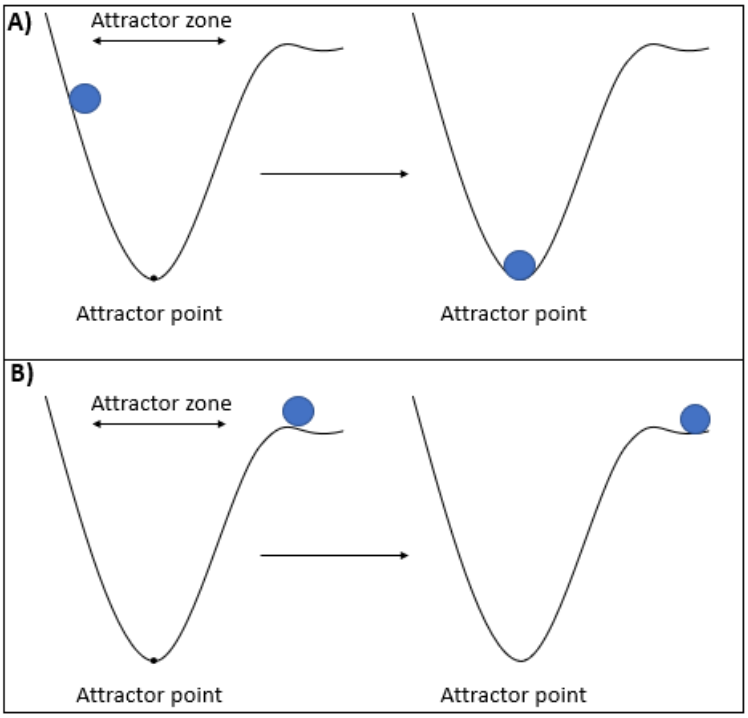


**Figure 2:** *a conceptual illustration of attractor dynamics. The blue ball represents the current dynamics of a system while the black line represents different dynamical system configurations as an attractor field. A) depicts a point attractor. Here the dynamics are pushed away from the attractor point, but because this is still within the zone of attraction the network stabilizes back into the attractor point. Much like putting a ball in a either side of a half pipe. B) depicts the event when a system is push out of its attractor zone and hence is no longer attracted to its attractor point.*

Self-organized criticality (SOC): SOC is a type of neural dynamic where the attractor point of a network is a state displaying critical dynamics (20). The concept of SOC is illustrated in Figure 3 below.

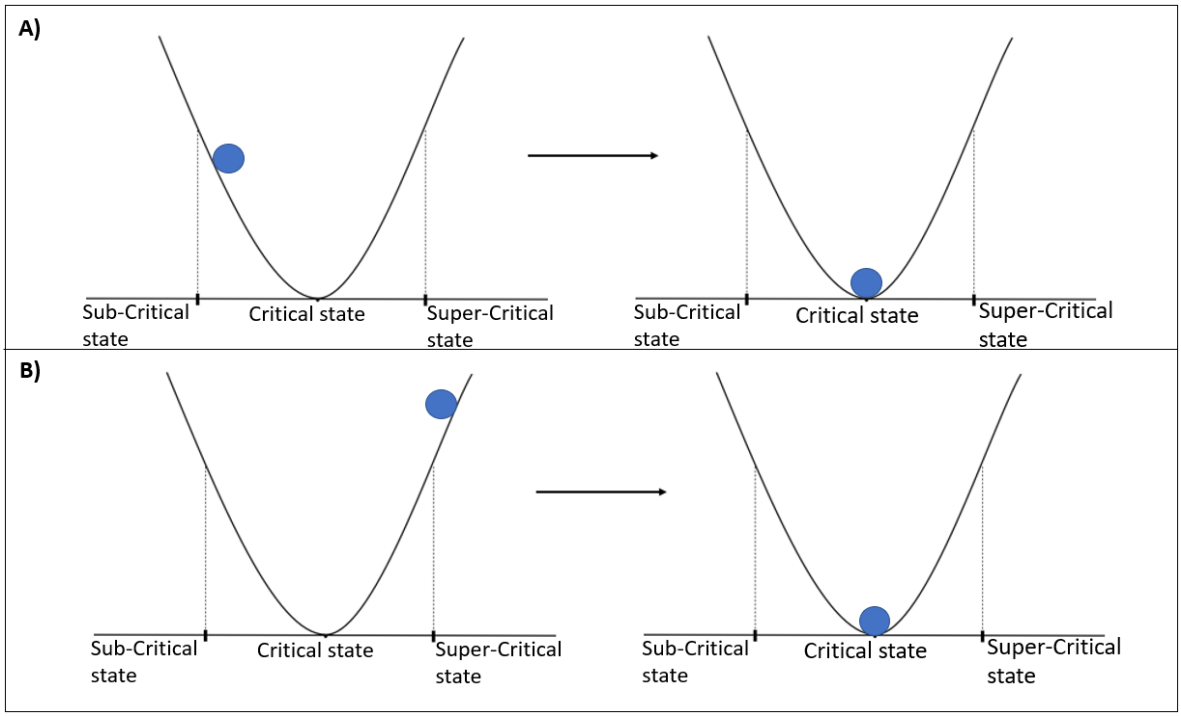


**Figure 3:** *a conceptual illustration of SOC. The blue ball represents the current dynamics of a system while the black line represents different dynamical system configurations as an attractor filed. A) when the system is pushed in either direction, the system will stabilize back into a critical state. B) shows a system being pushed out of the critical state and into a super-critical state, the system then stabilizes back into a critical state.*

## 1.2 From the Critical point to critical brain dynamics; History

The origin of critical systems in the field of physics dates back to the discovery of the critical point in 1822 (21), however, the real story of SOC occurred over one and half century later (20). This phenomenon, in which emergence relates to phase transition dynamics, would later be the founding idea of the dynamics explored in this thesis.

The concept of SOC was first presented in the field of physics in 1987 by Per Bak, Chao Tang and Kurt Wiesenfeld (20, 22). Their model, known as the "1/f noise" model, originated from the idea that a system with attractor dynamics would stabilize at a critical point. In the two-dimensional case the model describes the effect of placing a sand grain on the top of a sand pile, thereby perturbing the model. When initiated, the model starts off on an empty board, with the only condition being that sand grains are added to the model. The model then describes how the grain interacts with its neighbors displacing them in x and y directions, subsequently changing the whole sand pile slope. These perturbations to the system resulted in event cascades which ripple through the system, these event cascades were termed avalanches. They did this system perturbation to see when the model converged into a stable state. In the two-dimensional case, the models did not reach the most stable state, but it did

stabilize in what they called the minimally-stable state. When the system was in the minimally-stable state, they observed that the model produced what is called 1/f noise (or fractal self-similar behavior) in terms of the distribution of the sand pile avalanche sizes (height differences caused by the avalanche) and durations. This scale invariant behavior was observed through a power law distribution for variations in temporal durations and size (20, 22).

The sand pile model is the way Bak et al. (20, 22) chose to metaphorically visualize their SOC model (shown in Figure 4 below). Reviewing the dynamical regimes that emerges from this simple model, one can differentiate between three different states. The first state, named the sub-critical state, is observable when the sand pile slope is low. Low incline levels cause the addition of grains to be unlikely to displace the grains in the pile. As more grains are added, the slope increases, and each perturbation (added grain) has a greater possibility of displacing a larger number of grains. The grain addition eventually organizes the slope into the second dynamical regime, the critical state, which we will get back to. Skipping forward we reach the third state, named the super-critical state. This state is observed once the slope becomes too steep. When the slope incline is too high, each grain is more likely to displace a large number of other grains.

Lastly there is the critical state, which is reached when the system evolves itself into its minimally stable state; the state where maximum number sand grains are added to the system without the system necessarily undergoing dynamical changes and destabilizing the sand slope. This state emerges at the precise point of phase transition when the system is halfway between the two aforementioned phases. In the critical state the addition of more grains will cause varied responses due to the instability in the system. With each new grain addition it is impossible to predict if the addition of a grain of sand will cause avalanches displacing a few or many grains, or if the addition will have no effect on the sand pile. When there is a collapse into an avalanche, the slope will intrinsically converge on a given steepness, where new grains can displace a wide range of existing grains in the pile, resulting in a wide range of differently sized avalanches (20). This also ensures that the slope stays close to the critical steepness, since smaller slopes will lead to smaller avalanches and steeper slopes will lead to larger avalanches. These self-organization principles cause the sand pile model to spend most of its time in a critical or near-critical state.


**Figure 4:** *This figure depicts Bak et al's sand pile metaphor, which is a SOC model. The addition of grains creates at some point a minimally stable point, the addition of more grains makes the model stabilize back to this minimally stable point (23).* ["The sand pile model", from Self-organized criticality as a fundamental property of neural systems, by Hesse et al. (2014). URL: https://www.researchgate.net/figure/The-sandpile-model-The-classical-thought-experiment-motivating-self-organized_fig2_266626997, Figure license ( CC BY 4.0), full terms: Creative Commons Attribution 4.0 International

The visualization described above initiated the experimental work to focus on examining real avalanches in granular matter (24). From these investigations, systems displaying SOC typically were observed to be slowly driven non-equilibrium systems with many degrees of freedom and strong nonlinear dynamics (15, 20, 24, 25). While it was shown that critical systems must contain a large portion of interacting nonlinear components, this condition alone is not sufficient for the emergence of criticality (15, 20, 24, 25). As more examination was done into SOC, it became clear that SOC schemes represent a great source for variability in a system, and the phenomena is theorized to be one of the ways complexity naturally emerges (26). Following the publication of the Bak et al.'s article (20), many systems demonstrating SOC have been found in nature, including, but not limited to, earthquakes, forest fires and sand piles (27).

Around the 1980s, Wolfram (28) established a model out of curiosity of how computational abilities could spontaneously arise from interacting simple elements. This model was created from the cellular automat model, a model made from a regular grid of cells where each cell can inhabit a finite number of states. Wolfram's model was called the Cellular automata model IV (28) and this model had many similarities to artificial neural networks, and could conceptually be viewed as one. The model was later shown to operate near criticality, functioning as an SOC system (29). Later, Langton (15) studied cellular automata as a critical model, a model that could be tuned into ordered, critical or chaotic regimes, as depicted in Figure 5. These regimes are further described in the following sections.

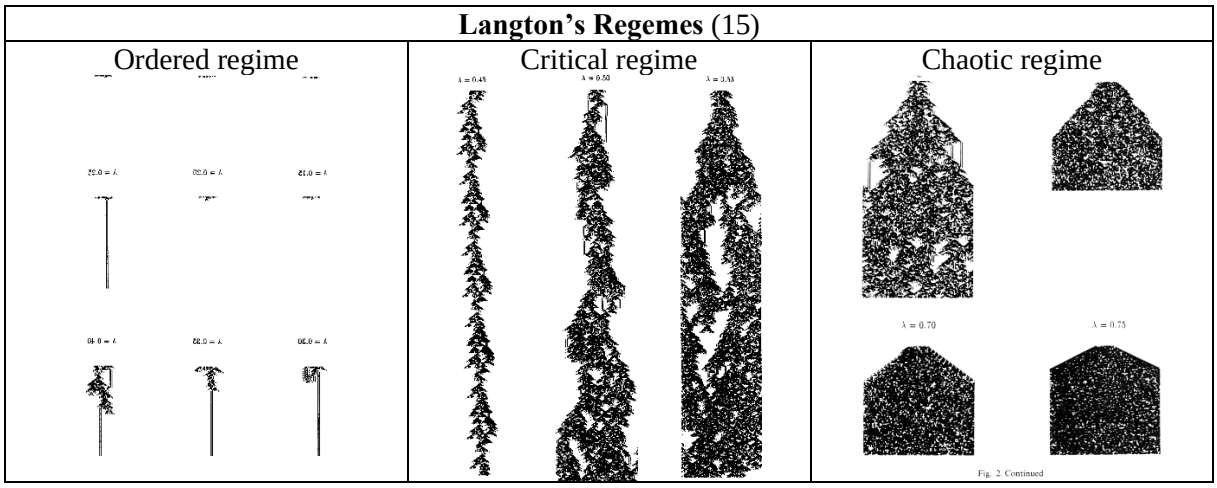


**Figure 5***: This figure shows Langton's Ordered, Critical and Chaotic regimes. From these depiction can one also see that the critical regime hade the longest transition length (15).[Figure are from Langton's conference (1990): Computation at the edge of chaos: Phase transition and emergent computation]*

Langton examined three different aspects of the cellular automata IV: the transition length of activity in the model, the information capacity through Shannon's entropy and the mutual information (MI) (15), these parameters are explained in Table 1.

**Table 1:** *Describes the three technical terms of Degree of freedom, Entropy, and Mutual information (30-32)*

| Technical term | description |
|---|---|
| Degrees of freedom | The number of different ways the system is allowed to evolve by. |
| Entropy (Shannon's) | The minimum amount of bits needed to store and send information |
| Mutual information | A measure of the reduction in uncertainty for one variable given a known value of the other variable, this uncertainty is represented through entropy. |

For different degrees of freedom with different lambda values; which is stated to be a measure of possible states each cell can position into (i.e., lambda reflected the amount of chaos in the environment), three qualities vary in the model: the average transition length; the distance of nodes through which the signal propagated, the entropy, and MI. Varying lambda from 0.0 to 1.0 (highly ordered to fully chaotic and random) the transition length, entropy and MI all had a clear cutoff point where the values suddenly peaked, as show in Figure 6 below. The transition length was close to zero before a sharp increase, followed by rapid decrease. The entropy went from low entropy to high entropy after the cutoff point, then it gradually

evolved towards a maximal value. The MI was nearly zero before it jumped after the cutoff point, then it gradually decayed again toward a limit value.

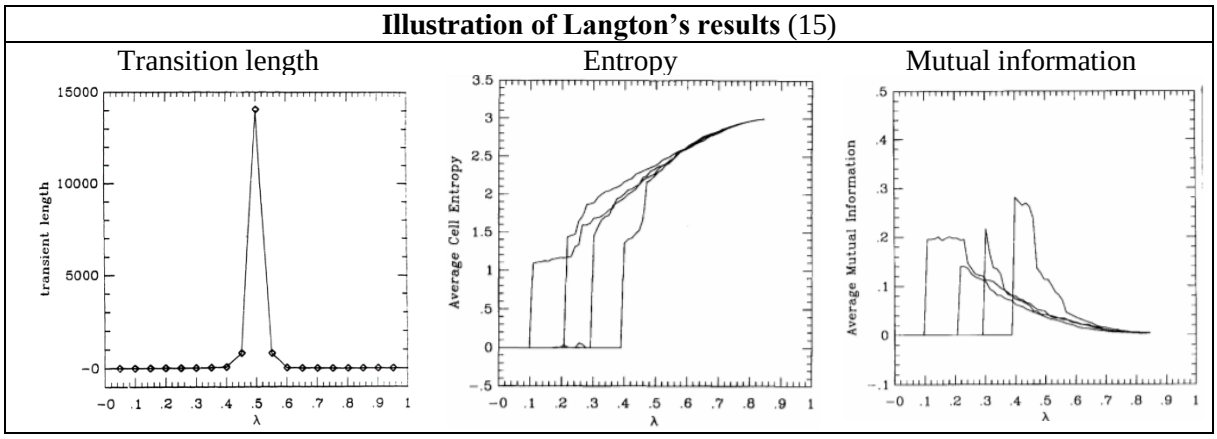


**Figure 6:** The following pictures show Langton's results of transition length, entropy and mutual information respectively. These factors were used to discriminate between Langton's three different regimes for his model (15). [Figure are from Langton's conference (1990): Computation at the edge of chaos: Phase transition and emergent computation]

This state before the cutoff points was called the ordered state, the state after was called the critical state, and the last state after the second transition length cutoff, where the entropy and MI gradually started to change was called the chaotic regime (15). The conclusion to Langton's experiments on Wolfram's model suggested that computations such as signal transduction and adaptability were performed best by systems near the critical point, where signal propagation lies between order and chaos (15). This state between total chaotic randomness and deterministic order he described as 'at the edge of chaos' (15).

Langton's results with the cellular automata model together with the coincidental similarities between artificial neural networks and the cellular automata model sparked ideas of the brain as a potential candidate for an SOC system, as the branching regimes of neuronal signaling were highly comparable to Langton's model on signal transduction where both could be classified into sub-critical, critical, and super-critical regimes. Around the year 2000, SOC started to be investigated as a potential brain phenomenon; with most of the investigations being grounded in statistical physics with regards to the work by Bak et al. (20). This led to the creation of Beggs's Critical Hypothesis in 2008 (10), the article where Beggs presented contemporary evidence suggesting that cortical networks operated in a critical state (10).

## 1.3 Evidence for SOC

Bak's "1/f noise" model showed that scale invariance and power laws emerged at the critical point through a signaling cascade type called avalanches and that input to SOC systems forms avalanches following power law distributions for both size (in terms of participating units) and duration (20). Similar attributes to the ones found in the "1/f noise" model have since been found in signaling cascades in brain networks.

Neural branching ratios can be categorized into different regimes, each branching regime relating to a particular critical state. Because of this, critical states in the brain are measured according to the average signal branching as branching ratios are quantifiable features of the different critical states (sub-critical, critical, or super-critical). The branching of neural signals may be classified as different phases, varying from a branching of under 1 to 1 to over 1. This led to the application of phase transition dynamics to neural signaling. Branching under 1 were designated as a sub-critical feature, branching of 1 were attributed as a critical feature, and branching of over 1 as a super-critical features (9, 13, 14, 17). This is visualized in Figure 7.

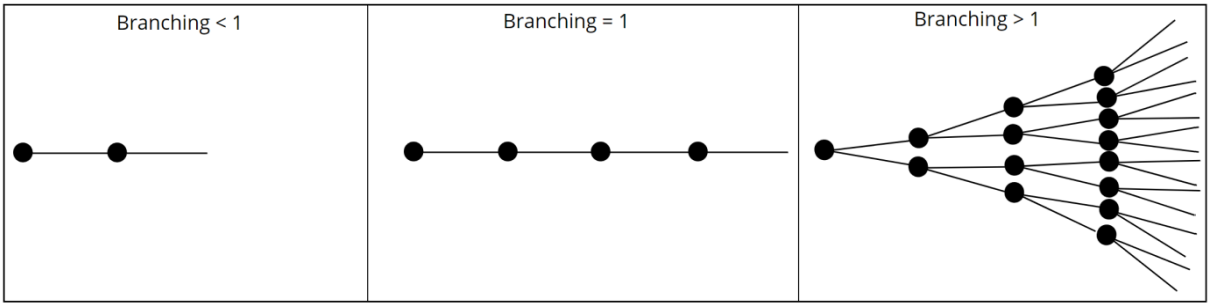


**Figure 7:** *This illustration shows the branching dynamics of neural signal. The three branching regimes shown are branching < 1 where the signal abruptly stops, branching of 1, and a branching > 1 in which the branching cause widespread activity.*

In addition to the phase transition dynamics, avalanche event cascades are present in neural networks. Neural signaling activity with avalanche properties and branching have been found in layer 2/3 of cats (33), rats (9), in primates such as monkeys and humans (34, 35) and in different brain states (during sleep and active/resting wakefulness) (35-38). Criticality has also been found on different scales, which supports the prediction of scale-freeness in critical networks, as avalanches have been observed in spiking behavior (microscale) (33), LFP (mesoscale) (9), and fMRI, ECOG, EEG, MEG (macroscale) (37-40). Furthermore, a large body of research shows this propagation behavior in acute brain slices (9), and in cell cultures

(41, 42), indicating this behavior both *in vivo* and *in vitro*. Lastly, properties similar to Langton's results (intermediate entropy, maximized transition length and MI) have also been observed from critical state dynamics (1, 41). These above-mentioned virtues combined with the fact that the brain is self-organizing led to the application of the name self-organized criticality for this phenomenon. Despite intriguing observations, critical dynamics are still a conflicting and debated topic, which is yet to be definitely proved and defined (17, 43-45).

## Evidence for E/I ratios involvement in SOC

A 2012 article analyzed the critical behavior of neural networks in pre-ictal and ictal states in epileptic patients (40). They found not only that excessive excitation disrupted the power law distribution of neural avalanches, which supported the notion of the brain operating with critical dynamics, but it also showed that different brain areas seemed to operate at different near-critical states under normal circumstances (40).

The result that interference with excessive excitation drives near-critical networks to a super-critical state, in the company of many other experiments including Beggs experiment (9) of perturbing critical networks with excitatory and inhibitory agonists and antagonists, indicated that the excitation to inhibition (E/I) ratio in the network was a vital aspect in the emergence of SOC (1, 9, 46, 47). E/I balance is prevalent on all neuronal scales and this may be why it is considered one of the most important factors for emergence of critical dynamics.

Several experiments have shown how tuning of different parameters may contribute to the emergence of criticality, with some of the more prevalent parameters being network topology (the coupling of network and the cell components) and the distribution of synaptic weights (14). However, criticality is not only defined by the mechanical coupling of the neuronal topology, as it takes networks longer to develop their topology than it takes to organize into the critical state (42, 48).

Around the year 2000, multiple experimental observations were reported supporting the notion that the E/I ratio was one of the parameters important for the emergence of SOC. Evidence supporting this claim includes observations from perturbation experiments. Networks without the configuration to stay critical, specifically those that fall into super-critical states, can be artificially moved and held in the critical state through pharmacological intervention with GABA (49). Additionally, critical networks can be moved out of criticality through pharmacological intervention targeting AMPA, NMDA and $GABA_A$ receptors (1, 9).

## 1.4 Aspects of critical self-organization

Extensive research into SOC has focused on understanding the mechanisms of the attractor dynamics underling the self-organization. These investigations focus on four main categories: the self-organization during development, the attractor state(s) which networks organize into, self-organization after perturbation (self-organization in mature networks), and factors that can control the self-organization.

### Development

Evidence shows that developing networks grow through a sub-critical and a super-critical state and before they stabilize in a near-critical state (42, 48), indicating that criticality develops through overshooting before it is tuned into the critical state. The emergence of SOC is likely to be dependent on multiple factors, from genes, to molecules, initial growth of axons, to neurons, to networks of neurons, to plasticity and homeostatic mechanisms (13). Critical emergence seems to be an inbuilt intrinsic mechanism of the neurons in the brain, as critical power law distributed avalanches occur in developing networks (41, 42). Additionally, neural networks have been shown to produce avalanches predicted by critical dynamics even when developing with elevated firing rates (41, 47), showing self-organization in varied environments, further suggesting that innate mechanisms upholds and regulates critical dynamics.

Network E/I firing balance is hypothesized to help regulate and maintain avalanche size and duration distributions (41, 42). Combined, these results indicate that network development into states of balanced E/I firing may be intrinsically regulated. However, little is known about how the E/I ratio affects the neurons' ability to develop, self-organize or establish critical dynamics. Considering that developing neurons wire differently based on molecular ques for different neuronal subtypes (50), and the observations that different brain areas have different E/I populations and different topologies (51-53), one would assume that the E/I population affects the topological development of a network. With the E/I firing balance being a tuning parameter for critical emergence, increased inhibitory populations are also expected to alter a network’s ability to produce critical dynamics to some capacity, as this would alter the dynamics of the firing balance.

## Attractor state

Several studies suggest that *in vitro* neural networks develop into a near-critical state (1, 37, 40), and not a critical one (40). The different brain areas are also observed to be in a near-critical sub-critical states (35, 54), and many theories have tried to describe this phenomenon. Some suggest it is an artefact of other underling neural mechanisms, or an evolutionary compromise between metabolic requirements and computationally gains (55), while other models indicate that it is beneficial for operating in noisy environments (56), yet others again claim it to be a defense mechanism from being pushed into a pathological super-critical state (23). The critical state has also been hypothesized to be less metabolically demanding to maintain compared to strong plastic circuits (57). Disregarding the definitive purpose of developing into near-critical dynamics, the matter that critical dynamics 1) can emerge from different network configuration and 2) can stabilize in more nuances than strictly sub-critical or critical are in themselves important traits.

An article by Ma et al. demonstrated that SOC may be the homeostatic state of networks in layer 2/3, thereby important for generic information processing in these layers (58). Different regions of the brain have also been shown to be separately tuned to different configurations of near-criticality (40), and these separate configurations may possibly represent multiple unique attractor states. This has led many to hypothesize that critical brain dynamics operate with critical regions rather than a sole critical point. This would allow the different brain regions to optimize for different computational purposes (14, 23). Further elaborating on the idea that critical dynamics can be established in different network topologies, it can be hypothesized that networks with different topologies may have different E/I firing balances which causes critical dynamics to emerge. Or oppositely, there is a chance that the E/I firing balance established from different inhibitory populations may cause changes to development of networks and thereby which attractor state a network develops into.

## SOC Resilience and homeostatic plasticity

Resilience of critical states and attractor dynamics are observed through the re-stabilization into critical dynamics after small and moderate perturbations. On a short-term scale this is shown through the regain of critical measurements after critical exponents dwindle then shifting back towards a critical-state during a switch in mental states (35, 37); from rest to mindful meditation (38) or from ictal to post ictal states (40, 59). On a long term scale this is shown through homeostatic mechanisms regulating the overarching excitability of the network (58, 60).

Electrical stimulation in the brain showed that the branching of neural signal increase with the onset of applied stimuli but quickly regained resting values, this shows an example of short term critical resilience (35). Similarly, incoming signal inputs can lead to deviations from critical dynamics followed by rapid tuning back to the critical regimen (3), although bigger perturbation may require more time to re-tune to criticality (3, 58). There is growing evidence that one of the main contributing mechanism to the attractor dynamics of SOC is homeostatic mechanisms such as synaptic scaling or synaptic depression (58). *In vivo* experiments of monocular deprivation caused destabilization of critical readings which was adapted to and restored over a 48h period (58). This is brought about by the slow working homeostatic plasticity, as seen by the observations that perturbations often cause slow tuning back to criticality (58). Given that networks can self-organize to different near-critical states, one possibility is that some attractor states create more stable dynamics then others or that the self-organizing mechanisms such as homeostatic plasticity operate differently in order to attract to different attractor states. One might speculate that differences in the action of attracting or the differences in the attracting state could alter a network's critical resilience both on a short and long term. If it is true that some network configurations are better at resisting perturbations or self-organizing back after perturbations than others, then tuning of parameters for critical emergence such as E/I balance may yield networks which shows differences in resilience.

## SOC associated factors

Accompanying topology and E/I firing balance, network wide bursts and the balance of synchrony/asynchrony have been associated with networks operating with critical dynamics (41, 61). Due to the scale invariance of critical dynamics for avalanche sizes, high levels network bursts (NBs) are expected (61). Intermediate levels of synchronous activity are also observed during critical dynamics, hence should relative intermediate levels of network bursts to synchronous activity (NB/S) also be expected during critical dynamics. Interestingly, burst activity and synchronous activity have also been associated with E/I balance (62-65). Which might indicate that these concepts, in some way, are interconnected. Exploration of critical and synchronous dynamics have indicated that a critical state can occur in a synchronization phase transition, at which oscillations and scale-free avalanches both occur (5, 44). Furthermore, in 2020 Li & Shew (57) showed through modeling that a balance of the synaptic strength between E/I neurons could cause both the emergence of criticality (in which they

observed synchrony-like behavior) and asynchrony (57). These observations together hint at a correlation between synchronous activity patterns and emergence of critical dynamics with different E/I ratios, as emergence of synchronous activity and critical dynamics both seem dependent on E/I ratios, and since synchrony-like behavior is observed under critical dynamics.

## 1.5 Critical topology

It is widely recognized that the topology of the brain provides a physiological basis for its information processing and dynamics, and this is also true for the emergence of criticality. The structure of brain networks is commonly referred to as being hierarchical and modular, and the average brain network is said to be share traits of three different network topologies: a regular (lattice), a random and a scale-free network (14, 66). The small-world (SW) topology shares some features of lattice and random networks. Many experiments and observations point to brain networks having a SW organization, due to graph theory measurements which coincide with SW qualities; short average path length and high local clustering (terms are described in detail in section 2.2) (14, 66-70). Network topologies which are regarded as more efficient for computation such as modular, SW and scale-free topologies have also been shown to be better suited for the emergence of critical dynamics compared to computationally inefficient topologies such as random and regular networks (14, 16, 68). These results tie into the observations of critical dynamics having ideal processing properties.

Neural avalanches following size distributions predicted from critical dynamics have so far only been observed in the superficial layers; layer 2/3 of the brain (71). These layers are normally described as being composed of mostly small and medium pyramidal cells and stellate cells. The cells in these layers are found to have many subtypes with genetic and functional differences (52, 53, 72) and layer 2/3 is even shown to contain area and cell type specific microcircuits (73-75). The GABAergic cells in layer 2/3 are estimated to amount to approximately 10-15% of the cortex in rodents (72) and 18-27% in monkeys (51), and 15-30% for humans (53). Interestingly, despite all these specialized cell-type populations and circuits in layer 2/3, neural avalanche following critical size distributions are also observed in simple *in vitro* cultures made of excitatory and inhibitory neurons, both in IPSC and organotrophic derived cultures (9, 41, 76). *In vitro* networks also tend to develop small-world topologies (77, 78). In addition, these networks also develop as single compartment networks, meaning that they do not get any external input, and that all activity is locally generated.

Considering these virtues, *in vitro* neural cultures provide a less complex system with fewer variables, which allows for less complications regarding data analysis when studying SOC in biologically relevant networks.

## 1. 6 Criticality *in silico*

Criticality was first described in physics, therefore mathematical models are the natural starting place for recreating a critical system. However, many *in silico* models operate with few and simplified neural mechanics, limiting their biological realism. Hence, model results alone should not be considered proof of system limitations or exact behavior without experimental data to back it up. For most neural network models translated from theory to reality, we expect to find the same core dynamics, but also some deviations. Therefore, when estimating general properties, it is easier to start from simple systems, as core behaviors are less likely to vary between different models and between *in silico* and *in vitro* systems.

The Izhikevich model (79) is a simple firing model derived from the Hodgkin–Huxley model, which is both biologically plausible and computationally efficient compared to other models (80). The Izhikevich firing model has the ability to reproduce spiking and burst behaviour of several types of excitatory and inhibitory neurons, and the model even accounts for noise through random thalamic input. While initial investigations with the model sacrificed its plastic qualities in exchange for staying simple and robust (79, 80), explorations of the Izhikevich model with spike-time dependent plasticity rules have been shown to produce similar behaviors, regardless whether the rule is active or not (81). This simplicity and robustness make the Izhikevich model a good candidate for estimating simple or generic network features.

## 1. 7 Study aim

Inhibitory interneurons seem to be important to “tune” the excitatory activity of neural networks to criticality, even though the excitatory activity can vary greatly and even change without disrupting the criticality of the system (58). The importance of balance between excitation and inhibition is indicated in multiple published papers (9, 47, 82), yet there is a lack of knowledge concerning the balance of excitatory to inhibitory neurons in the context of affecting and establishing critical dynamics. This project aims to investigate that balance and its significance for neural networks to self-organize to a critical state, and its capability to

alter the resilience of critical dynamics. Additionally, factors such as synchrony and network bursts which is associated with E/I balance and emergence of critical dynamics will be explored. Criticality is usually assessed from electrophysiological spiking data, especially when working with the balance between excitatory to inhibitory firing (1, 9, 47). Microelectrode arrays (MEAs) are a common tool used to study this aspect of criticality due to their temporal and spatial resolution and were used for investigating critical dynamics in this thesis. Additionally, MEAs gives us the ability to control the environment to a degree which is not available in other systems, for instance the fraction of inhibitory neurons in the population of the networks.

In this project, a neural network simulation was used to predict the ratio of excitatory to inhibitory neurons where criticality spontaneously emerged. Several networks were then grown on MEA interfaces with different ratios of excitatory to inhibitory induced pluripotent stem cell (iPSC)-derived neurons to try to find the optimal ratio for emergence of SOC. The exact ratios were informed by the results of the simulated model. The developing activity of the networks was analysed to assess for criticality and network features such as topology.

Furthermore, the differences in the simulated networks and the biological ones were examined, and the simulated model was then updated to better capture the experimentally observed behaviour of the biological network by tuning topological factors. Finally, the resilience of critical dynamics was also examined through pharmacological perturbation of biological networks. This was done to investigate whether critical networks with different inhibitory populations differed in perturbation resiliency. The information gained from exploring emergence and resilience of critical network dynamics might give new insight on the subject of SOC, and potentially be of benefit for future research on the topic, as well as studies on E/I balance in general.

# 2. Material and methods

## 2.1 Material

### *Induced Pluripotent Stem Cells*

The cells used in this project were fully differentiated cells purchased from BrainXell. These cells originated from human fibroblasts and were driven through cell fate determination stages observed during embryonic development, to increase their similarity to primary neurons. The neurons used were Cortical Glutamatergic Neurons (BX-0300) and Cortical GABAergic Neurons (BX-0400). The astrocytes used in this project were purchased from Gibco. These astrocytes were human brain progenitor-derived astrocytes, derived from human brain tissue.

### *Material for cell culturing*

Below are the chemical-solutions and reactants used in the project. The material for all solutions listed here are further detailed in the appendix A Table A-1, where producer, catalogue and lot numbers are presented. The material for the laminin coating includes 0.05% PEI in HEPES, and 20µl/mL Mouse laminin diluted in PBS.

All solutions used in the neuronal culturing includes Seeding medium, Day 4 medium, Day 10 and onward medium, and Gibco® Astrocyte Medium. The individual cell culture media material for astrocytes and Glutamatergic and GABAergic neuron solutions are shown in further detail in appendix A Table A-2 to A-4, while the composition of the solution is shown in appendix B.

The chemicals and solutions used in the immunostaining were PBS, 4% Paraformaldehyde in PBS, Block (PBS, 5% Goat serum, 0.3% Triton-X), Primary antibodies, Secondary antibodies, Flouroshield, and Hoescht. The materials for staining medias are described in appendix A Table A-5, while the antibodies of the immunocytochemistry (ICC) staining is depicted in appendix A Table A-6.

## 2.2 Methods

### *Computation and models*

The firing model used in this thesis, The Izhikevich model (79), is described by the equations

$$v' = 0.04v^2 + 5v + 140 - u + I, \quad (1)$$

and

$$u' = a(bv - u). \quad (2)$$

The parameters of the model include the membrane potential, *v*, thalamic input (the driving force of the model), *I*, and the membrane potential recovery value, *u* (79). The update rule, which is given by

$$\text{if } v \geq 30 \text{ mV, then} \begin{cases} v \leftarrow c \\ u \leftarrow u + d, \end{cases}$$

dictates the firing threshold, and how the recovery and rest factors affect the neurons after a firing (79).

The *a*, *b*, *c*, and *d* components are parameters which help the model behave like a Hodgkin-Huxley model. Parameter *a* related to the length of the recovery period after a firing (refractory period and hyper polarization) and *b* is involved determining the recovery of membrane potential (tunes the sensitivity, simulates $Na^+/K^+$ pumps decreasing effect on membrane potential). Parameter *c* is related to determining the membrane resting potential after spikes, and parameter *d* concern the reset of the recovery variable after firing (simulates a reset of internal $Na^+/K^+$ concentrations). The *a*, *b*, *c* and *d* parameters effect on the excitatory and inhibitory neurons are shown in Table 2 below.

**Table 2:** *Shows the model parameters a, b, c, and d, and their respective effects to excitatory and inhibitory neurons.* $r_i$ & $r_e$ are the lists of the inhibitory and excitatory neurons membrane potential respectfully.

| Parameter | Excitatory neurons | Inhibitory neurons |
|---|---|---|
| *a* | 0.02 | $0.02 + 0.08r_i$ |
| *b* | 0.2 | $0.25\text{-}0.05r_i$ |
| *c* | $-65 + 15r_e^2$ | 65 |
| *d* | $8\text{-}6r_e^2$ | 2 |

$r_i$ and $r_e$ are the lists of the inhibitory and excitatory neurons membrane potential respectfully (79).

To approximate the SW topologies in biological networks, we used the Watts-Strogatz networks implemented through NetworkX (83). For the random topology a simple randomly connected graph was used. The generation of SW topologies through Watts-Strogatz networks was kept at 30% chance to rewire as the *in vitro* networks are expected to have slightly different small-world topologies, hence would the average over a wide range of SW topologies give a better understanding of the effects of tuning the E/I ratio.

The Izhikevich model is a stepwise model, where each step represents 1 ms. To allow the model to equilibrate and saturate, the first 1000 ms were discarded for all simulation runs, leaving 1000 ms for analysis. The networks used for analysis all had 650 nodes with randomly placed inhibitory nodes. For simplicity's sake synaptic weights were put on a static 0.25, because the original Izhikevich model used randomly distributed weights between 0-0.5. It was tested beforehand that this static changed did not greatly alter any outcomes, this was tested by comparing results with and without the static weights.

The Izhikevich model was tested with the varying parameters of clustering values ranging from 0.5 to 0.9 in steps of 0.1, and inhibitory percentage from 0 to 50% in steps of 2%. Each parameter variation was tested with 500 model iterations. The code for the model is assessable via (84).

As the Izhikevich model does not have spontaneous activity from the neurons, the networks were driven using a random input to model thalamic input (79). It was tested that the external noise the model received (the models driving force) was not also the drive for the model's critical behavior. This was tested by only applying input of the same strength to a fixed spot of the network.

## Analysis with Graph theory

The graph theory analysis were performed on the functional connectivity between electrodes. This connectivity was based on temporal cross-correlations in spiking data i.e. the similarities between two sequences of spiking data from different electrode based on the displacement of one relative to the other. The networks functional connectivity was represented through undirected adjacency matrixes; undirected meaning that the connection between the electrodes does not inform which way information is transmitted. The adjacency matrix was computed by searching 2 ms bins of the electrophysiological recordings using the MATLAB function *xcorr* to find the cross-correlation between all pairs of electrodes (varying from 0 to

1). This cross-correlation function tries to synchronize two temporal sequence by shifting one sequence back or forth and gives points for every event (spike) that could be synchronized within the sequences. The mean of the cross-correlations output was given as an output matrix. The adjacency matrix was subsequently filtered to remove weak correlations not considered as viable connections. The filtering was based on connection persistence, filtering away correlations levels found to be ≤ 25% of the total data, following previously work on topological assessments of MEA data (77). Additionally, another filtering method of empirically testing thresholds was used to make sure that the mean degree of each recording was not more than the total active electrodes of the recording in question.
Once the topology was established the network describing measurements average pathlength, average clustering, average mean degree, and Small-world metric ω were computed. These parameters are explained in Table 3.

**Table 3:** I*nformation table Graph theory measurements. This table informs about the basic graph theory parameters: Path length, Clustering, Mean degree, and small-worldness metric Omega.*

| | |
|---|---|
| Average Pathlength | A measure of the distance between nodes in the network, calculated as the mean of the shortest distances (measured in connections) between every pair of nodes (85). |
| *Clustering* | The percentage wise measurement of the edges that exist between the neighbors of a node compared to the total number of possible edges between the neighbors if the neighbors were fully connected (85). |
| Mean degree: | A measurement of how many other nodes the average node is connected to (86). |
| Small-world metric (ω) | Omega (*ω)* is a measurement for a networks small-worldness. Computed as the difference between ratios of the networks clustering against clustering of a comparable lattice network and the ratio of the networks path length against pathlength of a comparable random network (66): topologies with $-0.5 < \omega < 0.5$ was considered to have small-world features. |

The topological analysis was made using the python package NetworkX (83), using built in functions to compute topological measurements, average pathlength, clustering, mean degree, and ω.

The graph theory analysis script was also used for the Izhikevich model. The topological parameter was only computed for the network configurations which was predicted to yield the best critical emergence, and only on readings considered critical.

After the topological measurement were taken, the *in vitro* networks were classified and grouped into one of 16 groups based on clustering, average pathlength, mean degree and small-world metric ω, where each measurement was characterized binary as either low or high depending highest and lowest data values found from the analysis.

## *Biological experiments and neuronal cultures*

18 neural networks were cultured, 6 per E/I ratio tested, according to the following procedures. General information about the cell cultures are shown in Table 4.

PEI + Laminin coating

To prepare the MEAs for seeding the surface of each MEA well was coated with PEI and laminin to mimic an extracellular environment permissive to neural growth. This was done following a previously established inhouse protocol Fig C-1 in Appendix C.

Cell Seeding

The seeding was carried out following a modified version of BrainXell's seeding protocol for Human mixed cortical neurons. For both glutamatergic and GABAergic neurons the seeding steps were identical following Appendix C Fig C-2 with a few alterations, while the astrocytes were treated differently.

The seeding of all cell types was done in 5 main steps:

- The frozen cells were thawed in water baths
- Warm Seeding media was added to the cells
- Cells were centrifuged and cryovial fluid was removed and replaced with seeding media.
- Viable cells were counted with the trypan blue method
- The cells were seeded

Protocol step 1-8 (Appendix C Fig C-2) were followed normally for the cortical neurons with the exception that the antibiotic Penicillin Streptomycin was added to the seeding media, while the astrocyte seeding used Gibco® Astrocyte medium instead of seeding medium for the thawing process. The neurons were centrifuged at 160xg for 3 minutes, while the astrocytes were centrifuged at 290 × g for 5 minutes. The supernatant was then fully removed, and the cell pellets were then gently resuspended in 1mL seeding media.

The trypan blue exclusion method was used to count the cells. The number of viable cells per mL was counted with the automated cell counter Countess™ II from life technologies. Then the necessary amount of seeding medium was added to achieve a desired concentration of viable neurons/µl. The equation used to calculate the volume of viable cells per milliliter needed to achieve desired cell density is given:

$$mL = \frac{\text{Desired number of cells}}{\text{Viable cells per mL}}. \quad (3)$$

Before the seeding a small volume of seeding media was placed onto the MEAs to prevent the surfaces from drying. Each MEA was plated with different volumes to achieve the desired ratio of excitatory to inhibitory neurons and each culture contained 10% viable astrocytes, totaling a cell count of 110,000 viable cells/MEA for all cultures. The three different ratios were each seeded in two random MEAs per plate as to avoid systemic errors in treatment. After seeding, the cells were left in the laminar flow hood for 15 minutes to allow the cells to settle to the bottom of the wells.

BrainXell protocol steps 13-15 (Appendix C Fig C-2) were followed with the only differences being that the media in each well was filled to a final volume of 1 mL and that cells were left to incubate in an incubator for 1 hour to allow neurons to attach to the laminin instead of 30 min.

Network maturation

The networks were visually inspected with light-microscope to ensure the neurons were healthy and that they attached to the MEA surface. The networks were incubated with water reservoirs, and more media was added if the pH indicator showed signs of turning from pink to yellow.

On day 4 and 10, half the media (500 µL/MEA) was replaced with appropriate media according to the protocol in appendix B, Fig B-3 and B-4 respectively (with 1% Penicillin Streptomycin). After day 10, half the media was replaced every fifth day.

**Table 4:** *Information about the cultured cells*

| Cell culturing information table | |
|---|---|
| Origin | Fibroblast in humans |
| Cell type | Cortical |
| Culture media | BrainXell media |
| Ph, temperature, Co2 | 37C°, 5% |
| Cell density under seeding | 110,000 viable cells |
| ml of culture media | 1 |
| Media Change | Every 5th day |
| Nr of networks | 6 per inhibitory ratio tested |

## *Immunocytochemistry (ICC)*

The cultures used for ICC were prepared on microscope plates ("*8 well chamber slide w/, removable wells"* Nunc™ Lab-Tek™ Chamber Slide System, Thermo Scientific™). ICC was carried out to confirm the presence of the different cell types in the cultures. The staining was accompanied by a negative test, to test for false positives. In the wells housing the negative controls were the primary antibodies not added. Three different sets of markers were used to stain the networks, additionally all sets also contained Hoechst. These marker-antibodies where added in triplets.

**Table 5:** *The four sets of antibody triplets used in the immune staining. A =astrocytes, N= neurons, E = excitatory neuron, I =Inhibitory neuron*

| Antibody marker cocktails | | |
|---|---|---|
| | Marker targets | Cocktail purpose |
| Marker set 1 | AMPA-r1, GABA β-R1, βIII-tubulin | Marker for: N |
| Marker set 2 | TBR-1, βIII-tubulin, NeuN | Marker for: N & E. |
| Marker set 3 | GABA, NeuN, GFAP | Marker for: I, N & A. |

ICC Indirect Staining

The immuno-staining was done following a slight alteration of the internal staining protocol shown in Fig C-3 in Appendix C. This protocol can be divided into 6 steps over 2 days:

Day 1

- Preparation and fixation: the networks are rinsed with warm PBS (37$^{o}$C) and then fixated with PFA, which causes covalent binding in the tissue, preventing degradation (87).
- Non-specific site blocking: PFA was rinsed away and the block solution is added to block non-specific binding sites.
- Primary staining: The primary antibodies were added. The primary antibodies are listed in appendix A Fig A-6, while antibody markers and general information can be found in Table 5 and 6 respectively.

Day 2

- Rinsing: PBS is used to rinse networks excess primary antibodies.

- Secondary staining: Secondary antibodies are added. Secondary antibodies are shown in appendix A Fig A-6, while antibody markers and general information can be found in Table 5 and 6 respectively.
- Fluorescent preservation and coverslip fixation: Fluoroshield was used to preserve fluorescence over a longer period of time and to attach glass coverslips.

**Table 6:** *General information on immuno-staining.*

| ICC | |
|---|---|
| Microscope type | EVOS™ M5000 Imaging System |
| Antibody type | IgG |
| Fluorescent specter | 488 nm, 546 nm, 647 nm |
| Antibody pairing | Mouse-anitmouse, chicken-antichicken, rabbit-antirabbit |
| Antibody specificity | Polyclonal |

## *MEA set up / analysis*

Electrophysiology recordings used Axion CytoView MEA plates, and the recording was done with Maestro Pro (Axion Biosystems) together with the AxIS navigator 2.0.4 software (Axion Biosystems). The MEA plate specifications are described below in Table 7. Recordings from days *in vitro* (DIVs) 18- 21 and 41-65 were taken for all 18 networks, which amounted to a total of 286 single well recordings (including recording data from perturbation experiment). However, only recordings from 41-55 DIV were used for electrophysiological analysis. Networks of 21 DIV and below did not show electrophysiological behaviors associated with mature networks, namely the lack of network bursts. Networks older than day 55 showed signs of ageing like more varied electrophysiological measurements. Prior to each recording the networks were equilibrated through incubation for 15 min in the Maestro Pro. Each individual recoding was 30 min at approximately the same time of day. Spike detection was performed using ± 7 standard deviations from the median of the signal. The sampling frequency was 12.5kHz. Data from all networks were filtered. Networks with firing rates of

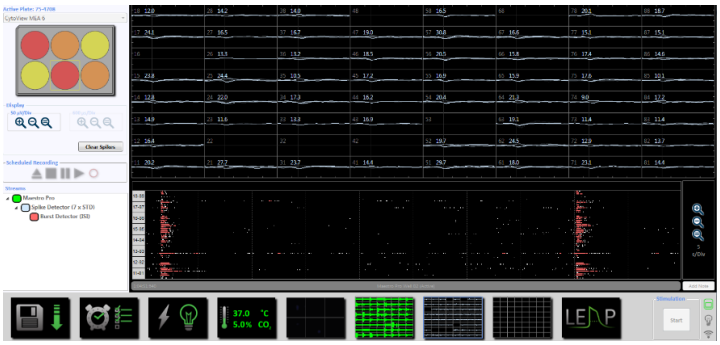

**Figure 8:** *Display of the MEA recorder maestro Pro (Axion biosystems)*

under 5 spiks per min were deemed silent networks, and no networks with 4 or fewer active electrodes were considered active.

**Table 7:** *General information about MEA plates*

| MEA information table | |
|---|---|
| MEA type | Axion biosystems Cytoview MEA 6 |
| Plate Name | M384-tMEA-6B |
| Nr of electrodes | 64 (PEDOT) |
| Layout | 8x8 grid (centered) |
| Nr of well | 6 |
| Electrode spacing | 300 µm |
| Electrode diameter | 50 µm |
| Recording area | 2.1mm X 2.1 mm |

## *Analysis of electrophysiological data*

The firing rates, synchrony and network burst detections were all captured through preexisting inhouse MATLAB scripts. The firing rate was computed from the total number of spikes divided by the length of the recording, while network burst and the synchrony analysis were computed as described below.

Network bursts (NB) were found by binning the recording into 50ms bins. The mean firing rate was then found for each bin. Any bin where the firing rate exceeded the firing threshold (mean firing + 5*SD from the whole recording) and more than 20% of the network was active, was considered part of a network burst. Consecutive bins that met condition of being in a network burst, were counted as parts of the same burst. From this analysis the frequency of NBs in each recording were found, and the measurement frequency of NBs were used for all analysis concerning NB in this thesis.

The synchrony (or coherence index) was found following the definition in (88). Here, the recording was binned by 2ms, and the firing rate was found in each bin. The mean firing rate over all bins was found and divided by the standard deviation (SD). Synchronous networks which have a low SD would obtain large coherence index value, while asynchronous firings with high SDs would have low coherence values.

## *Analyzing avalanches; detection and measurements*

Avalanche detection

Neuronal avalanches were detected based on the work by Beggs et al. (9). MEA recordings were divided by silent periods larger than Δt. The observation of an avalanche event was defined by sequences of activity bounded before and after by inactive time bins larger than Δt. In this project the size of an avalanche was defined by the total number of electrodes active during the avalanche, and the duration of an avalanche was defined by the number of active time bins spanning the avalanche. The interspike interval (ISI) for each individual recording was chosen as Δt. A numerical testing of different bin sizes was also done to test for linearly decreasing relationships between critical exponent and chosen bin size, as true critical recordings are observed to have this feature (9). As with the electrophysiological data, the networks which spiked under 5 spikes per minute were considered silent. In addition, networks with five or less data points for either the size or duration distribution were removed from further analysis.

The inter electrode distance (IED) was also accounted for following previously established methods (61). It was tested that the different ISI bins size was not so small that the velocity needed to move between electrodes (IED/Bin size) to be captured by the bin size did not surpass previous reported propagation velocity for neuronal activity in MEA networks (ranged from 30 to 350 mm/s) (89, 90). To make sure that the bin size at least captures the time frame a neural transduction theoretically would need to propagate along the length between electrodes were bin sizes from 0.9ms and upward put as a limit. However, because of the common input problem and indirect signaling problem (described in Figure 9), this Δt threshold was lowered to 0.5ms.

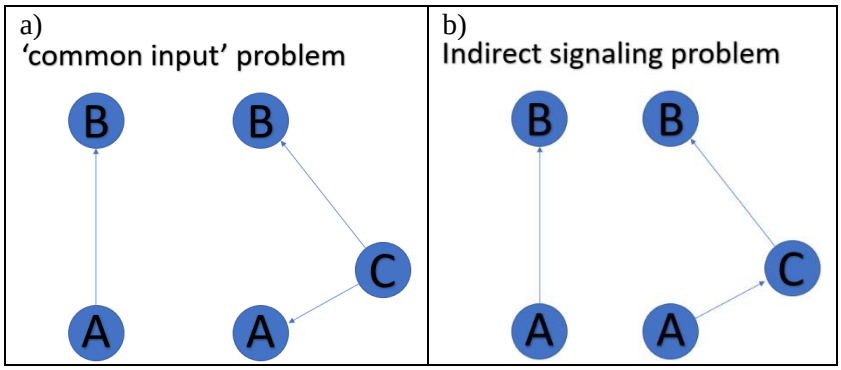


**Figure 9:** *The common input problem and indirect signaling problem: a) depicts the common input problem. This is the issue that it is difficult to distinguish connection correlations from temporal correlations in spiking activity between pairs of neurons and correlations from common input from a third unobserved neuron. b) shows the indirect signaling problem. A signal may not be sent directly from electrode A to B but instead A to an unobserved C, then C to B.*

ISI

Through visual inspection was it seen that most of the spike recordings had ISI distributions where 75-95% of the data were binned < 1ms. This made it problematic to use a mean estimation of ISI as the remaining 5-25% of data varied form 1-100ms, making the mean ISI significantly larger (typically between 0.4-4 sec) than the majority of the data, as shown in Figure 10. Therefore, when 75% or more of the ISI data was binned at <1 ms, the median of the interspike interval was used instead of the mean. Note that this is not the normal convention, but due to the power law distribution of spike times, this method was tried out.

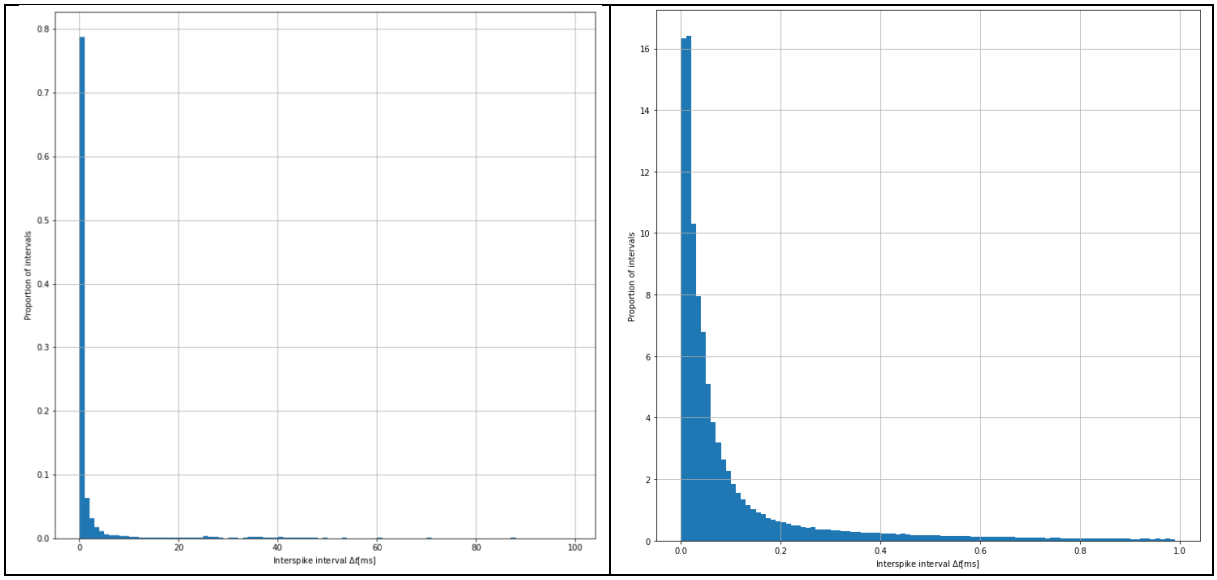


**Figure 10:** *This figure shows the ISI distribution from 0-100ms for 41 DIV, plate 13, well A3, in the left picture we see that over 70% is binned under 1 ms, but that a few ISI even goes over 80ms. The right shows the ISI distribution of the data binned under 1ms ranges 0.0-1ms.* Mean ISI = 4 sec, media ISI = 0.08 sec**.**

Branching parameter

The branching ($\sigma$) of neural signal is one of the parameters used to estimate true critical networks. Here, branching is defined as the average number of spikes detected in a time bin compared to the spike count in the previous time bin. This formula is mathematically defined as (9)

$$\sigma = \sum_{n=0}^{n_{max}} \left(\frac{N_p}{N_a}\right). \quad (4)$$

For this equation $n_{max}$ is the total amount of occurrences of active time bins (bins where at least one spike was detected). $N_a$ is the number of active electrodes observed in the starting time-bin, and $N_p$ is the number of active electrodes in the preceding time bin of an avalanche (9).

Probability distribution

The probability distribution was computed from the total active electrodes within each avalanche. The probability distribution was made through binning all occurrences of a frequency (total active electrode in an avalanche), which then was divide by total number of avalanches.

Finding the Power law exponent

A power law distribution is defined as $Y = CX^{\alpha}$, where: $X$ and $Y$ are the variables in question, α is the law's exponent, and C is a constant. When taking the logarithm of $Y$, the power law distributed data can be approximated by a line with slope number = $\alpha$.

$$\log(Y) = \alpha \log(CX) \quad (5)$$

The power law exponent ($\alpha$ -value) was found by make a plot of log occurrences and log probability distribution.

Maximum-likelihood estimations and best fit regression

MEAs have good spatial and temporal recording resolution but can only partly capture network activity due to their inter-electrode spacing, which creates unrecorded regions between electrodes. These unrecorded regions cause problems when analyzing propagation of avalanches. Furthermore, biological spiking data is notoriously accompanied by noise. Therefore, the empirical data was constrained using a Maximum likelihood estimation (MLE).

The MLE is a statistical method which finds the most likely estimator for describing data distributions. Here MLE is used to find the $\alpha$-value of a continuous sub-population in the data which most likely originated from the same sample set. This means that it finds the α-value from the range of data which is most likely to not have been affected by sub-sampling or noise.

The MLE was preformed following the works of Marshall et al. (91), which describes an MLE technique for truncated, discrete power laws. This method also compares the $\alpha$ value of the truncated data set against the full data set when estimating the likelihood, unlike other MLEs. The truncated ranges were found through numerically testing different variations of $x_{min}$ and $x_{max}$, which are positional numbers in the avalanche data distribution which varies

from zero to the total number of data points ($N$). The power law exponent was found though fitting the data with least square linear regression with goodness of fit test. $x_{min}$ and $x_{max}$ was constrained to at least cover 40% of the avalanche data as it was seen that small $x_{min}$ and $x_{max}$ intervals at the ends of the avalanches were preferably selected when the MLE analysis was done on heavy tailed distributions.

For the truncated, discrete power law, the log likelihood function, which here simply is referred to as the likelihood function, is given by

$$L(\alpha) = -\log\left(\sum_{x=x_{min}}^{x_{max}} \left(\frac{1}{x}\right)^{\alpha}\right) - \frac{\alpha}{N}\sum_{i=1}^{N}\log(x_i). \tag{6}$$

In equation 6 is $L(\alpha)$ the likelihood estimation for a given $x_{min}$ to $x_{max}$ interval, $\alpha$ is the predicted power law exponent following the $x_{min}$ to $x_{max}$ interval in question, while $N$ is the total number of data points for a given avalanche. Once all likelihood estimations were found for all $x_{min}$ to $x_{max}$ intervals, was a search algorithm used to choose the $\alpha$-value that gave the highest $L(\alpha)$ score.

Scaling relationship and Shape collapse

Scale freeness in critical dynamics predicts that avalanches of different lengths share a universal shape, which only differs from the mean temporal profile of any avalanche because of scaling when the duration is normalized. i.e. avalanche data is predicted to be collapsible through rescaling. The scaling relationship, Y, between the power law exponents of avalanche duration and size distribution was shown by Friedman et al. (92) this relationship is described by

$$Y = \frac{1}{\gamma} = \frac{\alpha - 1}{\tau - 1}, \tag{7}$$

where $\tau$ is the critical exponent, $\alpha$ is the avalanche duration exponent and $\gamma$ is the scaling constant. In critical networks $\gamma$ is typically described as 0.5 while $Y$ is typically described as 2 in critical networks (92). Note that the scaling relationship is calculated with absolute values for the power law exponents.

The shape collapse was done through dividing all avalanches by the ISI and binning all active electrodes in each time bin for the whole duration of the avalanche (92). The temporal profiles were normalized by dividing each time bin of each avalanche by the avalanche's total

duration, this way are the avalanches normalized with a duration between 0 and 1. Each avalanche size was then scaled accordingly to equation 8, where the scaling relationship between avalanches of different durations and the universal shape is described as

$$\frac{S_{mean}(\mathrm{t},\mathrm{T})}{T^{Y-1}} \sim f(t,T). \tag{8}$$

$S_{\mathrm{mean}}(t,T)$ is the function describing mean active electrodes per time $t$, for the whole duration $T$, for any avalanche, $Y$ is the scaling relationship from equation 7, and $f(t,T)$ is the universal scaling function that determines the shape of the average temporal profile (92).

Data which have α values within the range -1.5 ±0.2 , scaling constant of 0.5 ±0.3, are collapsible, have a branching of 1±0.1, has linearly decreasing relationship between bin size and critical exponent, and can be observed in all different critical phases are considered critical. The analysis code for critical detection is available via (84).

## *Perturbation methods*

Pharmacological perturbation

Networks were perturbed through addition of inhibitory γ-Aminobutyric acid (GABA) and excitatory NMDA diluted in water. The initial dosage of GABA and NMDA was given based on the predictions from the Izhikevich model as seen in Table 8 below. The different inhibitory population networks were tested with each other's predicted perturbation volumes in order to compare their responses.

**Table 8:** *Table of the Perturbation trial. This table shows all the perturbation trial with GABA and NMDA. 0.2µM of GABA was additionally tested reasoned limitations of available pipets.*

| GABA | 0.1 µM | 0.15 µM | 0.2 µM | 0.3 µM | Controls |
|---|---|---|---|---|---|
| Low Inhibitory Culture | - | 2 | 1 | 1 | Low: 4 |
| Medium Inhibitory Culture | - | - | 2 | - | |
| High Inhibitory Culture | 3 | 2 | 1 | - | Medium: 4 |
| NMDA | 0.4 µM | 6 µM | 18 µM | | |
| Low Inhibitory Culture | 1 | 1 | 3 | | High: 5 |
| Medium Inhibitory Culture | - | 4 | 3 | | |
| High Inhibitory Culture | - | 3 | 2 | | |

The predictions were found though combining the E/I firing ranges in the Izhikevich model in which critical readings occurred with the Hill–Langmuir equation (93, 94) 9.

$$\theta = \frac{[L]^n}{K_d + [L]^n}. \quad (9)$$

Here, $\theta$ is the percentwise saturation of receptors, L is the concentration of unbound ligand, n is how many binding sites the receptors have, and $K_d$ is the dissociation constant for the receptor in question. This was done in order to predict the percentwise saturation of GABA and NMDA receptors which would cause a decrease or increase in activity to make the Izhikevich model fall out of the predicted E/I firing range observed in critical networks.

Prior to adding the neurotransmitters, a 30-min baseline measurement was obtained. The recording was limited to 15-min and conducted directly after applying the neurotransmitter solution, to avoid effects of plasticity. After recording the media was replaced both to limit plastic changes and to prevent pathological conditions like excitotoxicity (95) and networks were left 48h to let homeostatic mechanisms undo any potential plastic changes from the recording.

# 3. Results

## 3.1 Modeling

The *in silico* model was shown to produce critical readings for the ranges 0-50% inhibitory populations by tuning with different the clustering levels. Figure 11 shows typical critical reading. Assessing the firing and ISI distributions, the model appeared to have biologically plausible firing regimes, as biological spikings rates average around 1-50 spikes per sec, although it is not uncommon to observe firing rates up to 200 spikes per sec (96-101). Single neuron interspike interval varied from ~10-11ms, which is plausible even when considering the refractory time of biological neurons (102).

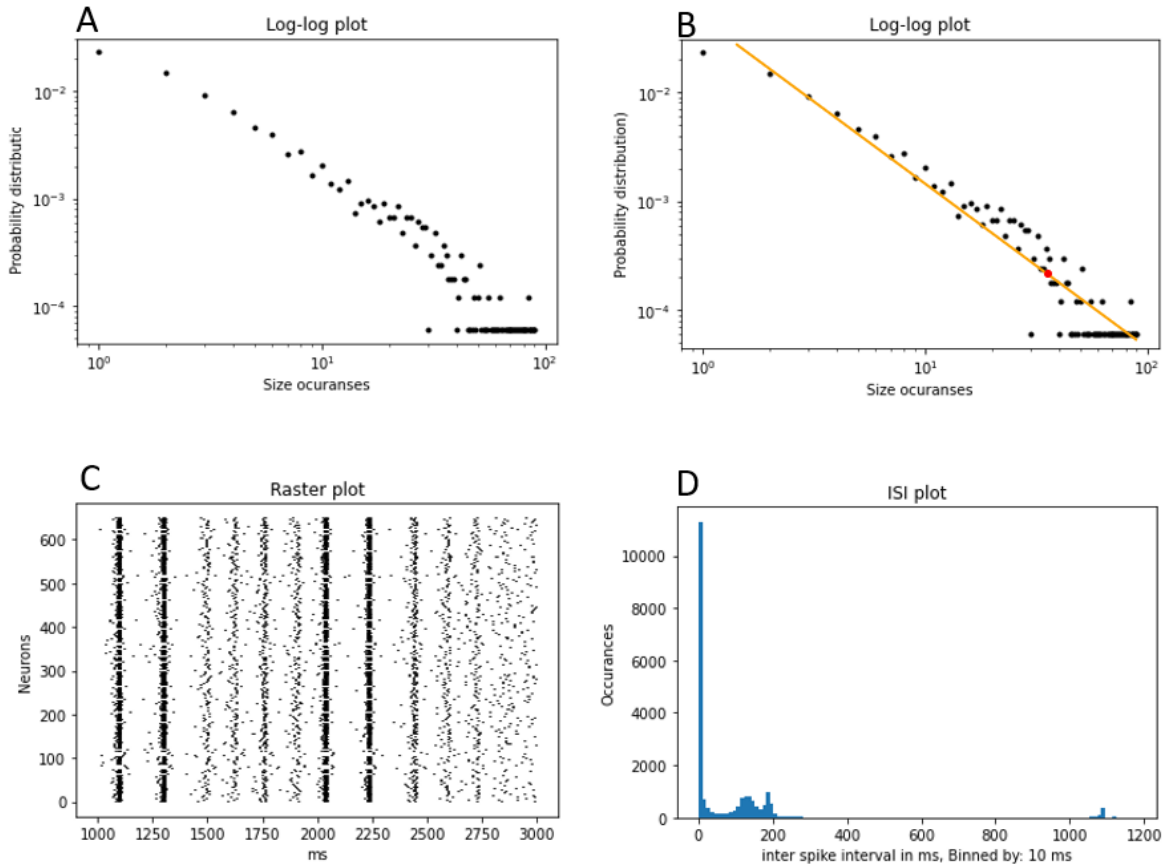


**Figure 11:** *Results from a critical reading in the izhikevich model, A) is the Log-log plot of the probability distribution plotted against the ocuranses of sizes. B) is the same plot as A with a regresion line to calculate the powerlaw exponent. C) is the raster plot of the spikes, and D) is the ISI distribution.*

To make sure these results were not biased, excitatory input was appiled to a fixed position in the izhikevich model with every milisecond. The izhikevich model was shown to be able to produce critical readings despite having fixed “thalamic” input. This meant that the models

internal dynamic and topology cause the critical readings and not just happenstanse from random noise.

Criticality in the models could only be detected with sufficient time for sampling data, and clustering and the the inhibitory population played a big role in the generation of critical readings. Figure 12 shows the critical emergense rates of networks with 70-90% clustering (50% clustering had no occurrences and 60% clustering only had one occurrence and were therefore omitted from the graph). The networks shown were able to create critical readings with the inhibitory populations from 0-5.5%, 8.3-24%, and 21.5-50.2% respectivley.

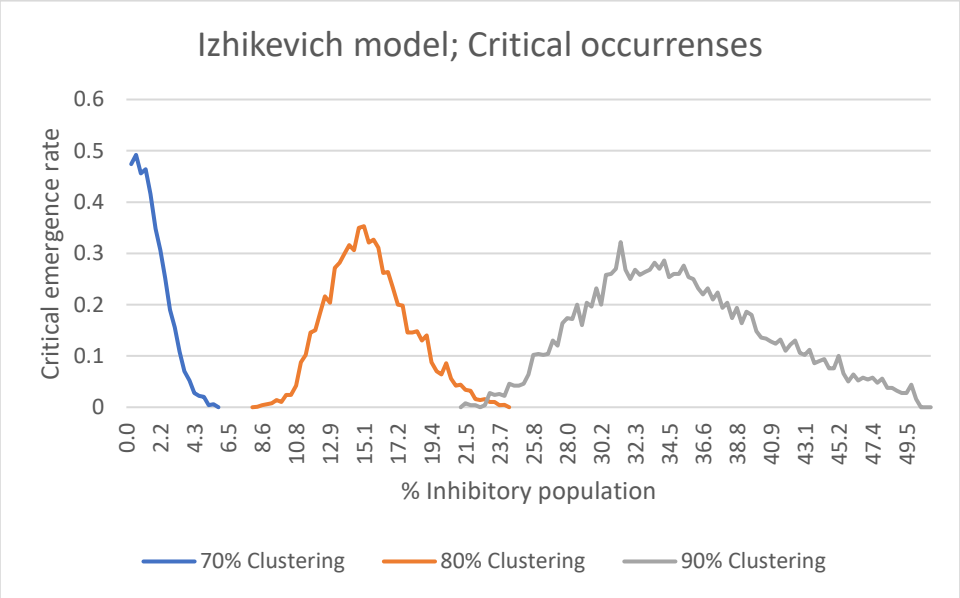


**Figure 12:** *The predicted ratios of inhibitory neurons which enables critical networks to emerge. These predictions were done by the Ichikevitch model on 70-90% clustered networks with Small-world topologies. All itterations had static weights of 0.25, as statics weights of under 0.2 casues the itterations to be sub-critical, while weight over 0.3 caused super critical itterations.*

SW networks with clustering of 80% were chosen as the starting point based on the observations that 70% clustering networks favored no inhibitory neurons, while SW networks with 90% clustering branched over the branching limit of 1±0.1. Ciriticality most commonly emerged in different topologies with an inhibitory population of about 8.3-24% of the total population for networks with clustering of 80%, as shown in Figure 12. Networks which had 80% clustering also yielded the best critical readings, with highest number of critical occurances along side best fit of branching ratios. The firing ratios between exciatatory and inhibitory neurons in networks with 80% clustering is shown in Figure 13.

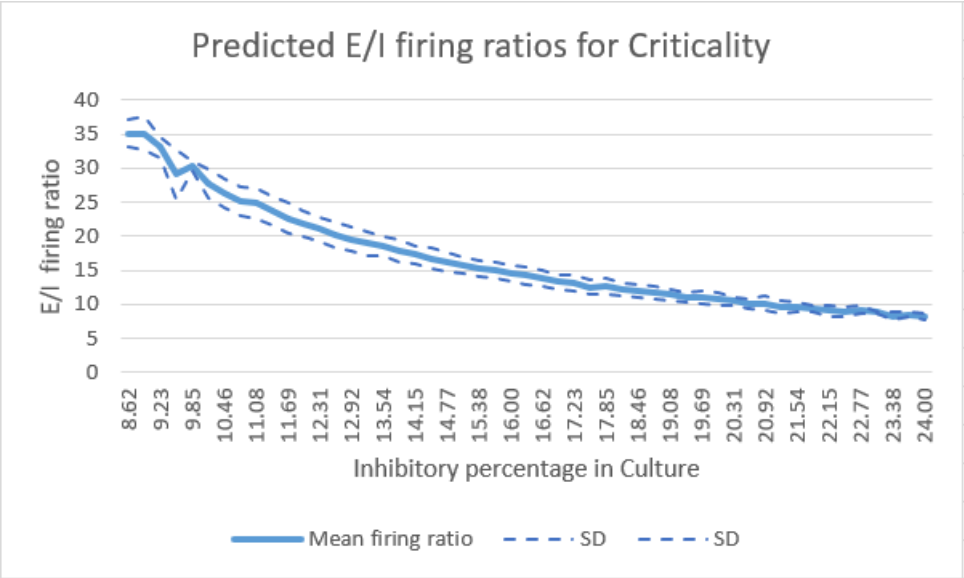


**Figure 13:** *Figure depicts the exitatory to inhibitory firing rates with the standatd deciation for critical readings in netwroks with 8%-24% inhibitory neurons.*

The critical emergence rate was compaired between *in silico* Izikevich neworks with small-world and random topologies with 80% clustering, to see if different topologies altered the rate of critical emergence, this is depicted in Figure 14.

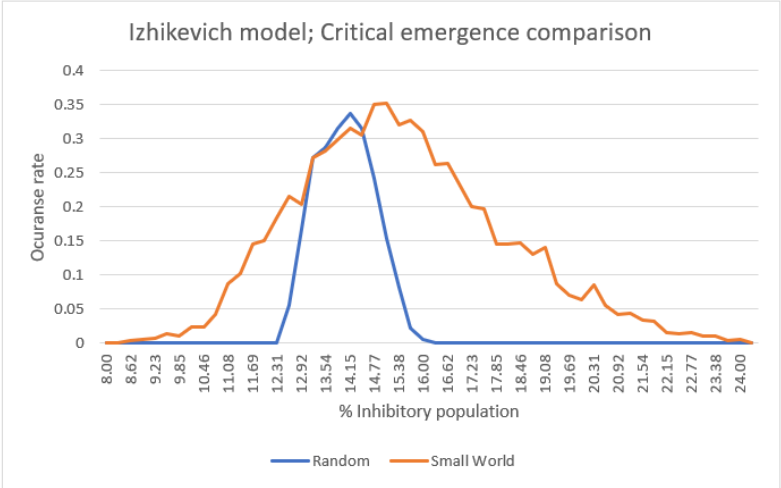


**Figure 14:** *A comparison of the critical emergence rates between a random and a small-world Izhikevixh model. The random topology is shown in blue, while data from the small-world topology is shown in orange.*

The model was also used as a basis to predict the concentrations of GABA and NMDA needed to disrupt critical dynamics in the different inhibitory population networks. Combining the E/I firing ratios from Figure 13 with results of the concentration prediction in Appendix D Fig. D-1, the different inhibitory ratio networks were predicted to fall out of

criticality following treatment with the neurotransmitter concentrations doses presented below in Table 9.

**Table 9:** *Initial dosage of agonists. The dosages were found using the Izhikevich model, by looking at the E/I firing ratio predicted of each culture it was calculated from $GABA_A$ and AMPA receptors drug binding kinetics how much concentration would need to be added to transform the E/I firing ratio of the culture in question into lower and higher E/I firing ratios, this we predict should push the network into a sub- or super-critical state, which also was predicted by the model. The data used is found in appendix D Fig D 1-2 and Table D-3.*

| | Initial Dose trial 1, GABA | Initial Dose trial 1, Glutamate |
|---|---|---|
| Low Inhibitory Culture | 0.1 µM | 18 µM |
| Medium Inhibitory Culture | 0.15 µM | 6 µM |
| High Inhibitory Culture | 0.3 µM | 0.4 µM |

## 3.2 Immunostaining

Figure 15 A shows glutaminergic neurons expressing GABA & AMPA receptors. C shows glutaminergic neurons expressing glutaminergic specific marker TRB-1 & neuron specific marker NeuN. Figure 15 B, and D illustrates the individual pictures taken with different light filters, which composes figure 15 A, and C respectfully. Figure 16 A shows GABAergic neurons expressing GABA & AMPA receptors. While C shows GABAergic neurons expressing intracellular GABA molecules and proteins GFAP for astrocytes. Figure 16 B, D illustrates the individual pictures taken with different light filters, which composes figure 16 A, and C respectfully. In the control tests no protein expression was visible in the primary exclusion assays, as shown in the supplementary results appendix (Appendix D D-4).

The staining results show both neuronal types have inhibitory and excitatory receptors, through the overlap of the orange and green fluorescents in Figure 15 A and 16 A. The excitatory neurons have a glutamatergic specific marker (Fig 15 C, orange fluorescents) and the inhibitory neurons have intracellular GABA, signatures of GABAergic neurons (Fig 16 C, green fluorescents around Hoescht stained nuclei). Additionally, astrocyte marker GFAP were found (Fig 16 C, orange fluorescents), indicating that all cell types were present in the networks of the thesis. In all trials the anti-rabbit antibodies were barely visible, this could be due the light filters of the microscope not fully matching the emission wavelengths from the anti-rabbit secondary antibody.

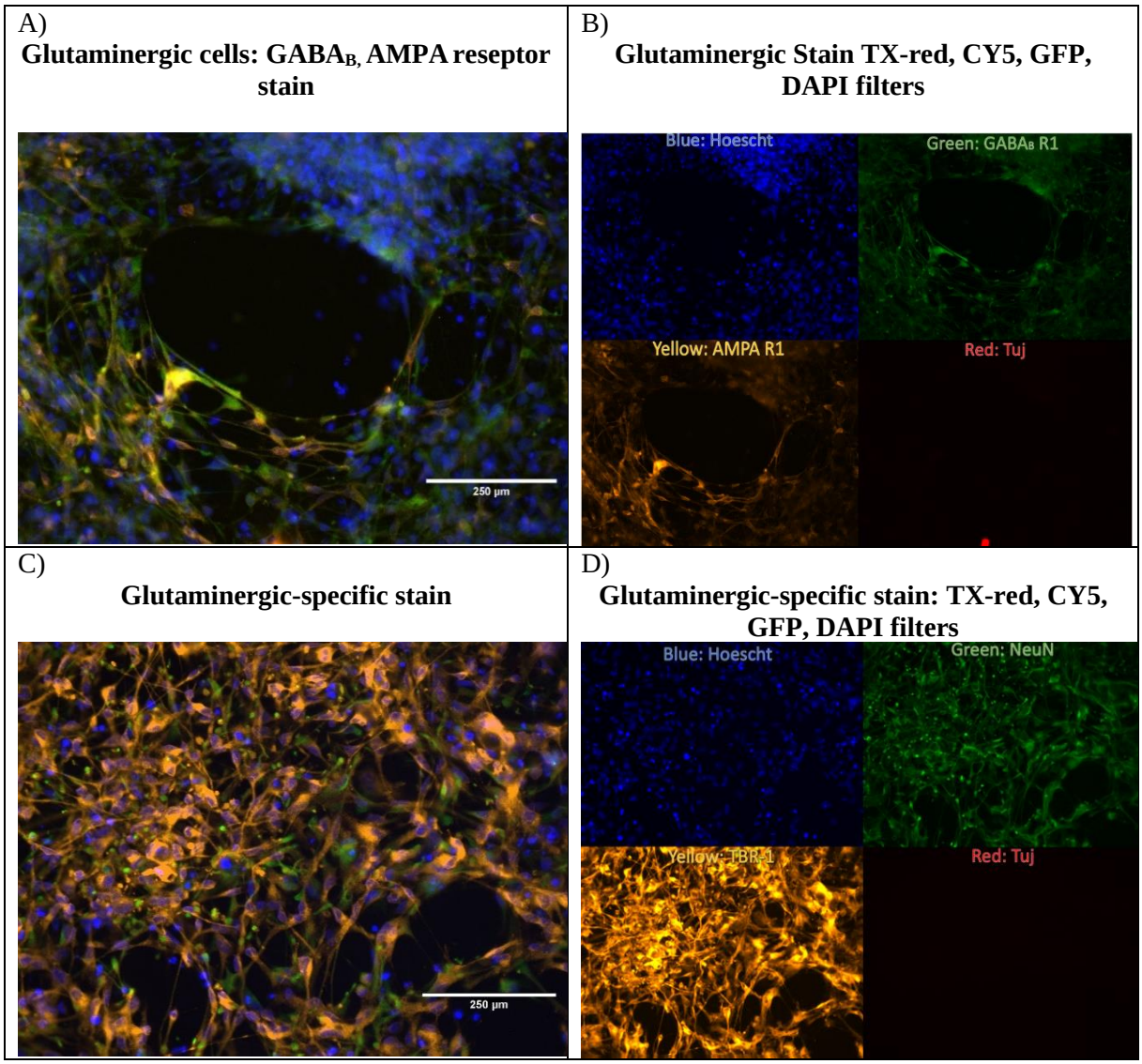


**Figure 15:** S*hows the immunostaining of three sets of three different antibodies all also containing Hoescht in blue: A) Stains for GABA$_B$-R1, AMPA-R1, beta III tubulin on Glutaminergic neurons, in the colors green, orange, red respectfully. B) Illustration of Glutaminergic stains view with* DAPI (blue) ,GFP (Green), CY5 (orange) and TX-red (red) light filters. The DAPI filter is for finding nuclei stains, the GFP filter is for finding *GABA$_B$-R1stains, the CY5 filter is for finding AMPA-R1 stains, and the TX-red filter is for finding beta III tubulin stains. C) Glutaminergic specific stains for NeuN, TBR1, βIII-tubulin on Glutaminergic neurons, in the colors Green, orange. Red respectfully. D) Illustration of Glutaminergic specific stains view with* DAPI (blue) ,GFP (Green), CY5 (orange) and TX-red (red) light filters. The DAPI filter is for finding nuclei stains, the GFP filter is for finding NeuN *stains, the CY5 filter is for finding TBR1 stains, and the TX-red filter is for finding beta III tubulin stains.*

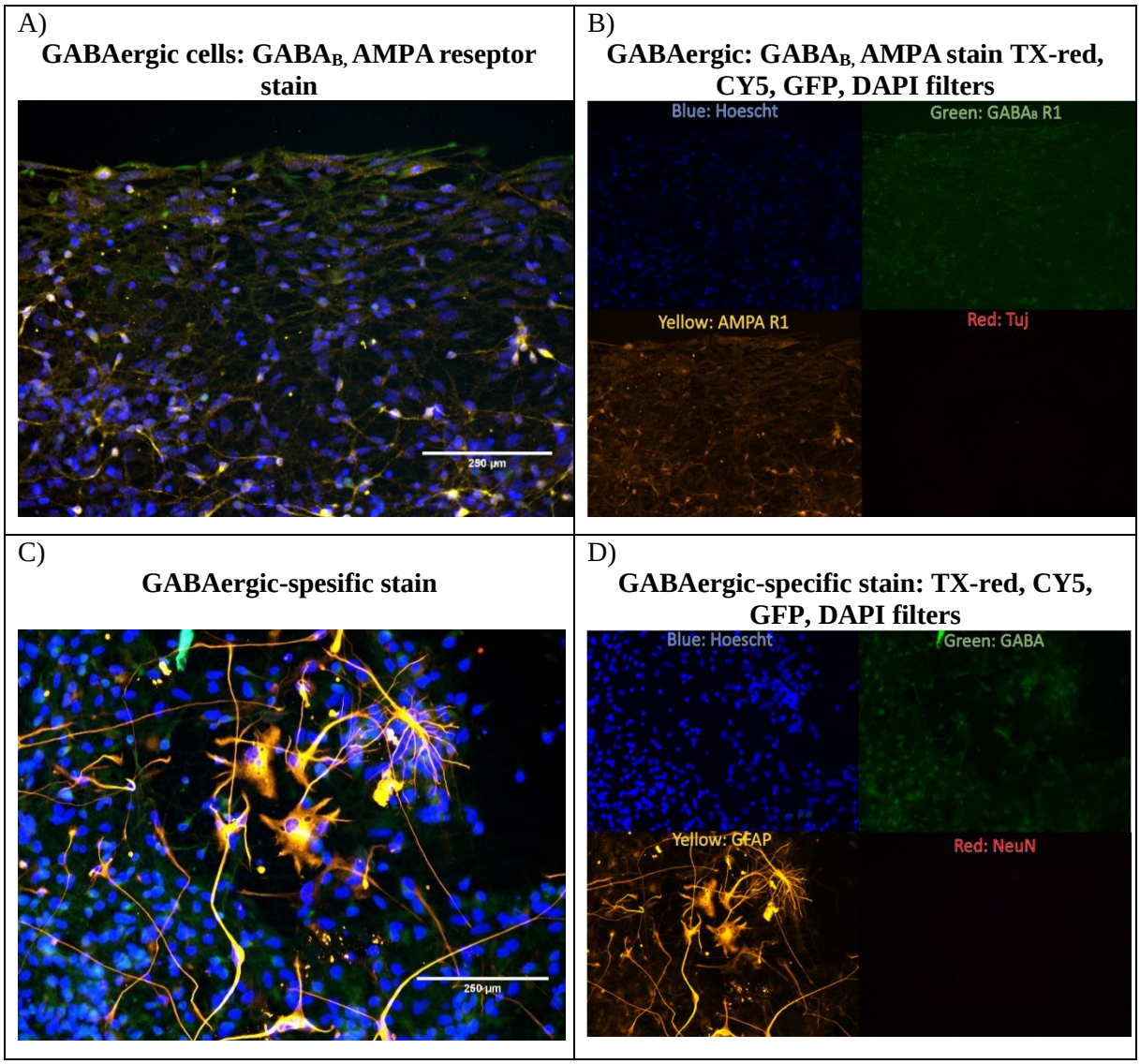


**Figure 16:** *Shows the immunostaining of three sets of three different antibodies all also containing Hoescht in blue: A) Stains for GABA$_B$-R1, AMPA-R1, beta III tubulin (Tuj) on GABAergic neurons, in the colors green, orange, red respectfully. B) Illustration of GABAergic stains viewed with DAPI (blue), GFP (Green), CY5 (orange) and TX-red (red) light filters. The DAPI filter is for finding nuclei stains, the GFP filter is for finding GABA$_B$-R1 stains, the CY5 filter is for finding AMPA-R1 stains, and the TX-red filter is for finding beta III tubulin stains. C) GABAergic specific stains for GABA, GFAP, NeuN on GABAergic neurons, in the colors green, orange, red respectfully. D) Illustration of GABAergic and astrocyte specific stains view with DAPI (blue) ,GFP (Green), CY5 (orange) and TX-red (red) light filters. The DAPI filter is for finding nuclei stains, the GFP filter is for finding GABA stains, the CY5 filter is for finding GFAP, and the TX-red filter is for finding NeuN stains.*

## 3.3 Electrophysiology

The overarching trends for all networks (after the networks were considered mature, 41 DIV) were that the firing trended downwards while both synchrony and NB trended upwards. In addition, the fraction of network burst to synchrony coefficient (NB/S) remained stable from 40 DIV. The 24% inhibitory populations tended to have the largest mean readings in all tested

factors. However, as seen in Table 10 no significant difference between the inhibitory ratio networks were found. Figure 17 shows the results of the electrophysiological analysis of the networks.

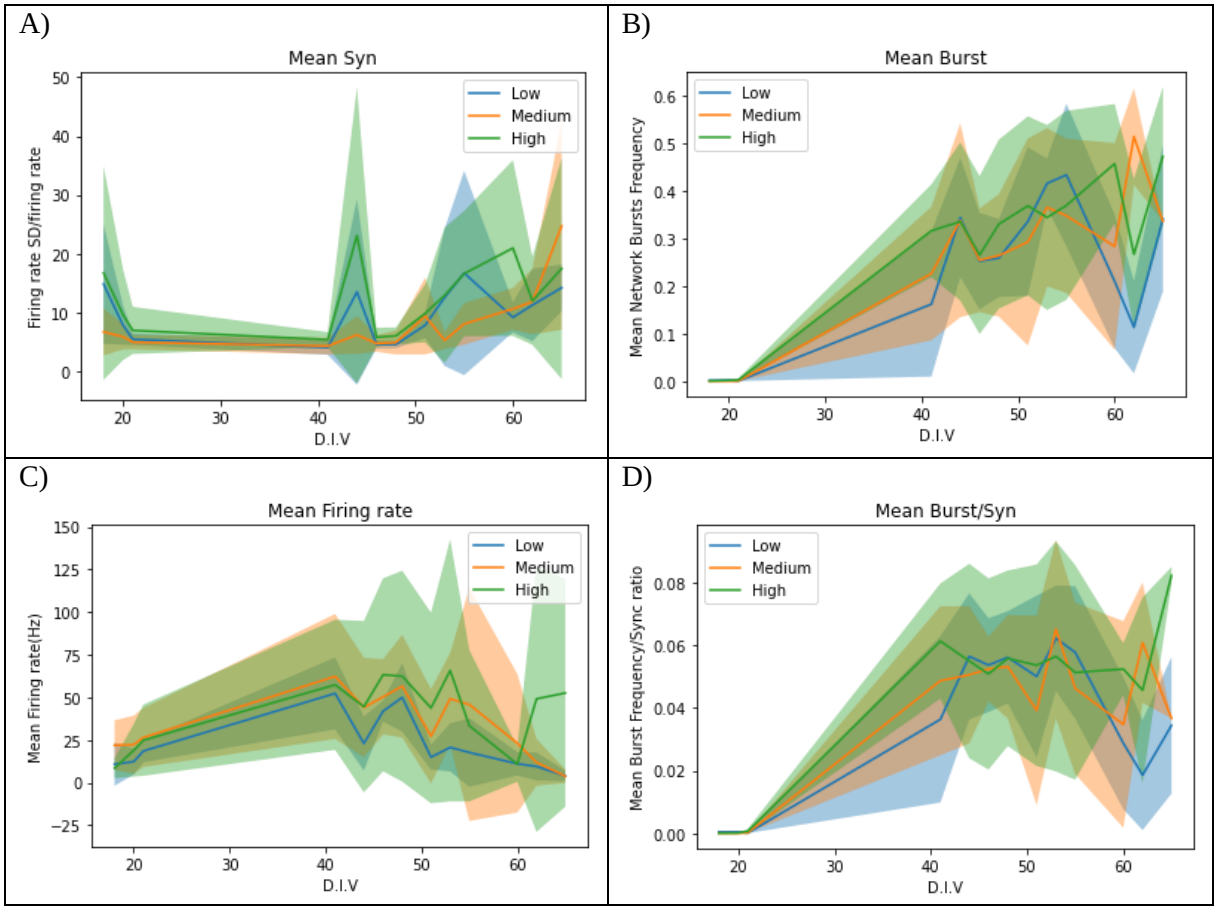


**Figure 17:** *Electrophysiological results. The line represents the mean of the data while the shaded regions is the SD. The Low, medium and high reffers to the networks with inhibitory population percentage 8%,15% and 24% respectfully. A) shows the synchrony coefficient for all networks over 21-65 DIV. B) Network burst frequency for all networks over 21-65 DIV. C) shows the firing rate for all cultures over 21-65 DIV. D) shows the Burst to synchrony ratio(I.e. measurment of B/A) for all networks over 21-65 DIV.*

To check for significant differences between the three network types, a one-way ANOVA test was used to compare the electrophysiological data from the three different inhibitory percentages (from 41 DIV), Table 10 depicts the results. These values come from Appendix D, Figure D-5, which also depicts the mean differences between the samples in the electrophysiological recordings. The total count of active networks of each inhibitory population is shown in appendix D Figure D-11.

**Table 10:** *A table of the statistical differences between the three different inhibitory population networks regarding the electrophysiological measurements. Samples gathered from 41 DIV*

| Parameter | p-value |
|---|---|
| Firing rate | 0.17 |
| Synchrony | 0.28 |
| Frequency of Network bursts | 0.78 |
| Bursts/Synchrony | 0.56 |

MEA recordings were preformed varying from 1-5 days following media changes. To make sure that this did not cause bias in the electrophysiological analysis, the effects of recoding on different days away from media changes was tested with one-way ANOVA, as seen in Table 11. Electrophysiological data from all cultures were compared against the data from all other days away from media change (1 day, 2 days, 3 days, 4 days, and 5 days). These values come from appendix D D-6 which also depicts mean differences between the samples.

**Table 11:** *A table of the statistical significance between days away from last media change and changes in electrophysiological measurements.*

| Parameter | p-value |
|---|---|
| Firing rate | 0.00041 |
| Synchrony | 0.00013 |
| Frequency of Network bursts | 0.092 |
| Bursts/Synchrony | 0.0088 |

These results suggest that the media change affected all electrophysiological measurements except for the NBs. Firing rates and the synchrony coefficient tends to decrease with more days without media change (Appendix D D-6).

## 3.4 Graph theory measurements

Visual inspections of the mature networks showed that the networks mostly developed into condensed clusters, but some had sparse regions of neurons. Typical healthy networks are shown in Figure 18.

The functional topology of the networks was assessed by graph theory. A typical topological MEA network description is depicted in Figure 19. Additional, pictures of stability of functional network over time is shown in appendix D Fig D-7.

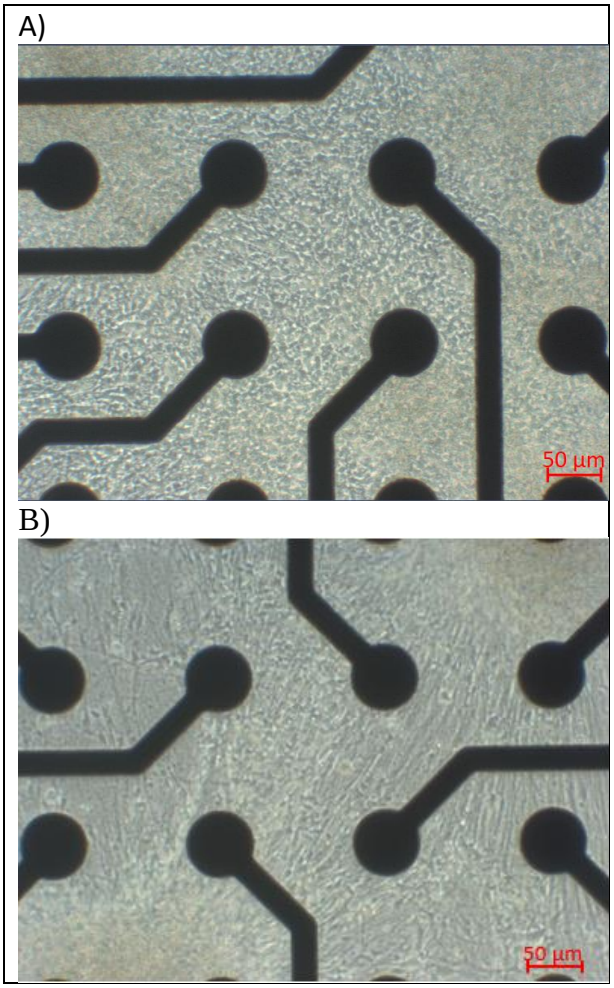


**Figure 18:** A) *mature cells 41 DIV. This picture shows a common mature culture B) mature cells 41 DIV with sparse neural density.*

The *in vitro* networks were classified based on their clustering, average pathlength, mean degree distribution and small-world metric ω, these classifications are shown in Table 12 below. The classification was binary and based on whether the values were in the lower (state 1) or upper (state 2) half of the maximum and minimum measured data. The clustering ranged from 0.3-0.75, the average pathlength varied from 1.6-2 and the mean degree varied from 10-26. All networks had small-worldness metrics counted as having small-world features ($0.5 > \omega > -0.5$), these networks were classified based on which side of the specter the ω value was located on. The two sides of the ω specter were the positive side (state 1) and the negative (state 2), $\omega > 0$ and $\omega < 0$ respectfully.

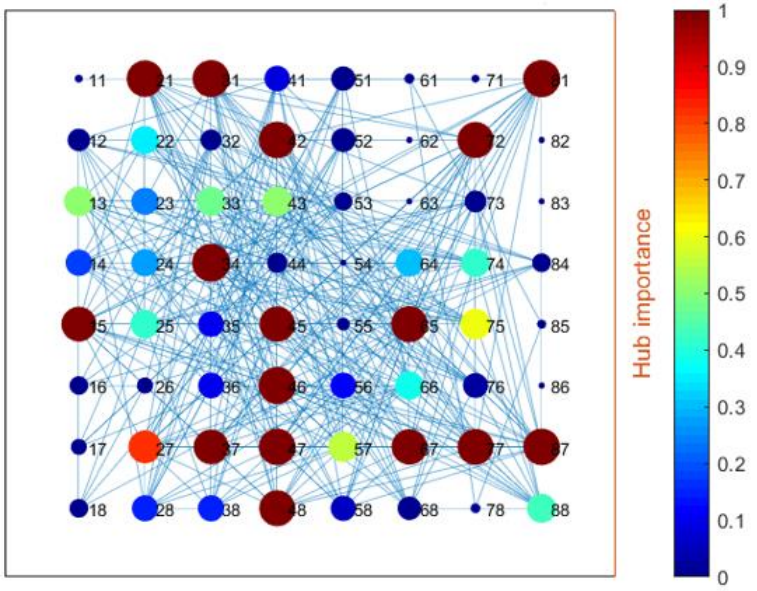


**Figure 19:** *Topological description of networks 08 A2 D.IV 41. This figure is representative of the typical visual, following the topological description.*

**Table 12:** *Classification table. This table shows the binary classification of all networks from the different E/I ratio groups. This data was found from appendix D Table D-8 and D-9, which shows the binary classification for each network. The mean measurements from the in vitro data of the graph theory measurements: clustering, average path, ω, and mean degree is also shown for all different inhibitory populations and collectively for all networks.*

| Collective values | State 1 | State 2 | Mean |
|---|---|---|---|
| Clustering | 14 | 4 | 0.43 |
| Average pathlength | 16 | 2 | 1.74 |
| Small-Worldness | 6 | 12 | -0.088 |
| Mean degree | 14 | 4 | 17 |
| 8% inhibitory population | State 1 | State 2 | Mean |
| Clustering | 6 | 0 | 0.37 |
| Average pathlength | 4 | 2 | 1.76 |
| Small-Worldness | 0 | 6 | 0.01 |
| Mean degree | 6 | 0 | 14.7 |
| 15% inhibitory population | State 1 | State 2 | Mean |
| Clustering | 6 | 0 | 0.44 |
| Average pathlength | 5 | 1 | 1.72 |
| Small-Worldness | 5 | 1 | -0.008 |
| Mean degree | 2 | 4 | 17.6 |
| 24% inhibitory population | State 1 | State 2 | Mean |
| Clustering | 4 | 2 | 0.49 |
| Average pathlength | 5 | 1 | 1.74 |
| Small-Worldness | 3 | 3 | -0.09 |
| Mean degree | 3 | 3 | 18.8 |

Table 12 shows that the clustering and mean degree trended upwards with the increased inhibitory population, the ω trended more towards the negative side of the specter, while the average pathlength seemed to fluctuate between the different inhibitory population networks. Additional data can be seen in Appendix D D-8, which shows the mean values of the graph theory measurement for all networks, and D-9 which shows the binary classification of all networks. Further, the number of strong cross-correlations were found to increase with increasing inhibitory populations (Appendix D D-10). It was found that half of the networks had the same topological description following these binary classifications, and 6 of the remaining 9 networks differed from having this description by one parameter category (Appendix D D-9). This shows that the functional topology was fairly similar for most networks. The most reoccurring graph theory measurements from all the networks are shown in Table 13. These values were used when trying to update the *in silico* model with the *in vitro* data.

**Table 13:** *Median measurements from the in vitro data of the graph theory measurements: clustering, average pathlength, ω, and mean degree.*

| Median | Clustering | Average pathlength | Small-worldness | Mean degree |
|---|---|---|---|---|
| values | 0.41 | 1.73 | 0.01 | 16 |

Additionally, all networks had what were considered small-world features, with low average pathlengths and high clustering, consistent with earlier topological assessments of MEA networks (69, 77, 78). Supplementary data comparing the mean topological measurements of the connection persistence and hard threshold filters is shown in Appendix D Fig D-12.

## *In vitro in silico comparison*

The topology of the *in silico* model and the MEA *in vitro* networks were compared. The *in silico* results were produced from average of the 10 best critical *in silico* networks, while the *in vitro* results for each of the three different inhibitory population networks stem from the average of the measurements collected in the 41-55 DIV period. These results are shown in Table 14.

**Table 14:** *Comparison of graph theory measurements between Izhikevich model data, and in vitro data filtered a hard threshold of 0.25 in correlations.*

| Model | Average clustering | Average Pathlength | Small-world metric ω | Mean Degree |
|---|---|---|---|---|
| *In Silico* | 0.801 | 1.18 | $7.5*10^{-4}$ | 519.81(80%) |
| *In Vitro* (MD < active electrodes) *8% inhibitory networks* | 0.370 | 1.76 | 0.01 | 14.7(23%) |
| *In Vitro* (MD < active electrodes) *15% inhibitory networks* | 0.440 | 1.72 | -0.008 | 17.6(27%) |
| *In Vitro* (MD < active electrodes) *24% inhibitory networks* | 0.490 | 1.74 | -0.09 | 18.8(29%) |

For all the graph theory measurements the *in vitro* results varied from the *in silico* data. The clustering, and the mean degree were lower in the *in vitro* measurements, and the average path length was higher for the *in vitro* measurement. Regarding ω, the two models were similar, however the ω values from the *in vitro* measurements were further away from 0 than the *in silico* model, if only marginally.

## 3.5 Critical analysis

*Critical readings of different inhibitory ratio networks*

The recorded data was analyzed with the critical analysis scripts available from (84) and Figure 20 shows the results for the predicted critical exponent and scaling relationship for all networks over all recordings (except recordings from the perturbation experiment), as well as box plots for the critical exponent and scaling constant with data restricted to the 41-55 DIV period.

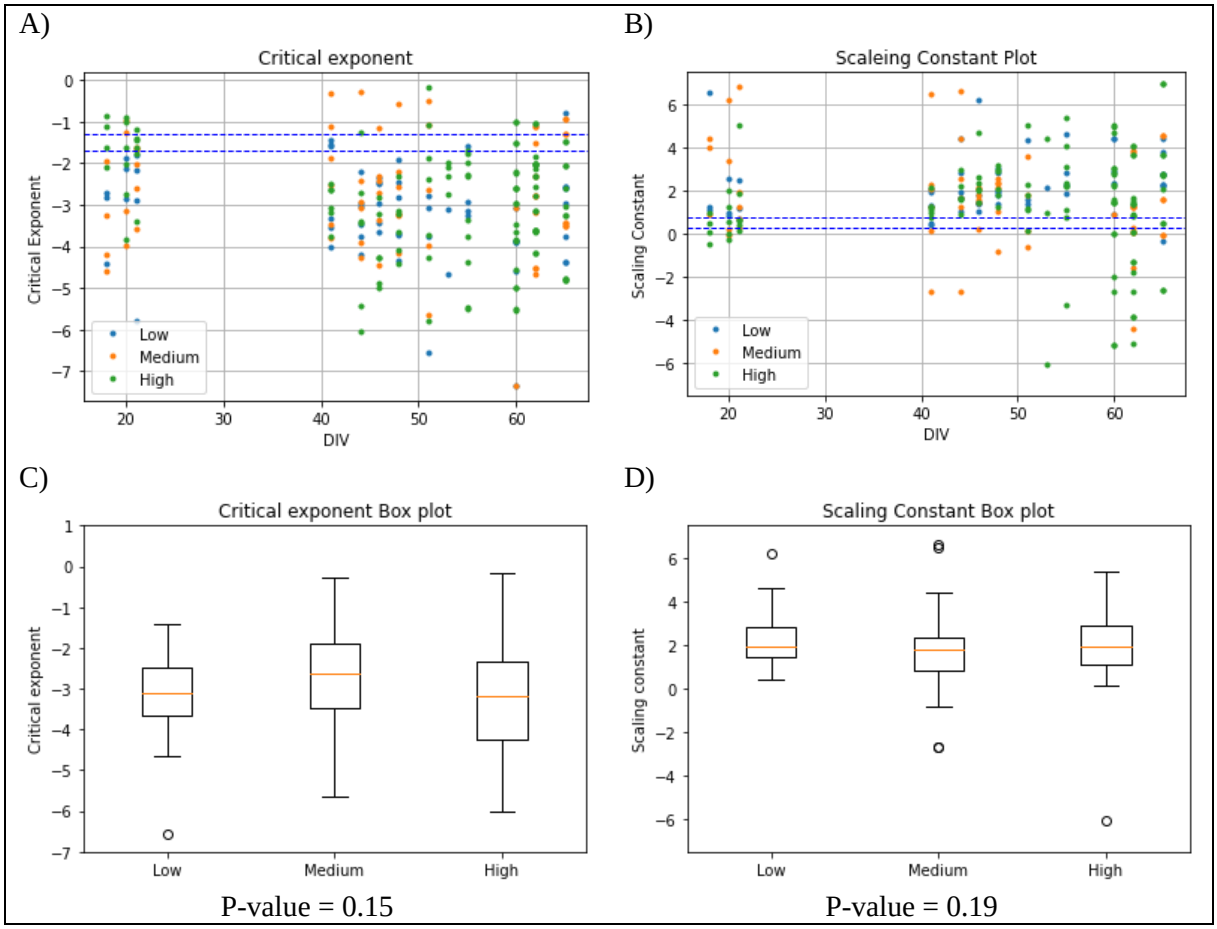


**Figure 20:** *critical and scaling values. A) shows a dot plot of the Critical exponents from 21-65 DIV, data within the blue stippled line is considered critical. B) shows a dot plot of the scaling constant from 21-65 DIV, data within the blue stippled line is considered critical. C) Shows a box plot of the Critical exponents from 41-55 DIV, where the orange line is the median off the critical exponents in the data. The box encases 50% of the data, and 95% of the data is within the whiskers. Additionally, the p-value from an ANOVA test comparing the critical exponent data from the three different inhibitory ratio networks is shown. D) Shows a box plot of the Scaling constant from 41-55 DIV, where the orange line is the median off the scaling constant in the data. The box encases 50% of the data, and 95% of the data is within the whiskers. Additionally, the p-value from an ANOVA test comparing the scaling constant data from the three different inhibitory ratio networks is shown.*

As seen in Figure 20 was no significant differences found between the critical exponent nor the scaling constant data form the different inhibitory percentage networks. Assessing the critical exponent and the scaling constant data, visual inspection of avalanche size

distribution, ISI distribution and avalanche durations (appendix D Fig D-13), it was seen that the networks past 41 DIV were all considered super-critical. Networks up to 20 DIV were found to be sub-critical, and some networks in the period 21 & 41 were considered critical. Additionally, some networks were observed in all critical states throughout the 65 DIV period, appendix D D-14.

When finding the mean critical exponent and scaling constant, single day anomalies (scaling constant data over 50 and under -50) were filtered away, and the unfiltered data is shown in appendix D Figure D-15. The mean results of the critical analysis are shown in Table 15 below.

**Table 15:** *Mean results for critical exponent, scaling constant, ISI, branching, and avalanches for the three different inhibitory population networks from recordings from DIV 41-55.*

| Culture | Mean critical exponent | Mean scaling constant | Mean Branching | ISI (ms) | Mean Avalanche nr |
|---|---|---|---|---|---|
| Low | -2.8±0.5 | 2.2±1.7 | 1.15±0.01 | 57±104 | 10773±5084 |
| Medium | -2.7±1.0 | 1.5±0.6 | 1.14±0.01 | 35±17 | 8468±5249 |
| High | -3.9±2.2 | 2.4±1.1 | 1.14±0.01 | 39±48 | 11818±7750 |

For the different network types the branching ratio trended downwards with increased inhibitory populations. The mean critical exponent showed a slight trend downward, however one must be mindful of the large variance. The other data categories varied between all network types with no clear trends.

The relative occurrence rate for the networks considered critical is shown below in Table 16, furthermore, the networks were also observed in all critical phases (Appendix D Fig D-5).

**Table 16:** *Shows count of networks which fit this thesis criteria for being considered critical, these networks were found between 21 and 41 DIV. Combined had each different inhibitory ratio network 12 recordings from 21 and 41 DIV.*

| | Low inhibitory Networks | Medium inhibitory Networks | High inhibitory Networks |
|---|---|---|---|
| Total Critical readings | 3/12 | 2/12 | 4/12 |

The 8% inhibitory networks had 3/12 and the 15% inhibitory networks had 2/12 critical recordings, however no same network was stable over DIV 21 & 41. 24% inhibitory networks had 4/12 where one network was stable over the period.

## *Critical readings filtered by topology*

The networks which were classified as having the same functional topology (appendix D Table D-9) were compared to see if similar networks provided results with less variance, the results are shown in Table 17. By only comparing networks of the same function topology the variance in the data decreased for most of the data, however some scaling constant values only decreased in mean measurement and increased in variance. However, there were still no significant differences found between the critical exponent or scaling constant of the different inhibitory population networks.

**Table 17:** *Critical exponent and scaling constant of networks classified with the same topology. ANOVA results for critical exponent and scaling constant from networks filtered by topology is also shown.*

| Culture | Mean critical exponent | Mean scaling constant |
|---|---|---|
| Low | - 3.9 ± 2.2 | 3.9 ± 2.2 |
| Medium | - 2.4 ± 0.1 | 1.5 ± 0.1 |
| High | - 3.7 ± 0.7 | 2.8 ± 1.0 |
| p-value | 0.3 | 0.1 |

One-way ANOVA test was used to test if the three inhibitory ratio networks significantly differed in critical exponents or scaling constants when comparing measurements from the same day away from media change, these results are shown in Table 18.

**Table 18:** *Critical exponent and scaling constant of networks classified with the same day away from media change (1 day). ANOVA results for critical exponent and scaling constant from networks filtered by same day away from media change (1 day).*

| Culture | Mean critical exponent | Mean scaling constant |
|---|---|---|
| Low | - 2.7 ± 0.84 | 1.48 ± 1.77 |
| Medium | - 2.4 ± 1.16 | 1.55 ± 1.99 |
| High | - 3.5 ± 0.85 | 1.93 ± 1.05 |
| p-value | 0.8 | 0.04 |

There was found no significant difference between the critical exponents from data taken the same day way from media change, but there was a significant difference between the scaling constants. For this filtering the standard deviation was lower for all critical exponent data and some scaling constant data, compared to the data in Table 19.

## *Shape collapse*

Data collapse was tried on all the data, and most of the data was not collapsible. Figure 21 depicts a typical successful collapse.

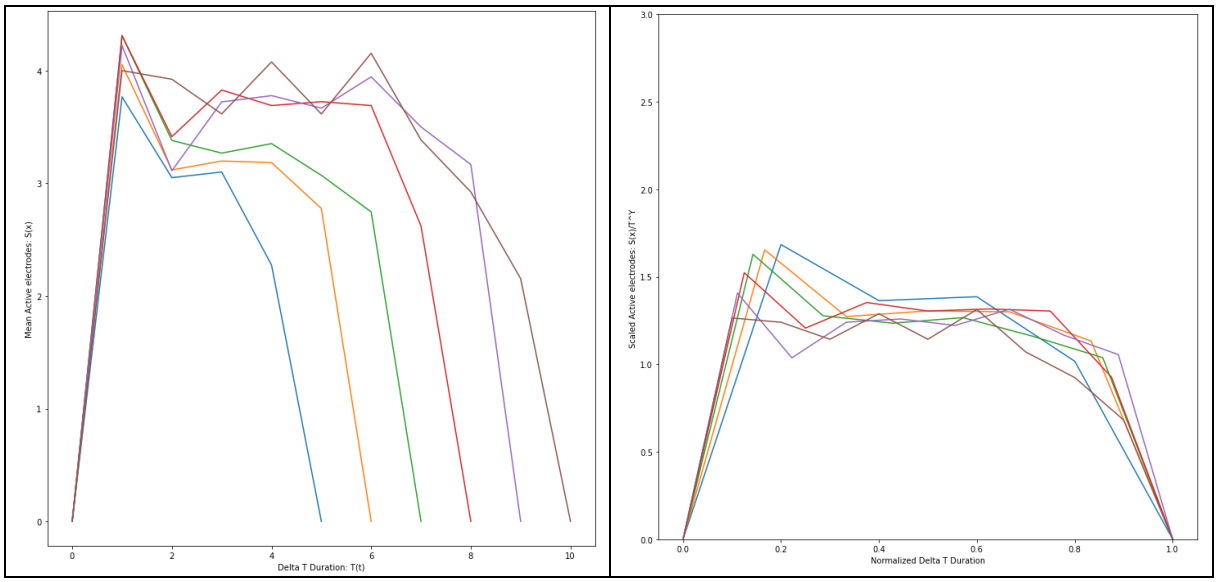


**Figure 21:** Figures *taken from DIV 41 13 A2. Mean shape of raw avalanches of durations 6-11 bin sizes. B) shape collapsed avalanche data (scaled with durations in $\Delta T$ and not T as in Friedman et al.)*

To show that this collapse was possible due to the sequential shape of an avalanche and that any data could not be collapsed, the data from Figure 21 was shuffled and the shuffled data was tried with a collapse. However, the shuffled the data was not collapsible, as seen in Figure 22.

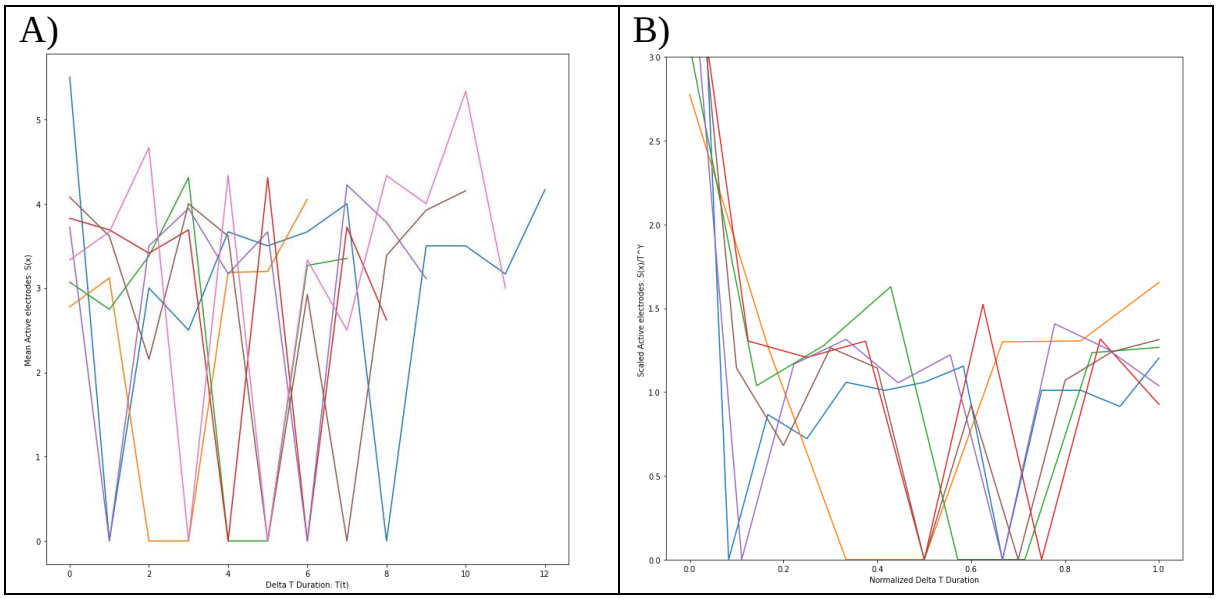


**Figure 22:** *Randomly shuffled data does not collapse. A) Re-shuffled data form Figure 21 A. B) results of collapse analysis on shuffled data from A.*

An example of what was not counted as a successful collapse is depicted in appendix D Figure D-16. Additionally, in appendix D Fig D-16 is a picture of collapsible data from a non-

critical recording. Appendix D Figure D-13 also depicts a full range of avalanche from the non-collapsible data.

## *Factors affecting critical stability*

The effect of media changes on the critical exponent was also tested to determine if recording on different days away from last media change could have caused some of the variance in the data (5 groups were used in this ANOVA test, the groups included 1-5 days away from last media change). Furthermore, critical exponent and scaling constant data from low synchrony value recordings were tested against critical exponent and scaling constant data of high synchrony value recordings to see if they produced differences in critical exponent. This method of testing for statistical differences was also done between critical exponent and scaling constant data in low and high frequencies of NBs and for high and low NB/S recordings. These values are all shown in Table 19, and the values are taken from Appendix D Table D-17.

**Table 19:** *Statistical significance of changes in critical exponent and scaling constant regarding changes in: Last media change, fraction of network bursts, synchrony, and ratio of burst/synchrony.*

| Name | P-Value exponent | P-vale scaling |
|---|---|---|
| Media changes effect on Critical exponent | 0.015 | 0.018 |
| Bursts effect on Critical exponent | 0.5 | 0.26 |
| Synchrony effect on Critical exponent | 0.012 | 0.042 |
| Intermediate Burst/synch level effect on Critical exponent | 0.21 | 0.051 |

Table 19 shows that media change had significant differences between values of both critical exponents and scaling constants on different days away from media change. The critical exponents trended downward with increased days away from media change while the variance of the scaling constant increased with increasing days away from media change (appendix D Table D-13). Significant differences between critical exponent and scaling constant data from days of high and low synchrony values were also found. It was also found that both the mean critical exponent and scaling constant and their SDs were lower on recordings with higher synchrony (appendix D Table D-14).

## 3.6 Perturbation and Resilience

To test if the networks differed in resilience to perturbation the networks were perturbed with GABA and NMDA. Figure 23 shows the effect of these neurotransmitters on firing rate, critical exponents and scaling constant.

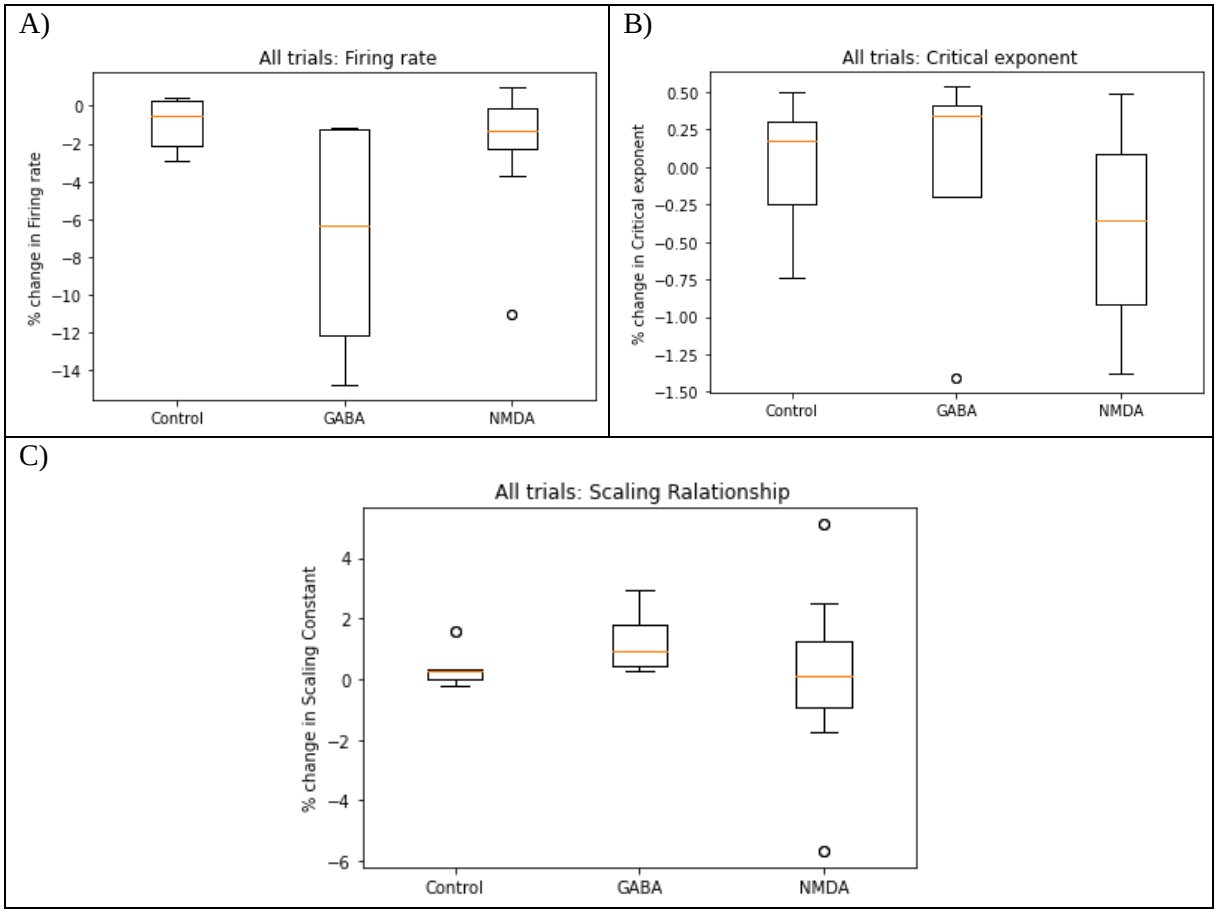


**Figure 23:** *Changes in firing rate from NMDA and GABA addition. A) is the perturbations effect on the firing rates compared to control, B) the perturbations effect on the critical exponent compared to control, C) the perturbations effect on the scaling constant compared to control.*

NMDA (and some GABA trials) caused firing rate changes overlapping with the control, some NMDA trial even causing a decrease in firing rates. Table 20 below shows comparison between all perturbations (where there were enough samples to compare). The networks were compared in two categories as seen in Table 20, percental differences in critical exponent and scaling relationship caused by acute perturbation, and percental differences between measurements before the perturbation and 48 h after the perturbation, to look at self-organization capabilities. GABA and NMDAs effect on the firing rates are shown in appendix D Table D-18, this data insinuates that firing of lower inhibitory networks are less affected by GABA interactions while no clear trends were found for NMDA effect on activity.

**Table 20:** *Perturbation data. The table shows all different trials of the perturbation. The table also shows the percental differences between critical exponent and scaling constant the perturbation, from value before the perturbation against values after perturbation. And the changes in critical exponent and scaling constant before perturbation against values 48h after the perturbation. Trial results without the SD were single trials.*

| Reactant | **Inhibitory Ratio** | **% Change to perturbation: Critical exponent** | **% Change to perturbation: Scaling constant** | **% Change 48h after perturbation: Critical exponent** | **% Change 48h after perturbation: Scaling constant** |
|---|---|---|---|---|---|
| **GABA** | | | | | |
| 0.1µM | 24% | 0.63±0.48 | 3.90±5.90 | 0.05±0.16 | -1.32±1.72 |
| 0.15µM | 8% | 0.06 | 0.10 | 0.15 | 0.62 |
| 0.15µM | 24% | 0.68 | 1.17 | 0.04 | -- |
| 0.2µM | 8% | -0.36 | 1.22 | 0.49 | -3.88 |
| 0.2µM | 15% | -0.58 | -1.50 | -0.03±0.27 | -0.19±0.29 |
| 0.2µM | 24% | -016 | -2.29 | 0.29 | 0.46 |
| **NMDA** | | | | | |
| 6µM | 15% | 0.16 | -4.02 | -0.03±0.79 | -0.84±0.82 |
| 6µM | 24% | -0.58 | -0.84 | -- | -- |
| 18µM | 8% | 0.00±0.65 | 20.77±43.28 | -0.40±0.19 | -0.35±2.29 |
| 18µM | 15% | 0.15±0.58 | -1.70±4.97 | -0.13±0.52 | -1.5±2.01 |
| 18µM | 24% | -0.52 | -0.63 | -0.66 | -0.81 |
| **Control** | | | | | |
| | 8% | 0.98 | 0.45 | -- | -- |
| | 15% | 0.00±0.61 | -0.93±1.29 | 0.60 | -0.26 |
| | 24% | -0.27±0.52 | -0.27±0.74 | 0.64±1.3 | 3.28±5.19 |

From Table 20 the 24% inhibitory networks collectively changed the least 48h after perturbation, compared to 15% and 8% networks. 15% collectively also beat 8% inhibitory networks in the 48h after perturbation categories. Changes to acute perturbation varied more. The data might hint to higher inhibitory populations resisting NMDA better than lower percentage networks, and that lower inhibitory percentage networks resist GABA perturbations better. Curiously, 24% inhibitory networks seem to be more effected by lower GABA concentrations than higher ones. Reviewing the perturbation data, the 8% networks were only consistently better at resisting changes to scaling constant during acute effects of GABA perturbation compared to the other network types, while the 24% was better in re-stabilization 48h after perturbation and in acute changes to NMDA perturbation. Interestingly, 8% and 24% each outperformed the other once in the effect of GABA on acute resilience to critical exponents.

## 3.7 Updated model results

The Izhikevich model was modified to mimic the functional topology found *in vitro*. This modification caused the model to be unable to create critical reading as seen in Table 26.

**Table 21:** *Critical emergence rate in updated model. Shows the mean critical exponent ant the critical occurrence rate.*

| Izhikevich model with *in vitro* topology values | Values |
|---|---|
| Critical exponent | 1.9±0.3 |
| Critical occurrence rate | 0% |

Additionally, the model only showed asynchronous behavior, with long ISI periods. A typical model simulation with the functional *in vitro* topology is depicted in Figure 24.

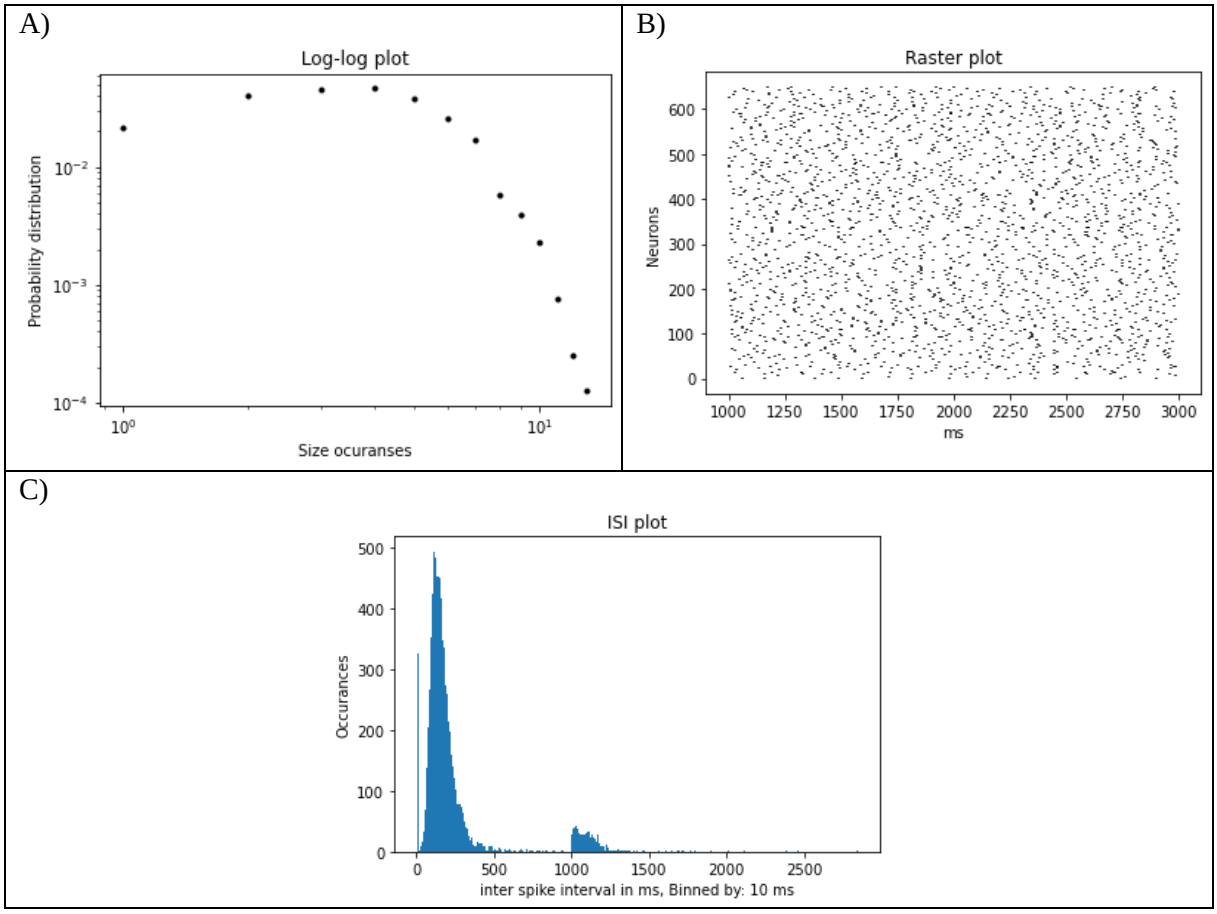


**Figure 24:** *Typical readins from the updated Izhikevich model. A) is the Log-log plot of the probability distribution plotted against the ocuranses of the sizes, B) is the raster plot of the spiking, C) is the ISI distribution.*

However, the network could be tuned to criticality with a change in the total neuronal population of the network (Appendix D Figure D-19). The critical emergence rates of size increased networks are shown in Figure 25:

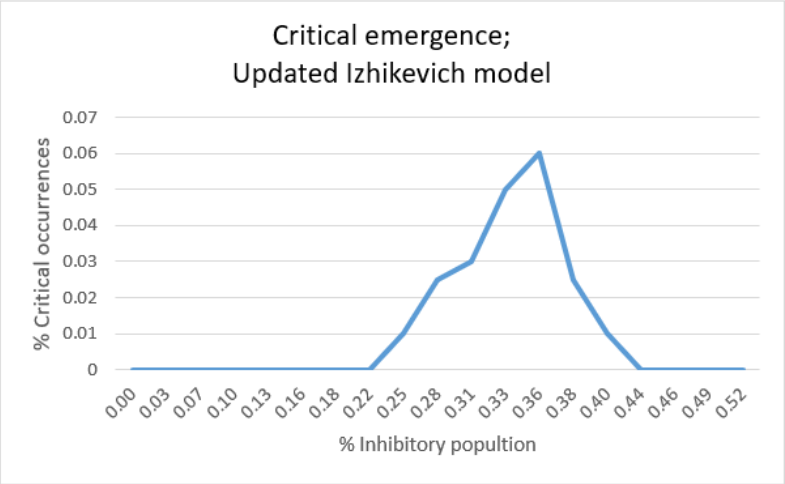


**Figure 25:** *The critical emergence rate of the updated Izhikevich model with 1.5 x increase in total neuronal population*

With the increased size the *in silico* model manage to produce critical reading between 22-45% inhibitory populations, but these occurrence rates were low varying form 1-7%.

# 4. Discussion

## 4.1 Results

### *In silico results*

From the *in silico* model it was predicted that many factors affected critical emergence. The critical readings of the model varied from iteration to iteration, this is probably due to differences in inhibitory placement, suggesting that the placement of the inhibitory nodes plays a large role for critical emergence. Assessing the results from the model, four factors seemed to tune critical occurrence rates: topology (both single parameter and overarching topology), E/I ratio, inhibitory placement, and synaptic weights. From our simple comparison, small-world topology seemed to have a better emergence rate than random topologies, both in highest occurrence rate and area of E/I population ratios in which critical configurations could occur in. This complements previous works stating that small-world topologies are better suited for critical emergence (14, 69). These results supports earlier observations of factors altering occurrence rates (14, 58, 103). In contrast to our model, other models with Small-world topology have found that 20-30% inhibitory neurons promotes criticality, although these results were produced from other firing model type than the Izhikevich firing model and each neuron was connected with only 4 other neurons and plasticity rules were in place (104).

### *Electrophysiological Data*

The different E/I population ratio networks differed in many ways. From the electrophysiological data no significant difference was found between the different inhibitory networks, however, 24% inhibitory networks did have a mean highest rating on all electrophysiological parameters, and 15% had higher mean electrophysiological readings than 8% in every category other than synchrony. The firing rate of the different inhibitory population networks interestingly had a trend of increased firing with increased inhibitory populations, contradictory to what was expected given the effect if GABAergic firing. Put in context with Appendix D Table D-11, it is seen that both 15% and 24% inhibitory networks have 10% more active networks then 8% inhibitory networks. This increase in spiking activity and active networks might suggest that these networks with higher inhibitory populations can be considered healthier, as they show more activity and have higher survivability. Synchronous activity was expected to be different for the different networks, as the interaction of excitatory to inhibitory input have been known to produce synchrony in spiking data (62, 64, 65).

However, increased inhibitory populations caused no significant differences in synchrony measurements. One possibility for this statistical insignificance might be due to the innate self-organizational abilities of neurons. Networks might have organized into similar E/I firing balances despite the different E/I populations, viewing as the different network types all had similar functional topologies. However, examining Appendix D Table D-5, there were trends of increased firing, synchrony and NB activity with increasing inhibitory population.

Following the trend of the other electrophysiological data, it is not unreasonable to speculate that similarly to the *in silico* model, the discrepancy in synchronous activity between 8% and 15% inhibitory networks is reasoned the inhibitory distributions in the networks, and that with more samples, the same increasing trend would occur between 8% and 15% inhibitory networks. These trends further suggest that a significant difference between synchronous activity and NBs in the different inhibitory networks might be found with larger sample sizes.

### *Topology data*

Although the 25% connection persistent method was tried, it was deemed unsuitable for use, as this way of filtering left a larger mean degree than there were active electrodes for some recordings. Because of this, the hard threshold method was used. As previously mentioned, it is hard to predict the right filtering threshold for the adjacency matrix. Visual inspection of the hard threshold showed that the data at least intuitively made sense as, i) mean degree distributions were lower than the number of electrodes active during each recording, and ii) an abundance of fully connected networks was lacking, iii) there were nuances in the remaining data with different electrodes both containing relatively low and high correlations with other electrodes, iv. the correlations are so high that we can be confident that it is an actual functional relationship between electrodes. Still, these results suggest a higher average path length and lower mean degree than predicted by the model. This was not surprising, given that the Izhikevich firing model is fitted with a static small-world topology. Even if the Izhikevich firing model reproduce biological spiking behavior (80), the symmetric equally spaced connections will affect the firing dynamics, which in turn alters the graph theory measurement which cause critical topologies to emerge. This argument is further elaborated on in section 4.2, *in silico model.*

As seen, the different E/I population networks slightly differed in all graph theory measurement with increased clustering, decreased average pathlength, and larger negative values of the $\omega$ metric with increased inhibitory populations. One would expect different

molecular profiles between inhibitory and excitatory neurons, and on this basis is it not unthinkable that these differences in profiles cause the developmental differences, which would be magnified with increased E/I populations. One such factor may be the increased GABA transmitters concentrations, as GABA transmitters have been observed to be a trophic (growth promoting) agent during neural development, promoting synapse and neurite formation (105-107). This may explain why there is a trend of increased clustering, decreased average pathlength and a trend of larger negative $\omega$ values with increased inhibitory populations, as this would cause networks to be more interconnected. It was also seen that networks with more inhibitory populations had more strongly cross-correlated electrodes (Appendix D Fig D-10), this supplements our previous observation that the synchronous activity in a network increases with inhibitory population. The observation of more clustering and increase in cross-correlated data following higher inhibitory populations coincides with the observation of increased bursting activity with the increased inhibitory populations, as synchronous activity in highly interconnected network will lead to NBs.

## *Critical Data*

**Is the observed data critical?**

As of now, we find that there has yet to come any evidence definitely proving that the behavior found originated from critical state dynamics and not other neural mechanisms. Power laws can commonly be observed in nature, independent of phase transitions or critical dynamics. As stated, power laws are indications of a network being in a critical or close to a critical state. However, since power laws can occur from other mechanisms, supplementary evidence is required to prove the presence of critical dynamics (17). In true critical systems one should be able to observe power laws emerging from networks that can undergo phase transitions from sub- to super-critical phases (42, 48), have the predicted power law relationships (size, durations, branching ratios) (1, 9), and scale invariance should be shown with data collapse (9, 17, 37, 38, 92); meaning that one can take the multivariable data and make it into a one variable function through scaling (108).

For some of the networks all the aforementioned factors were found, as seen by networks going through all critical phases during the 65-day period (Appendix D Fig D-14), and through the criticality analysis. This indicates that some networks operate with critical dynamics or to some degree, at least are similar to critical dynamics. It is possible that some networks were in a critical state in the unobserved time span between 21-41 DIV and since transitioned into a different state. This speculation is strengthened by other studies which have

observed critical readings in the 20-35 DIV (1, 48, 61, 78), although this period seems to vary with the experimental specifics (42).

**Variability in data**

Due to self-organization attractor dynamics, critical networks are ever evolving systems. Because of this, some day-to-day variation was expected. However, the data observed might be beyond what would be expected of such daily variations. Many factors seem to cause variability in the data. Recording on different days away from media change had a significant effect on many electrophysiological factors. The ageing is another cause of variation, especially under the developing stages and after 60 DIV. Differences in topology might have been another source of variation, filtering by similar topologies reduced the variance of the scaling constant and critical exponents. However, the variability caused by each individual network might have made it so that the variance would be decreased no matter which networks were excluded as seen in Appendix D Figure D-15.

Furthermore, some unknown event caused sharp increase in synchrony on 44 DIV, on this day the network bursting rate was also increased and firing rates went down. The functional topology was also affected by this event (Appendix D Figure D-7). This might have been caused by human error or seeing as 41 DIV is the last day any networks were considered critical, the 44 DIV results might be a transition period where the networks evolve towards a super-critical state, as every network from 44 DIV and onward were considered super critical. Further research would be required to confirm whether transitions from critical or critical-like states to super-critical states are associated with such dramatic changes in activity.

Networks with different dynamics and topologies seem to produce different attractor points with different ‘proximities’ to criticality (37, 40). As seen in Appendix D Fig D-15 A, C and E (although our data is considered super-critical) different networks of the same E/I population seem to produce different critical exponents. This might be because some networks develop into different attractor states, as illustrated in Figure 26. Hypothetically, this should give different nuances in the computational gain associated with critical dynamics. In fact, this is speculated to be the case with different superficial brain areas; each area operating at different near-critical configurations best suited for their particular function, hence balancing and optimizing their individual appropriate processing properties (13, 55). If indeed

our networks operate with different attractor stats, this could represent another potential source of variance.

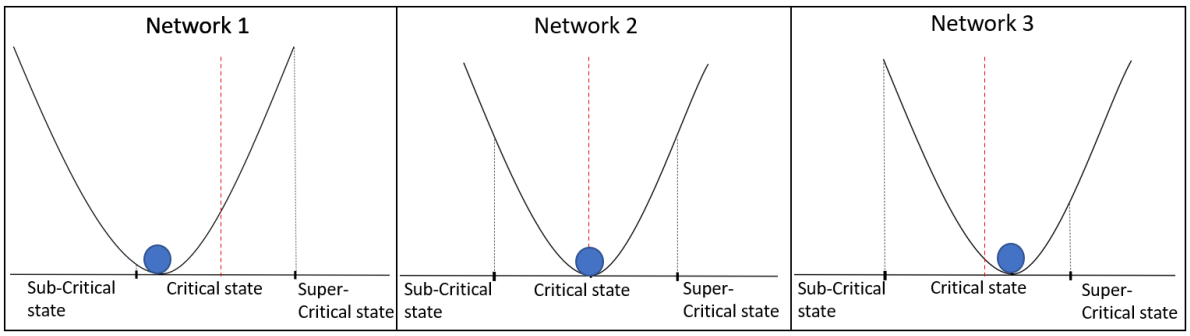


**Figure 26:** *Conceptual illustration of three different networks which have developed different attractor states. The blue ball represents the current dynamics of a system while the black line represents different dynamical system configurations as an attractor filed. The red line represents the system configuration which causes optimal critical dynamics (where gained processing abilities peaks).*

### Factors which might affect critical dynamics

Four factors were tested for associations to critical emergence, but associations were only found for half of them. High levels of NB is observed to be associated with critical dynamics, but low values of NB frequency and NB/S did not cause any significant effects on the critical exponents and scaling constants compared with data with higher NB or NB/S ratio values. Considering, that the critical exponent was calculated from size distribution of avalanches and that our measurement of NB is a direct measurement of the frequency of widespread activity. It was unexpected that the low and high NB levels did not cause differences in critical exponents. This is most likely due to the data being in a super-critical state, which would make the NB and NB/S values tested comparatively low to what would have been observed if the networks were not super-critical state. High levels of NB and Intermediate levels of NB/S might still be associated with critical dynamics and bursting activity might still affect critical dynamics, but this is not captured in the data.

Synchronous activity was shown to alter the critical exponent and scaling constant. Incidentally, the data from the model indicates that criticality emerges at intermediate levels of synchrony to asynchrony (Appendix D Fig D-19), which is similar to other research (41, 57, 61). An independent critical state have been associated with synchronous dynamics (14, 44, 57), this might mean that the observed dynamics from neural networks may be a mix of several critical dynamics, hence why synchronous activity affects the critical dynamics. However, uncovering the nature of critical dynamics is beyond the scope of this thesis.

The media change also looked to affect the critical dynamics. The media used to culture the networks was a combination of metabolites, survival factors, and pH regulating components. As networks goes without a change in media, these components become less available due to depletions from use. Li et al. stated that strong synaptic connections (plastically enforced) are more metabolically taxing to maintain (57). Considering this, it is possible that the changes in critical exponents are due to changes in synaptic weights, as a result of inadequate amounts of energy. However, the media also altered synchrony, which appeared to affect the critical exponent and scaling constant. With the current data it is not possible to distinguish if these are independent events both causing an effect or if only the change in synchrony caused an effect. Synaptic weights, and modulatory mechanisms such as Hebbian plasticity are other factors linked to critical emergence (14, 41, 103), however, none of these are directly explored in this thesis. An alternate explanation might be that changes in pH could cause slight alterations in some proteins and thus affect the critical exponent (109, 110). Still, for all these significant correlations found between the factors explored in this section and changes in critical exponents and scaling constants one must bear in mind that correlations are a far step away from causations.

**Critical emergence and E/I population ratios**

Most of the recorded data was considered super-critical, however, from the recordings considered critical, 24% inhibitory networks had the most critical readings. This data hints to increased inhibitory populations being better for emergence of critical dynamics. However, the nature of why this is remains unknown. Higher inhibitory populations may increase the synchronous activity, which our data suggest affecting critical dynamics though altering the critical exponent and scaling constant. Increased inhibitory populations also change topology, but it did not create networks with the best small-worldness ($\omega$ metric closest to 0). Based on these observations, one possible explanation for increased critical emergence with higher inhibitory populations is that higher inhibitory populations creates different tuning combinations of tuning parameters, based on alterations of many different factors (for instance, topology, firing dynamics, molecular environment), which together is better for critical emergence. Increased inhibitory populations cause complex alterations in many aspects, which cannot be captured as a single parameter.

## *Resilience data*

From the activity of lower inhibitory networks were less affected by GABA then higher percentage ones, and a case can be made for 15% networks resisting changes in firing rates better than 24% networks, both to GABA and low amounts of NMDA (Appendix D Table D-18). This could mean that inhibitory neurons contribute more to maintaining critical dynamics than just balancing firing. If true, this may be related to the topological changes it encourages during development or some innate cellular mechanisms.

From the samples eligible for use we could see a slight trend of 24% inhibitory networks having better resilience than the other networks, being better at restabilizing critical exponent and scaling constant values after perturbation. 24% network were also best in NMDA perturbation trials and even preformed best in one of the GABA perturbation trial. This data hints to larger inhibitory populations promoting better critical resilience. From the functional topology it was seen that some graph theory measurements trended with increased inhibitory populations, hinting to inhibitory population affecting development of networks or the functional topology of networks. Viewed together, larger E/I population ratios may cause better critical resilience both due to the alteration it causes to the functional (and physical) network topology and because of inhibitory firing interactions. One potential way increased inhibitory populations may help a network self-organize back to its attractor state after perturbation can be through the increase of available options for modulating firing dynamics. Critical dynamics can re-stabilize either through synaptic scaling or by balancing enhanced firing of one neuronal type with enhanced firing in the other, causing a counterbalance. For networks with small inhibitory populations, the option of counterbalancing firing may not be an available option in all areas of the network, simply due to the shortage of inhibitory neurons. Further speculating on this, possible ways inhibitory firing interactions may cause acute resilience are: 1. with increased inhibitory neuron populations there is more inhibitory firing, quenching the spreading of signals, which negates incoming excitatory signals. 2. For any percentage of inhibitory neuron populations there will be small concentrations of inhibition which will cause inhibition of inhibitory neurons, leading to a net positive effect on activity in the network. For some networks with high inhibitory populations will the effect of inhibiting the network, and thereby also inhibiting GABAergic neuron activity, lead to a less depressed networks then when the GABAergic neurons operated at full capacity. The GABA concentrations which cause this reaction to inhibition will increase with inhibitory population.

This trend of increased resilience following increased inhibitory populations will presumably have a gaussian distribution with a peak inhibitory population for resilience, as an abundance of inhibitory neurons presumably will cause an affinity towards silencing signals (negative feedback signaling). Regarding this, the trend of increased resilience will probably revert passing certain E/I population levels. However, as stated these results are in need of further exploration, considering that the networks were in a super-critical state which might alter the networks' ability to counteract perturbation and self-organize back to their attractor point.

## *Model improvement*

The topological measurements of the *in vitro* networks were the basis for the model update, which might be why the model could not produce any critical readings. The Izhikevich model operates with single neurons and the *in vitro* measurements were taken from multiple neurons (i.e. there is a difference of scales). The model with the *in vitro* data only managed to create sub-critical readings., however, when increasing the size of the network without changing any other measurements the model produced critical readings. The range of E/I population ratios from which critical networks could emerge over was comparable to the standard model, but the ratios shifted from 8.3-24% to 25-40%. However, the occurrence rates were significantly lower than the initial model. The reason why size differences made the model go from sub-critical to critical may be because the driving force of the network is externally driven, and with smaller networks there is a higher probability for inhibitory nodes to be distributed to ill-favored positions stopping signal propagation. This change in size allow for more distribution configurations and the increased excitability probably made the difference when tuning the networks. Only topology was changed when updating the model, as the model parameters of the Izhikevich model are tuned to best mimic cortical behavior (79), additionally the parameters have no direct biophysical meaning (79), which also means that we have no comparable data to use to update these parameters.

### Comparing model and *in vitro* data

Our model produced different emergence results compared to the *in vitro* data observed. These differences are probably due to the differences between the *in silico* model and biological networks. These differences can be divided into four main camps: extracellular dynamics, neural mechanisms, dynamical topology, and self-organization. The *in silico* models shortcomings regarding extracellular dynamics includes the lack of diffusion associated dynamics, neurotransmitter removal mechanics, environmental differences in

networks such as different local ion concentrations, astrocytes and pan glia networks, and upstate and down states created by local LFPs. Some of the neuronal mechanisms missing in the *in silico* model includes retrograde signaling, plasticity, no metabotropic signaling, back propagation of signals, no dynamics associated with firing depletions and different quantal releases, no auto receptors, nor any signaling pathways leading to changes in the gene expressions or protein profiles.

In contrast to the *in silico* model, biological networks have the ability to dynamically change and move. This gives biological networks the ability to modulate synapses, create new synapses and grow neurites. Furthermore, neuronal critical dynamics are predicted to be, to some degree, an innate behavior, emerging without the need of tuning of single parameters. While our rigid model, in the sense that it is not self-organizing, very much depends on singular parameter tuning when gathering data of critical emergence. These are probably some of the reasons why the model showed differences compared to the *in vitro* data. This is further discussed in 4.2 *in silico model.*

The updated model also showed critical emergence data different from the initial model. Viewing the data of the two models together suggests that critical dynamics can emerge with different E/I ratios depending on different topologies tuned by different synaptic strength. The model data with the *in vitro* parameters predicted higher inhibitory population values for critical emergence than what was tested in the experiments. Interestingly, the range at which we observed critical recordings was outside 15-30% inhibitory population ratios of the human brain (53) and the 10-15% in rodents (72). This might indicate that critical dynamics can emerge in other E/I ratios than what is observed in the brain, human or otherwise (9, 35). As critical dynamics emerge in 8% inhibitory networks and is predicted to occur up to 40% inhibitory populations, over and under the reported observations in the brain, this might give room for emergence of critical dynamics in other areas then just the superficial layers 2/3 of the brain.

## 4.2 Methodology

### *in silico* model

This *in silico* model was chosen for its simplicity, but the model might have been too simple. The model's first weakness is its symmetric connections, this connection regime is considered biologically improbable. Reciprocal connections between neurons are not common, and these are not expected to have the same synaptic strengths. All nodes coupled together in the model

are wired this way. Additionally, the model is a time-step model, where every connected node is spaced an equal distance apart. This causes a loss of temporal dynamics. When the model updates from time step t to t+1, the signal will be transduced at the same time to every other neuron the initial neurons are coupled to. Unlike biological networks all directly coupled neurons are equally spaced away from each other, disregarding the aspect of distance differences. This means that the model is to some degree primed towards synchronic interactions, due to the lacking diversity in temporal signaling.

Synaptic weight distribution were not studied in this model, as it was seen to produce comparable results to static weight distributions. There are no modulatory mechanisms introduced e.g. Hebbian plasticity, as this has been shown to not produce different results from the standard model (81). However, these aspects are still different when compared to biological networks.

## *Cell cultures*

When growing the networks, there were much cell debris as depicted in Figure 27. The cells looked to grow uninhibited, but the potential Damage-associated molecular patterns (DAMPs) in the networks can potentially have slightly altered to ratios of E/I cells or altered the topology under development. But these effects would probably be small as most of the free cytoplasmic spill probably was rinsed away quickly due to the solution change after the centrifugation in the seeding, and the media changes.

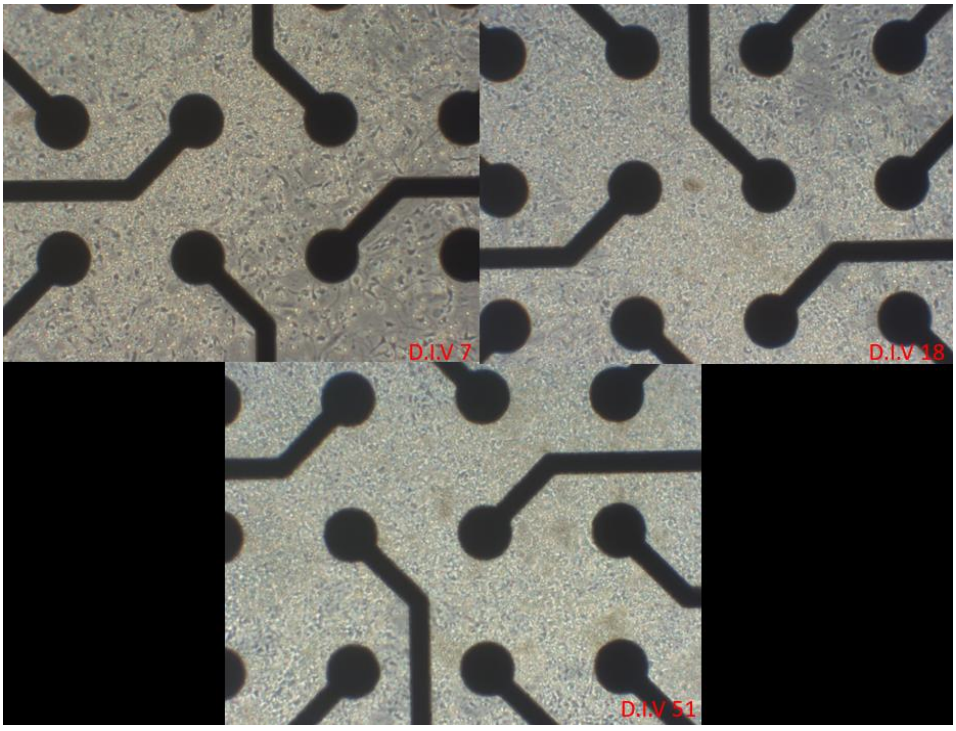


**Figure 27:** *cell debris in networks, networks from 7, 18 and 51 DIV.*

One of the weaknesses of culturing networks on MEAs is the inability to do ICC on the networks. Without any ways to visualize inhibitory neurons in the networks, it was impossible to know if the actual percentage of inhibitory neurons in the mature networks equaled the percentages mixed under cell seeding, nor was it possible to see if the inhibitory neurons clustered to such a degree that the functional effect would be less than the effect of an equivalent inhibitory population brain circuit with a more precise distributions of inhibitory neurons. Ideally the networks in question be examined for the distribution of inhibitory neurons in the networks.

For all their positive attributes, *in vitro* systems also have some limitations compared to *in vivo* models. For instance, we are restricted to 2D topologies compared to the normal 3D topologies of circuits in the brain. Besides, our *in vitro* networks are single compartment networks where all activity is internally driven and the networks develop without any external guidance, meaning that the networks develop with no purpose regarding functional/meaningful processing. These factors mentioned above may cause notable differences in the effects of increased inhibitory populations on electrophysiological data compared to cortical networks.

One of the biggest weaknesses of this thesis is the sample size used for the analysis, as only 6 networks for each inhibitory ratio were tested. This means that the data of each network has a large effect on the analysis. This bias can create results not representative of the true statistics, and it makes it hard to capture subtle effects in the data. Because of this small sample size together with variance in the data it is difficult to draw strong conclusions from the data.

### *Pharmacological Perturbation*

Concerning the methodology and choice of pharmacological reactants, $GABA_A$-receptor and NMDA-receptor agonists were chosen for use over the antagonist for the pharmacological perturbation. As antagonists effectively alter both the E/I ratio in the networks and also the functional topology by blocking the receptors efficiently making the neurons void of function, this would make it even harder to draw out information specific to the different inhibitory population networks.

Many factors might contribute to the indifference between control and NMDA effects on networks. One of the factors that might have made it hard to differentiate neurotransmitters effects compared to the controls, could have been the concentrations used. The dissociation constants used were predicted to be withing a range, the middle value of this range was used for the calculations. This gives a lot of room for modification as small changes in dissociation constants give large variations in predicted concentrations as seen in appendix D Fig D-2. Previous work using NMDA treatment demonstrated noticeable effect with similar concentrations (95) to what was used in this thesis. However, the GABA concentrations might have been too small and any effect may been too subtle to differentiate from control values. Some variance in control and samples might be a result of the way the perturbation agents were added to the networks. To add perturbation agents to the networks, the networks needed to be moved, and networks were not rested after movement to capture perturbation effects. Additionally, the neurotransmitters were diluted in water and added while cold. Preferably, the neurotransmitter should have been diluted in neuronal growth media tempered to 37˚C to prevent inadvertent change in activity as a result of changes in media composition.

The perturbation experiment was also done when the cells were old and started showing increased variance in the behavior of the electrophysiological measurements, this led to much data being filtered away by the standard filtering. Some of the data that made it through the filtering had low firing rates, which made the percentage difference from baseline very sensitive to changes. This may have made changes look bigger than they might have been.

## *Critical analysis*

As mentioned in section 2. *Avalanche detection,* subsampling is an issue when examining critical dynamics as current technology is not able to fully capture the entirety of neural signal transmissions. Although measures such as the MLE is used to make up for the loss of data, there is still room for error. Due to this lack of sampling can we not fully claim to observe avalanches predicted by critical dynamics. Researchers around 2009 observed that exponential distributions described the distribution of their neural data better then power laws (8). This was later shown to be bias formed from too few electrodes used in the electrophysiological recordings (i.e subsampling). Later studies with larger sets of electrodes all showed the predicted power laws in their data sets (15). With every new generation of recording equipment, resolution increases and we can observe an increasingly more complete

signaling transmission. But, even if we cannot fully claim to have observed power law distributions, the data gathered in this thesis can be approximated by power law distributions.

**Analysis Bias**

The way avalanches are detected from spiking data leaves room for some bias to form. In our analysis it is impossible to differentiate if the observed data is part of the same avalanche or if the spatial spreading of signals is a product of two independent avalanches happening at the same time. These are counted as one and the same avalanche in the analysis. Another potential form of bias in the data might come from electrode noise, as seen in appendix D Fig D-13. Electrode noise may arise from damaged electrodes or MEAs not properly connected to the Maestro Pro reader. Oppositely, rough handling of cells or improper maturation can lead to neurons not properly attaching to certain electrodes, which would reduce the activity recorded in some areas, affecting the critical analysis and the calculation of the functional topology.

The choice of bin sizes is a crucial point in the analysis process as too small $\Delta t$ leads to datapoints becoming separated, favoring sub-critical observations, if $\Delta t$ is too big, datapoints will be combined, favoring super-critical observations. By choosing the median of ISI instead of the mean (which is commonly used), the analysis favors a sub-critical regime as the median of our data was smaller than the mean. However, this was done to reduce the effects of outliers, as the mean was large due to long periods of inactivity followed by brief highly active periods. These activity patters are hard to account for, but in such cases can it be argued that the ISI median captures avalanche silence periods better, and thereby separate avalanches better, compared to the mean ISI. Lastly, some data might have been affected by electrode noise, and some avalanches could have prolonged tails due to single, highly active electrodes. Spike trains of the noisy electrodes might thus increase avalanche sizes and durations. This will cause longer avalanches and higher firing rates and thereby ISI, thus affecting the criticality analysis in two ways. However, the extent of these effects is unknown.

## *Topological analysis*

The functional topology of mature networks was observed to change in the 41 to 55 DIV period (appendix D Fig D-7). Since the topology measurements were not stable it was decided

to look at the collective average of the graph theory measurements over this period for each network. Some core nodes of the functional topology stayed the same throughout the maturation, but many nodes differed. Other articles predict that the network maturation should be more stable (68). This might be caused by differences in electrode numbers and dimensions, where bigger electrodes (such as the ones used in this thesis) cover more neurons and hence correlates signal more collectively, which would cause larger variations in the functional topology following the daily changes in firing rates.

**Graph theory measurements**

The threshold set on the correlations in the adjacency matrix was a hard threshold but there exist other ways of doing this. The correlations between electrodes also depend on the firing rate in the network, although the methods used in this thesis did not take this into consideration. Alternately, a link-persistence threshold could be computed for each individual network instead of from the total population data. The filtering greatly influences alle topological measurements, and too low filtering (and certain intermediary filtering) thresholds created fully connected networks. NetworkX graph theory analysis functions treat correlations between electrodes as binary edges, which was an issue as the code used for temporal correlations computes relative correlations, meaning that even inactive electrodes can be correlated with other electrodes. These weak correlations are small in comparison to real correlations, so big thresholds remove most of these non-existing correlations. However, there is no way to tell if all false connections were fully removed. This was the reason why a second threshold was used to make sure that at least the mean degree of electrode connections did not surpass the number of active electrodes from the recording. Additionally, the common input problem may have affected the functional topology. The functional connections with indirect signaling gets partially captured in our connectivity since the correlation between the start and the end is captured, but the common input problem may still cause a bias in representation of correlations between two electrodes.

**Small-world metric omega and bias in SW measures**

Small-world metric ω was chosen over other Small-world measurements methods because NetworkX's current available methods for small-world measurements only include the sigma and ω measurement methods, and the sigma measuring method has been shown to be heavily influenced by the size of the network in question (66). Further, one issue regarding the use of NetworkX functions for computing small-worldness (named omega) was to converted graphs

from external formats to NetworkX's class *graph*. The data class *graph* is the class networkx uses for all its computations, but this data class only works with quadratic matrices in which each row could not consist of only zero values. If the matrix had a row of only zeroes the graph was counted as a disconnected graph and the omega function could not be applied, however, the other graph theory measurements could be still computed from such matrices. To compute ω from none-quadratic matrices, extra rows with values were added to fully square the adjacency matrices before it was converted to the networkx class *graph.* For data in which ω was computable, the ω value was compared to the ω values with and without the aforementioned treatment, the standard deviation was found for differences between these measurements. The values computed this way had an SD of 0.13 compared to none treated data, but all data was still within the limits of being counted as SW networks even with addition of the variation.

# 5. Conclusion

One of the aims of this thesis was to explore E/I balance, and E/I related factors which might affect critical emergence, stability, and resilience. The majority of our data was considered super-critical, still, some networks showed all expected traits of critical dynamics. From these results it is suggested that networks with 24% inhibitory neurons have an increased a chance to develop critical regimes comparatively to networks with lower inhibitory populations.

With increased inhibitory populations firing activity, synchronous activity and bursting activity trend to increase. Additionally, the functional topology does seem to change with increasing inhibitory populations. These factors were also found to be associated with the stability of critical exponents and scaling constants. Our data suggested that the degree of synchronous activity in networks, networks topology, and media changes were the main factors which affected critical stability. Regarding the synchronous activity, it was observed from the model that critical readings appeared in intermediate states of synchrony to asynchrony, similar to previously established data, and variations in the synchronous activity had a significant effect on alterations in the critical exponent and scaling constant. Changes in the bursting activity and NB/S were tested in the context of changes in critical exponent and scaling constant but no significant difference was found, this is believed to be caused by bias from the analysis. Our *in silico* model predicts that SW topologies supports critical emergence better then random topologies, and from our functional topology analysis all networks were considered to have SW features. Furthermore, similar topological descriptions could explain

some of the variance in the data, suggesting that topology also affects critical dynamics. The addition of cell media (metabolites and pH regulating agents) also seemed to have a significant effect on firing rates, synchrony and critical stability. However, since synchrony seemed to affect criticality it is not known if media changes effect on criticality is independent of the changes it causes in synchronous activity.

The *in silico* model predicted that E/I ratios were important for critical emergence, and that criticality emerged at different E/I firing ratios within different E/I population networks, which was supported by the *in vitro* data. Additionally, it was indicated that the placement of the inhibitory neurons, small-world topology, and synaptic weights played an important role in the emergence rates in the model. There were slight trends showing that the 24% inhibitory networks were better at both promoting critical emergence and resilience compared to the networks with lower inhibitory neuron populations. Higher inhibitory networks trended to be better in both self-organizing back to initial values and momentary resistance to NMDA perturbation. In addition, 24% and 15% inhibitory networks produced higher neural activity, and had better survivability then 8% networks, suggesting that networks with moderate inhibitory populations might promote survival better than lower percentages. However, further research is needed.

As expected, critical emergence differed from the model and *in vitro*. The model estimated that criticality could only emerge between 8.3-24% inhibitory networks and 25-40% inhibitory networks, which *in vitro* data indicated to be wrong, as readings considered critical were found in both 8% and 24% inhibitory networks. Neither of these model ranges fully overlapped with the inhibitory estimations in the brain 15-30% (53). However, given the indications of our data it looks like criticality can emerge even outside of these ranges, suggesting that critical dynamics can emerge in more brain regions than just layer 2/3.

Viewed together, our data suggests that criticality can emerge in a large variation of combinations of different tuning parameters. It appears that tuning of single factors alone cannot guarantee that networks develop and stay in critical regimes but increase the chances of these events instead. Higher inhibitory populations seem to tune many factors simultaneously, causing changes in both topology and firing interactions. Collectively these changes may cause more eligible circumstances for emergences of critical dynamics.

# 6. Recommendations and future work

It would be of interest to further confirm these results and grow new networks with the new predicted inhibitory populations to examine if emergence of critical dynamics in these network configurations would be possible. With these new networks the new trial of perturbation should be tried with optogenetics to prevent and avoid the previously encountered complications. It would also be interesting to test same experimental setup utilizing sensory and motor neurons. A 2015 meta study on neuronal proteomics found that the proteome of cortical neurons were fairly similar while neurons from the cerebellum, brainstem and optical nerve (essentially those bordering sensory and motor neurons) deviated the most in protein expression (especially membrane proteins) (111). Repeating the experiment with motor and sensory neurons might give insight on the generality of neurons innate ability to self-organize into critical dynamics, if it holds true for the most varied neuron types one might assume the same holds true for less variable neuronal types.

It would be of interest to further explore the perturbation experiment to see if there are differences in resilience (critical and firing) to perturbation with increasing inhibitory populations. A more detailed test could try to find exact concentrations which push different inhibitory networks out of critical dynamics and compare these concentration ranges. *In vivo* models could even test electrical stimulations of brain areas with different E/I ratios in animal models, to test if some areas are more resilient to perturbation. Furthermore, E/I resilience could be investigated in the context of disease, if e.g. epileptic activity is prone to start in low inhibitory areas compared to high inhibitory areas.

Lastly, from our data it would be meaningful to examine the distributions of inhibitory neurons in different E/I network to see if the cells organize in similar patterns, or if there are reoccurring differences in the wiring distributions.

# References

1. Shew WL, Yang H, Yu S, Roy R, Plenz D. Information capacity and transmission are maximized in balanced cortical networks with neuronal avalanches. Journal of neuroscience. 2011;31(1):55-63.
2. Zimmern V. Why Brain Criticality Is Clinically Relevant: A Scoping Review. Frontiers in Neural Circuits. 2020;14:54.
3. Shew WL, Clawson WP, Pobst J, Karimipanah Y, Wright NC, Wessel R. Adaptation to sensory input tunes visual cortex to criticality. Nature Physics. 2015;11(8):659-63.
4. Shew WL, Yang H, Petermann T, Roy R, Plenz D. Neuronal avalanches imply maximum dynamic range in cortical networks at criticality. Journal of neuroscience. 2009;29(49):15595-600.
5. Gireesh ED, Plenz D. Neuronal avalanches organize as nested theta- and beta/gamma-oscillations during development of cortical layer 2/3. Proc Natl Acad Sci U S A. 2008;105(21):7576-81.
6. Silberberg M. Chemistry: The molecular nature of matter and change, 1.1 The States of Matter In: Neyens L, editor. 7 ed: McGraw-Hill Higher Education; 2014. p. 4-8.
7. Fisher ME. The theory of equilibrium critical phenomena. Reports on progress in physics. 1967;30(2):615.
8. Hoshino O, Kashimori Y, Kambara T. Self-organized phase transitions in neural networks as a neural mechanism of information processing. Proceedings of the National Academy of Sciences. 1996;93(8):3303-7.
9. Beggs JM, Plenz D. Neuronal avalanches in neocortical circuits. Journal of neuroscience. 2003;23(35):11167-77.
10. Beggs JM. The criticality hypothesis: how local cortical networks might optimize information processing. Philosophical Transactions of the Royal Society A: Mathematical, Physical and Engineering Sciences. 2008;366(1864):329-43.
11. Clauset A, Shalizi CR, Newman ME. Power-law distributions in empirical data. SIAM review. 2009;51(4):661-703.
12. Beggs JM, Plenz D. Neuronal avalanches are diverse and precise activity patterns that are stable for many hours in cortical slice cultures. Journal of neuroscience. 2004;24(22):5216-29.
13. Shew WL, Plenz D. The functional benefits of criticality in the cortex. The neuroscientist. 2013;19(1):88-100.
14. Heiney K, Huse Ramstad O, Fiskum V, Christiansen N, Sandvig A, Nichele S, et al. Criticality, connectivity, and neural disorder: A multifaceted approach to neural computation. Frontiers in Computational Neuroscience. 2021;15:7.
15. Langton C. Computation at the edge of chaos: Phase transition and emergent computation. Los Alamos National Lab., NM (USA); 1990.
16. Massobrio P, de Arcangelis L, Pasquale V, Jensen HJ, Plenz D. Criticality as a signature of healthy neural systems. Frontiers in systems neuroscience. 2015;9:22.
17. Beggs JM, Timme N. Being critical of criticality in the brain. Frontiers in physiology. 2012;3:163.
18. Moser EI, Kropff E, Moser MB. Place cells, grid cells, and the brain's spatial representation system. Annu Rev Neurosci. 2008;31:69-89.
19. Hopfield JJ. Neural networks and physical systems with emergent collective computational abilities. Proceedings of the national academy of sciences. 1982;79(8):2554-8.
20. Bak P, Tang C, Wiesenfeld K. Self-organized criticality: An explanation of the 1/f noise. Physical Review Letters. 1987;59(4):381-4.
21. Charles. Cagniard de la Tour. Nouvelle note sur les effets qu'on obtient par l'application simultan´eede la chaleur et de la compression a certains liquides. Phys. 1823(22 ):410-5.
22. Bak P, Tang C, Wiesenfeld K. Self-organized criticality. Physical review A. 1988;38(1):364.
23. Hesse J, Gross T. Self-organized criticality as a fundamental property of neural systems. Frontiers in systems neuroscience. 2014;8:166.

24. Frette V, Christensen K, Malthe-Sørenssen A, Feder J, Jøssang T, Meakin P. Avalanche dynamics in a pile of rice. Nature. 1996;379(6560):49-52.
25. Ricotta C, Arianoutsou M, Dıaz-Delgado R, Duguy B, Lloret F, Maroudi E, et al. Self-organized criticality of wildfires ecologically revisited. Ecological Modelling. 2001;141(1-3):307-11.
26. Bak P, Paczuski M. Complexity, contingency, and criticality. Proceedings of the National Academy of Sciences. 1995;92(15):6689-96.
27. Turcotte DL. Self-organized criticality. Reports on progress in physics. 1999;62(10):1377.
28. Wolfram S. Statistical mechanics of cellular automata. Reviews of modern physics. 1983;55(3):601.
29. Li W, Packard NH, Langton CG. Transition phenomena in cellular automata rule space. Physica D: Nonlinear Phenomena. 1990;45(1-3):77-94.
30. Walker HM. Degrees of freedom. Journal of Educational Psychology. 1940;31(4).
31. Vajapeyam S. Understanding shannon's entropy metric for information. arXiv preprint arXiv:14052061. 2014.
32. Kraskov A, Stögbauer H, Grassberger P. Estimating mutual information. Physical Review E. 2004;69(6):066138.
33. Hahn G, Petermann T, Havenith MN, Yu S, Singer W, Plenz D, et al. Neuronal avalanches in spontaneous activity in vivo. Journal of neurophysiology. 2010;104(6):3312-22.
34. Petermann T, Thiagarajan TC, Lebedev MA, Nicolelis MA, Chialvo DR, Plenz D. Spontaneous cortical activity in awake monkeys composed of neuronal avalanches. Proceedings of the National Academy of Sciences. 2009;106(37):15921-6.
35. Arviv O, Goldstein A, Shriki O. Near-critical dynamics in stimulus-evoked activity of the human brain and its relation to spontaneous resting-state activity. Journal of Neuroscience. 2015;35(41):13927-42.
36. Priesemann V, Valderrama M, Wibral M, Le Van Quyen M. Neuronal avalanches differ from wakefulness to deep sleep–evidence from intracranial depth recordings in humans. PLoS Comput Biol. 2013;9(3):e1002985.
37. Tagliazucchi E, Balenzuela P, Fraiman D, Chialvo DR. Criticality in large-scale brain fMRI dynamics unveiled by a novel point process analysis. Frontiers in physiology. 2012;3:15.
38. Dürschmid S, Reichert C, Walter N, Hinrichs H, Heinze H-J, Ohl FW, et al. Self-regulated critical brain dynamics originate from high frequency-band activity in the MEG. Plos one. 2020;15(6):e0233589.
39. Allegrini P, Paradisi P, Menicucci D, Laurino M, Piarulli A, Gemignani A. Self-organized dynamical complexity in human wakefulness and sleep: different critical brain-activity feedback for conscious and unconscious states. Phys Rev E Stat Nonlin Soft Matter Phys. 2015;92(3):032808-.
40. Meisel C, Storch A, Hallmeyer-Elgner S, Bullmore E, Gross T. Failure of Adaptive Self-Organized Criticality during Epileptic Seizure Attacks. PLOS Computational Biology. 2012;8(1):e1002312.
41. Plenz D. Neuronal avalanches and coherence potentials. The European Physical Journal Special Topics. 2012;205(1):259-301.
42. Tetzlaff C, Okujeni S, Egert U, Wörgötter F, Butz M. Self-organized criticality in developing neuronal networks. PLoS Comput Biol. 2010;6(12):e1001013.
43. Fosque L, Williams-Garcia RV, Beggs JM, Ortiz G. Evidence for quasicritical brain dynamics. arXiv preprint arXiv:201002938. 2020.
44. Di Santo S, Villegas P, Burioni R, Muñoz MA. Landau–Ginzburg theory of cortex dynamics: Scale-free avalanches emerge at the edge of synchronization. Proceedings of the National Academy of Sciences. 2018;115(7):E1356-E65.
45. Wilting J, Priesemann V. 25 years of criticality in neuroscience—established results, open controversies, novel concepts. Current opinion in neurobiology. 2019;58:105-11.
46. Poil S-S, Hardstone R, Mansvelder HD, Linkenkaer-Hansen K. Critical-state dynamics of avalanches and oscillations jointly emerge from balanced excitation/inhibition in neuronal networks. Journal of Neuroscience. 2012;32(29):9817-23.

47. Bellay T, Shew WL, Yu S, Falco-Walter JJ, Plenz D. Selective Participation of Single Cortical Neurons in Neuronal Avalanches. Frontiers in Neural Circuits. 2021;14(90).
48. Yada Y, Mita T, Sanada A, Yano R, Kanzaki R, Bakkum DJ, et al. Development of neural population activity toward self-organized criticality. Neuroscience. 2017;343:55-65.
49. Heiney K, Ramstad OH, Sandvig I, Sandvig A, Nichele S, editors. Assessment and manipulation of the computational capacity of in vitro neuronal networks through criticality in neuronal avalanches. 2019 IEEE Symposium Series on Computational Intelligence (SSCI); 2019: 247-54.
50. Maskery S, Shinbrot T. Deterministic and Stochastic Elements of Axonal Guidance. Annual Review of Biomedical Engineering. 2005;7(1):187-221.
51. Hendry SH, Schwark H, Jones E, Yan J. Numbers and proportions of GABA-immunoreactive neurons in different areas of monkey cerebral cortex. Journal of Neuroscience. 1987;7(5):1503-19.
52. Meng X, Winkowski DE, Kao JP, Kanold PO. Sublaminar subdivision of mouse auditory cortex layer 2/3 based on functional translaminar connections. Journal of Neuroscience. 2017;37(42):10200-14.
53. Markram H, Toledo-Rodriguez M, Wang Y, Gupta A, Silberberg G, Wu C. Interneurons of the neocortical inhibitory system. Nature Reviews Neuroscience. 2004;5(10):793-807.
54. Priesemann V, Wibral M, Valderrama M, Pröpper R, Le Van Quyen M, Geisel T, et al. Spike avalanches in vivo suggest a driven, slightly subcritical brain state. Frontiers in systems neuroscience. 2014;8:108.
55. Thivierge J-P. Scale-free and economical features of functional connectivity in neuronal networks. Physical Review E. 2014;90(2):022721.
56. Finlinson K, Shew WL, Larremore DB, Restrepo JG. Optimal control of excitable systems near criticality. Physical Review Research. 2020;2(3):033450.
57. Li J, Shew WL. Tuning network dynamics from criticality to an asynchronous state. PLOS Computational Biology. 2020;16(9):e1008268.
58. Ma Z, Turrigiano GG, Wessel R, Hengen KB. Cortical circuit dynamics are homeostatically tuned to criticality in vivo. Neuron. 2019;104(4):655-64. e4.
59. Yan J, Wang Y, Ouyang G, Yu T, Li Y, Sik A, et al. Analysis of electrocorticogram in epilepsy patients in terms of criticality. Nonlinear Dynamics. 2016;83(4):1909-17.
60. Stewart CV, Plenz D. Homeostasis of neuronal avalanches during postnatal cortex development in vitro. Journal of neuroscience methods. 2008;169(2):405-16.
61. Pasquale V, Massobrio P, Bologna LL, Chiappalone M, Martinoia S. Self-organization and neuronal avalanches in networks of dissociated cortical neurons. Neuroscience. 2008;153(4):1354-69.
62. Zou X, Wang D-H. On the Phase Relationship between Excitatory and Inhibitory Neurons in Oscillation. Frontiers in Computational Neuroscience. 2016;10(138).
63. Hájos N, Pálhalmi J, Mann EO, Németh B, Paulsen O, Freund TF. Spike timing of distinct types of GABAergic interneuron during hippocampal gamma oscillations in vitro. Journal of Neuroscience. 2004;24(41):9127-37.
64. Börgers C, Kopell N. Effects of Noisy Drive on Rhythms in Networks of Excitatory and Inhibitory Neurons. Neural Computation. 2005;17(3):557-608.
65. Hasenstaub A, Otte S, Callaway E. Cell Type-Specific Control of Spike Timing by Gamma-Band Oscillatory Inhibition. Cerebral Cortex. 2015;26(2):797-806.
66. Telesford QK, Joyce KE, Hayasaka S, Burdette JH, Laurienti PJ. The ubiquity of small-world networks. Brain Connect. 2011;1(5):367-75.
67. Bullmore E, Sporns O. The economy of brain network organization. Nature Reviews Neuroscience. 2012;13(5):336-49.
68. Avena-Koenigsberger A, Misic B, Sporns O. Communication dynamics in complex brain networks. Nature Reviews Neuroscience. 2018;19(1):17-33.
69. Bassett DS, Bullmore E. Small-world brain networks. Neuroscientist. 2006;12(6):512-23.
70. Bassett DS, Bullmore ET. Small-World Brain Networks Revisited. Neuroscientist. 2017;23(5):499-516.

71. Stewart CV, Plenz D. Inverted-U profile of dopamine–NMDA-mediated spontaneous avalanche recurrence in superficial layers of rat prefrontal cortex. Journal of neuroscience. 2006;26(31):8148-59.
72. Tremblay R, Lee S, Rudy B. GABAergic interneurons in the neocortex: from cellular properties to circuits. Neuron. 2016;91(2):260-92.
73. Schubert D, Kötter R, Staiger JF. Mapping functional connectivity in barrel-related columns reveals layer-and cell type-specific microcircuits. Brain Structure and Function. 2007;212(2):107-19.
74. Takata N, Hirase H. Cortical layer 1 and layer 2/3 astrocytes exhibit distinct calcium dynamics in vivo. PLoS One. 2008;3(6):e2525.
75. Opris I, Chang S, Noga BR. What is the evidence for inter-laminar integration in a prefrontal cortical minicolumn? Frontiers in neuroanatomy. 2017;11:116.
76. Lombardi F, Herrmann HJ, Plenz D, De Arcangelis L. On the temporal organization of neuronal avalanches. Frontiers in systems neuroscience. 2014;8:204.
77. Downes JH, Hammond MW, Xydas D, Spencer MC, Becerra VM, Warwick K, et al. Emergence of a Small-World Functional Network in Cultured Neurons. PLOS Computational Biology. 2012;8(5):e1002522.
78. Massobrio P, Pasquale V, Martinoia S. Self-organized criticality in cortical assemblies occurs in concurrent scale-free and small-world networks. Scientific Reports. 2015;5(1):10578.
79. Izhikevich EM. Simple model of spiking neurons. IEEE Transactions on neural networks. 2003;14(6):1569-72.
80. Izhikevich EM. Which model to use for cortical spiking neurons? IEEE transactions on neural networks. 2004;15(5):1063-70.
81. Khoshkhou M, Montakhab A. Spike-Timing-Dependent Plasticity With Axonal Delay Tunes Networks of Izhikevich Neurons to the Edge of Synchronization Transition With Scale-Free Avalanches. Frontiers in systems neuroscience. 2019;13(73).
82. Massobrio P, de Arcangelis L, Pasquale V, Jensen HJ, Plenz D. Criticality as a signature of healthy neural systems: multi-scale experimental and computational studies: Frontiers Media SA; 2015.
83. Hagberg A, Swart P, S Chult D. Exploring network structure, dynamics, and function using NetworkX. Los Alamos National Lab.(LANL), Los Alamos, NM (United States); 2008.
84. Jordbræk SV. SVJ_Maste_Codes. v1.0 ed. Github: Zendo; 2021. DOI: 10.5281/zenodo.4947163, available from: https://doi.org/10.5281/zenodo.4947163
85. Watts DJ, Strogatz SH. Collective dynamics of 'small-world'networks. nature. 1998;393(6684):440-2.
86. Newman ME. The structure and function of complex networks. SIAM review. 2003;45(2):167-256.
87. Thavarajah R, Mudimbaimannar VK, Elizabeth J, Rao UK, Ranganathan K. Chemical and physical basics of routine formaldehyde fixation. J Oral Maxillofac Pathol. 2012;16(3):400-5.
88. Wang XJ. Pacemaker neurons for the theta rhythm and their synchronization in the septohippocampal reciprocal loop. J Neurophysiol. 2002;87(2):889-900.
89. Jacobi S, Moses E. Variability and corresponding amplitude–velocity relation of activity propagating in one-dimensional neural cultures. Journal of neurophysiology. 2007;97(5):3597-606.
90. Bonifazi P, Ruaro ME, Torre V. Statistical properties of information processing in neuronal networks. European Journal of Neuroscience. 2005;22(11):2953-64.
91. Marshall N, Timme NM, Bennett N, Ripp M, Lautzenhiser E, Beggs JM. Analysis of power laws, shape collapses, and neural complexity: new techniques and matlab support via the ncc toolbox. Frontiers in physiology. 2016;7:250.
92. Friedman N, Ito S, Brinkman BA, Shimono M, DeVille RL, Dahmen KA, et al. Universal critical dynamics in high resolution neuronal avalanche data. Physical review letters. 2012;108(20):208102.
93. Hill AV. The possible effects of the aggregation of the molecules of haemoglobin on its dissociation curves. j physiol. 1910;40:4-7.

94. Gesztelyi R, Zsuga J, Kemeny-Beke A, Varga B, Juhasz B, Tosaki A. The Hill equation and the origin of quantitative pharmacology. Archive for History of Exact Sciences. 2012;66(4):427-38.
95. Zhou X, Hollern D, Liao J, Andrechek E, Wang H. NMDA receptor-mediated excitotoxicity depends on the coactivation of synaptic and extrasynaptic receptors. Cell Death Dis. 2013;4(3):e560.
96. Grenier F, Timofeev I, Steriade M. Focal synchronization of ripples (80–200 Hz) in neocortex and their neuronal correlates. Journal of neurophysiology. 2001;86(4):1884-98.
97. Traub RD. Fast Oscillations and Epilepsy. Epilepsy Currents. 2003;3(3):77-9.
98. Petersen Carl CH, Crochet S. Synaptic Computation and Sensory Processing in Neocortical Layer 2/3. Neuron. 2013;78(1):28-48.
99. Kerr JND, Greenberg D, Helmchen F. Imaging input and output of neocortical networks in vivo. Proceedings of the National Academy of Sciences of the United States of America. 2005;102(39):14063.
100. Abeles M, Vaadia E, Bergman H. Firing patterns of single units in the prefrontal cortex and neural network models. Network: Computation in Neural Systems. 1990;1(1):13-25.
101. Hengen Keith B, Lambo Mary E, Van Hooser Stephen D, Katz Donald B, Turrigiano Gina G. Firing Rate Homeostasis in Visual Cortex of Freely Behaving Rodents. Neuron. 2013;80(2):335-42.
102. Yeomans JS. The absolute refractory periods of self-stimulation neurons. Physiology & Behavior. 1979;22(5):911-9.
103. Rubinov M, Sporns O, Thivierge J-P, Breakspear M. Neurobiologically realistic determinants of self-organized criticality in networks of spiking neurons. PLoS Comput Biol. 2011;7(6):e1002038.
104. Lombardi F, Herrmann HJ, de Arcangelis L. Balance of excitation and inhibition determines 1/f power spectrum in neuronal networks. Chaos: An Interdisciplinary Journal of Nonlinear Science. 2017;27(4):047402.
105. Gao XB, van den Pol AN. GABA release from mouse axonal growth cones. J Physiol. 2000;523 Pt 3(Pt 3):629-37.
106. Belhage B, Hansen G, Elster L, Schousboe A. Effects of gamma-aminobutyric acid (GABA) on synaptogenesis and synaptic function. Perspectives on developmental neurobiology. 1998;5(2-3):235-46.
107. Ben-Ari Y, Tseeb V, Raggozzino D, Khazipov R, Gaiarsa J. γ-Aminobutyric acid (GABA): a fast excitatory transmitter which may regulate the development of hippocampal neurones in early postnatal life. Progress in brain research. 1994;102:261-73.
108. Bhattacharjee SM, Seno F. A measure of data collapse for scaling. Journal of Physics A: Mathematical and General. 2001;34(33):6375.
109. Jaspe J, Hagen SJ. Do Protein Molecules Unfold in a Simple Shear Flow? Biophysical Journal. 2006;91(9):3415-24.
110. Gupta P, Khan FI, Roy S, Anwar S, Dahiya R, Alajmi MF, et al. Functional implications of pH-induced conformational changes in the Sphingosine kinase 1. Spectrochimica Acta Part A: Molecular and Biomolecular Spectroscopy. 2020;225:117453.
111. Sharma K, Schmitt S, Bergner CG, Tyanova S, Kannaiyan N, Manrique-Hoyos N, et al. Cell type–and brain region–resolved mouse brain proteome. Nature neuroscience. 2015;18(12):1819-31.
112. Jain KK. Neuropharmacology: Molecular Neuropharmacology: A foundation for clinical neuroscience. Chapter 5: Molecular neuropharmacology A foundation for clinical neuroscience. 23. Trends in Pharmacological Sciences2002. p. 217-62.
113. Cupello A, Hydén H. Binding experiment KD values and physiologically active GABA concentrations: an only apparent contradiction? Int J Neurosci. 1986;30(4):297-301.
114. Herman MA, Jahr CE. Extracellular glutamate concentration in hippocampal slice. J Neurosci. 2007;27(36):9736-41.
115. Hutchinson PJ, O'Connell MT, Al-Rawi PG, Kett-White CR, Gupta AK, Maskell LB, et al. Increases in GABA concentrations during cerebral ischaemia: a microdialysis study of extracellular amino acids. J Neurol Neurosurg Psychiatry. 2002;72(1):99-105.

# Appendices

## Appendix A: Material

For the chemicals used in this thesis, could not all lot numbers be found e.g. for the astrocytes. And the lot number is neither show for chemical for which it is deemed irrelevant.

**Table A-1:** *Laminin coating. This table shows all chemical and procurers of the reactants used in the laminin coating protocol.*

| Name | Producer | Catalogue nr | Lot nr |
|---|---|---|---|
| Polyetylenene (PEI) | PolySciences | 24765-1 | MKCJ3787 |
| HEPES | Gibco | 15630-080 | 1837669 |
| Natural mouse Laminin (NML) | Gibco | 23017-015 | 2175110 |

**Table A-2:** *Astrocytes. This table shows the astrocyte types used in the project and the supplier of these cells.*

| Name | Producer | Catalogue nr | Lot nr |
|---|---|---|---|
| Gibco® Human Astrocyte Kit | Gibco® | N7805-200 | – |
| Gibco® Human Astrocytes | Gibco® | K1884 | – |
| Gibco® Astrocyte Medium | Gibco® | A1261301 | – |
| | | | |
| N-2 Supplement, 100X | Gibco® | 17502-048 | – |
| Dulbecco′s Modified Eagle Medium (DMEM) (1X) | Gibco® | 10569-010 or 31966-021 (Europe only) | – |
| One Shot™ Fetal Bovine Serum (FBS), Certified | Gibco® | 16000-077 | – |

**Table A-3:** *Culturing kit. This table shows the neuron types used in the project and the supplier of these cells.*

| Name | producer | Catalogue nr | Lot Nr |
|---|---|---|---|
| Human Glutamatergic Neurons (BX-0300) | BrainXell | BX-0300 | 200107 |
| Human GABAergic Neurons (BX-0400) | BrainXell | BX-0400 | 190116 |
| Neuron Seeding Supplement at 1000X | BrainXell | BX-0300 | 200625 |
| Neuron Day 4 Supplement at 1000X | BrainXell | BX-0300 | 200522 |

**Table A-4:** *Culturing reactant. This table shows the reactants used in the cell culturing medias.*

| Name | producer | Catalogue nr | Lot nr |
|---|---|---|---|
| DMEM/F12 Medium | Gibco | 21331-020 | 2124980 |
| Neurobasal Medium | Gibco | A24775-01 500ml | 2074220 |
| B27 Supplement | Life Technologies | 17504-044 | – |
| N2 Supplement | Thermo Fisher Scientific | 17502-048 | – |
| GlutaMAX | Ginco | 35050-061 | 2088878 |
| Geltrex | Thermo Fisher Scientific | A1413202 | – |
| BDNF | R D SYSTEMS | 248-BD/CF | VQ2215082 |
| GDNF | R D SYSTEMS | 212-GD/CF | NGG515031 |
| TGF-β1 | Peprotech | 100-21C | 1218209 |
| BrainPhys Medium | STEMCELL Technologies | 05790 | 1000014709 |
| Trypan blue | Sigma-Aldrich | T6146-5G | 02596LH |

**Table A-5** *Immuno-Staining. This table shows the reactants used in the staining protocol and the supplier of these chemical.*

| Name | producer | Catalogue nr | Lot nr |
|---|---|---|---|
| Goat Serum (GS) | Merck | G9023 | – |
| Primary antibody | Table A-6 | Table A-6 | – |
| PBS | Sigma-Aldrich | D8537-500mL | RNBG6525 |
| Triton-X | Sigma-Aldrich | T8787-60ML | SLBH4329V |
| 4 % paraformaldehyde (PFA) | Merck | P6148 | – |
| Secondary antibodies | Table A-6 | Table A-6 | – |
| Hoescht | Merck | 94403 | – |
| Mounting media (Fluoroshield) | abcam | ab104135 | – |
| Kim wipes | Merck | Z188956 | – |
| Distilled H20 | In-house | – | – |

**Table A-6:** *Antibodies. This table depicts the antibodies used in this thesis and their suppliers, catalogue number and binding specificity.*

| Antibody | producer | Catalogue nr | Binding site | Fluorescents |
|---|---|---|---|---|
| Rabbit monoclonal Anti-GluA receptor-1 IgG antibody | abcam | ab109450 | AMPA-R1 | – |
| Mouse polyclonal Anti-GABA B receptor-1 IgG antibody | abcam | ab55051 | GABA β-R1 | – |
| Mouse monoclonal Anti-GABA IgG antibody | abcam | Ab86186 | GABA | – |
| Chicken polyclonal Anti-Beta III tubulin IgG antibody | abcam | Ab41489 | βIII-tubulin | – |
| Mouse monoclonal Anti-NeuN IgG antibody | abcam | Ab104224 | NeuN | – |
| Rabbit polyclonal Anti-GFAP IgG antibody | abcam | Ab7260 | GFAP | – |
| Chicken monoclonal Anti-NeuN IgY antibody | abcam | Ab134014 | NeuN | – |
| Rabbit monoclonal Anti-TBR IgG antibody | abcam | Ab183032 | TBR-1 | – |
| Goat polyclonal Anti-mouse IgG antibody | Thermo Fisher Scientific | A-11001 | Mouse- IgG antibody | 488 nm |
| Goat Anti-chicken IgY antibody | Thermo Fisher Scientific | A-11040 | Chicken- IgG antibody | 546 nm |
| Goat polyclonal Anti-rabbit IgG antibody | Thermo Fisher Scientific | A-21244 | Rabbit- IgG antibody | 647 nm |

**Table A-7:** *Neurotransmitters. Shows the neurotransmitters, catalogue nr and suppliers used for the pharmacological perturbation*

| Name | Producer | Catalogue nr |
|---|---|---|
| GABA | Sigma-Aldrich | A2129-10G |
| NMDA | Sigma-Aldrich | M3262-25MG |

# Appendix B: Media formulas

| Component | 100 mL complete medium | 500 mL complete medium |
|---|---|---|
| DMEM | 89 mL | 445 mL |
| N-2 | 1 mL | 5 mL |
| FBS | 10 mL | 50 mL |
| *Optional:* EGF | 2 µg | 10 µg |

**Figure B-1:** *Astrocyte media. This figure shows the components and mixing ratios of the solutions used in the astrocyte seeding media.*

Culturing media

| | | Component | Stock Conc. | Final Conc. | Volume |
|---|---|---|---|---|---|
| Seeding Medium | 1 | DMEM/F12 Medium | 1X | 0.5X | 9.6 mL |
| | 2 | Neurobasal Medium | 1X | 0.5X | 9.6 mL |
| | 3 | B27 Supplement | 50X | 1X | 400 µL |
| | 4 | N2 Supplement | 100X | 1X | 200 µL |
| | 5 | GlutaMAX | 200 mM | 0.5 mM | 50 µL |
| | 6 | BDNF | 10 µg/mL | 10 ng/mL | 20 µL |
| | 7 | GDNF | 10 µg/mL | 10 ng/mL | 20 µL |
| | 8 | TGF-β1 | 1 µg/mL | 1 ng/mL | 20 µL |
| | 9 | Seeding Supplement | 1000X | 1X | 20 µL |
| | 10 | Geltrex | 15 mg/mL | 15 µg /mL | 200 µL (of 1:10) |

**Figure B-2:** *Seeding medium. This figure shows the components and mixing ratios of the solutions used in the seeding media*

| | | Component | Stock Conc. | Final Conc. | Volume |
|---|---|---|---|---|---|
| Day 4 Medium | 1 | DMEM/F12 Medium | 1X | 0.5X | 9.6 mL |
| | 2 | Neurobasal Medium | 1X | 0.5X | 9.6 mL |
| | 3 | B27 Supplement | 50X | 1X | 400 µL |
| | 4 | N2 Supplement | 100X | 1X | 200 µL |
| | 5 | GlutaMAX | 200 mM | 0.5 mM | 50 µL |
| | 6 | BDNF | 10 µg/mL | 10 ng/mL | 20 µL |
| | 7 | GDNF | 10 µg/mL | 10 ng/mL | 20 µL |
| | 8 | TGF-β1 | 1 µg/mL | 1 ng/mL | 20 µL |
| | 9 | Day 4 Supplement | 1000X | 1X | 20 µL |

**Figure B-3:** *Day 4 medium. This figure shows the components and mixing ratios of the solutions used in the day 4 media.*

| | | Component | Stock Conc. | Final Conc. | Volume |
|---|---|---|---|---|---|
| Day 10 Medium and Onwards | 1 | BrainPhys | 1X | 0.5X | 19.3 mL |
| | 2 | B27 Supplement | 50X | 1X | 400 µL |
| | 3 | N2 Supplement | 100X | 1X | 200 µL |
| | 4 | GlutaMAX | 200 mM | 0.5 mM | 50 µL |
| | 5 | BDNF | 10 µg/mL | 10 ng/mL | 20 µL |
| | 6 | GDNF | 10 µg/mL | 10 ng/mL | 20 µL |
| | 7 | TGF-β1 | 1 µg/mL | 1 ng/mL | 20 µL |

**Figure B-4:** *Day 10 and onward medium. This figure shows the components and mixing ratios of the solutions used in the day 10 media.*

# Appendix C: Protocols

## Axion multiwell MEAs, PEI + Laminin coating

Vegard Fiskum, 27.01.2020

Axion MEA plates arrive in sterile packaging and new plates do not require any disinfection, cleaning or treatment prior to coating. If you are reusing plates, first follow the Axion Biosystems "Cleaning Protocol for Microelectrode Arrays (MEAs)". This protocol follows the following timeline:

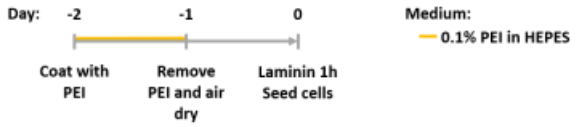


1. Cover the surface of each well with 0.05% polyethylenimine (PEI) diluted in HEPES (both Sigma-Aldrich). 48-well plates: 70µL per well, 6-well plates: 210µL per well. Fill the water reservoirs to prevent evaporation and leave the plates in the incubator (37$^0$C, 5% $CO_2$) overnight.
2. The next day, remove the PEI and rinse 4 times with distilled water. Remove the water, including in the water reservoirs and leave the plates to air dry overnight. If left in the laminar flow hood, cover them with aluminium foil as the plates must not to be exposed to UV light.
3. The next day, coat with laminin diluted in PBS. For example, Natural Mouse Laminin at 20 µg/mL (ThermoFisher) for 1 hour. 48-well plates: 70µL per well, 6-well plates: 210µL per well.
4. Remove the laminin and plate cells directly without washing. It is recommended to seed the cells in small volumes carefully seeded within the reference electrodes, see the figure below. When using astrocytes in co-culture, it is important that these are not seeded in advance but are mixed with neurons to obtain the desired ratio and then seeding the mixed cell solution.
5. Leave the plates in the incubator for 1 hour to allow the cells to begin to attach. Then, fill the wells to their final volume. 48-well plates: 300µL per well, 6-well plates: 1000µL per well.

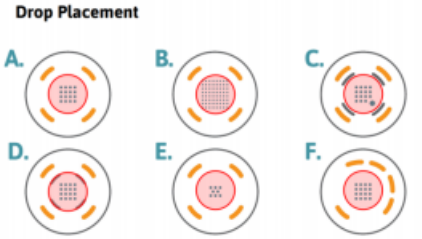


**Figure 1: Drop Placement Diagram**
The layouts above represent the bottom surfaces of wells in (A) a 48-well MEA, (B) a 6- or 12-well MEA, (C) a 24-well MEA or 48 well E-Stim+ MEA, (D) a 48-well AccuSpot MEA, (E) a 96-well MEA, and (F) a 48-well CytoView MEA. The number of electrodes per well is different across the plate formats, however the drop placement is the same, with the drop (red circle) centered on the recording electrodes and staying within the ground electrodes. On plate types with the addition of the stim-paddle in the lower right corner of the array, it is important to make sure the droplet covers this feature. The droplet may need to be manipulated after placement of the pre-treatment to ensure stim-paddle coverage.

**Fig C-1:** *in-house protocol of laminin coating of MEA plates.*

The second part of appendix C-2 is continued below

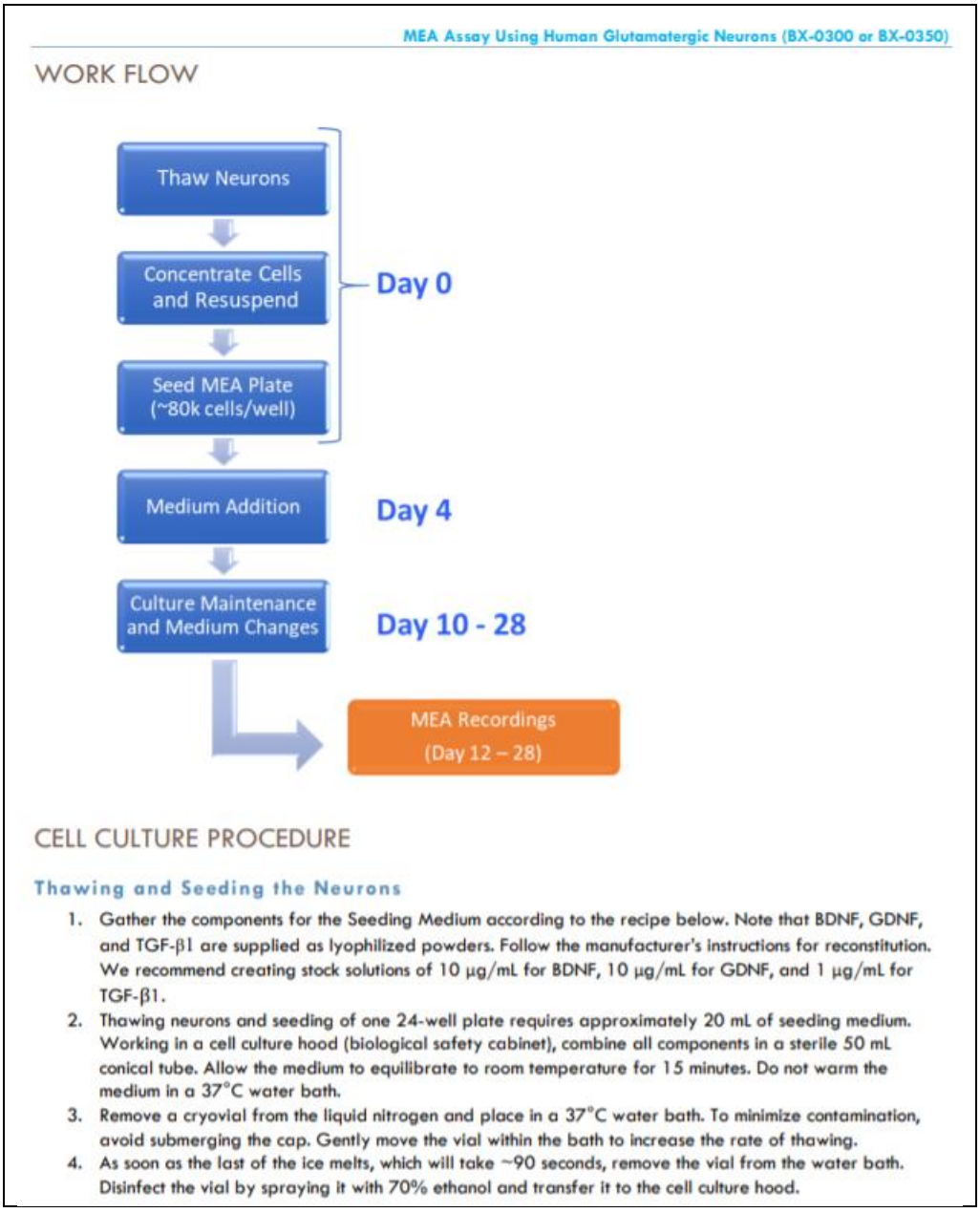

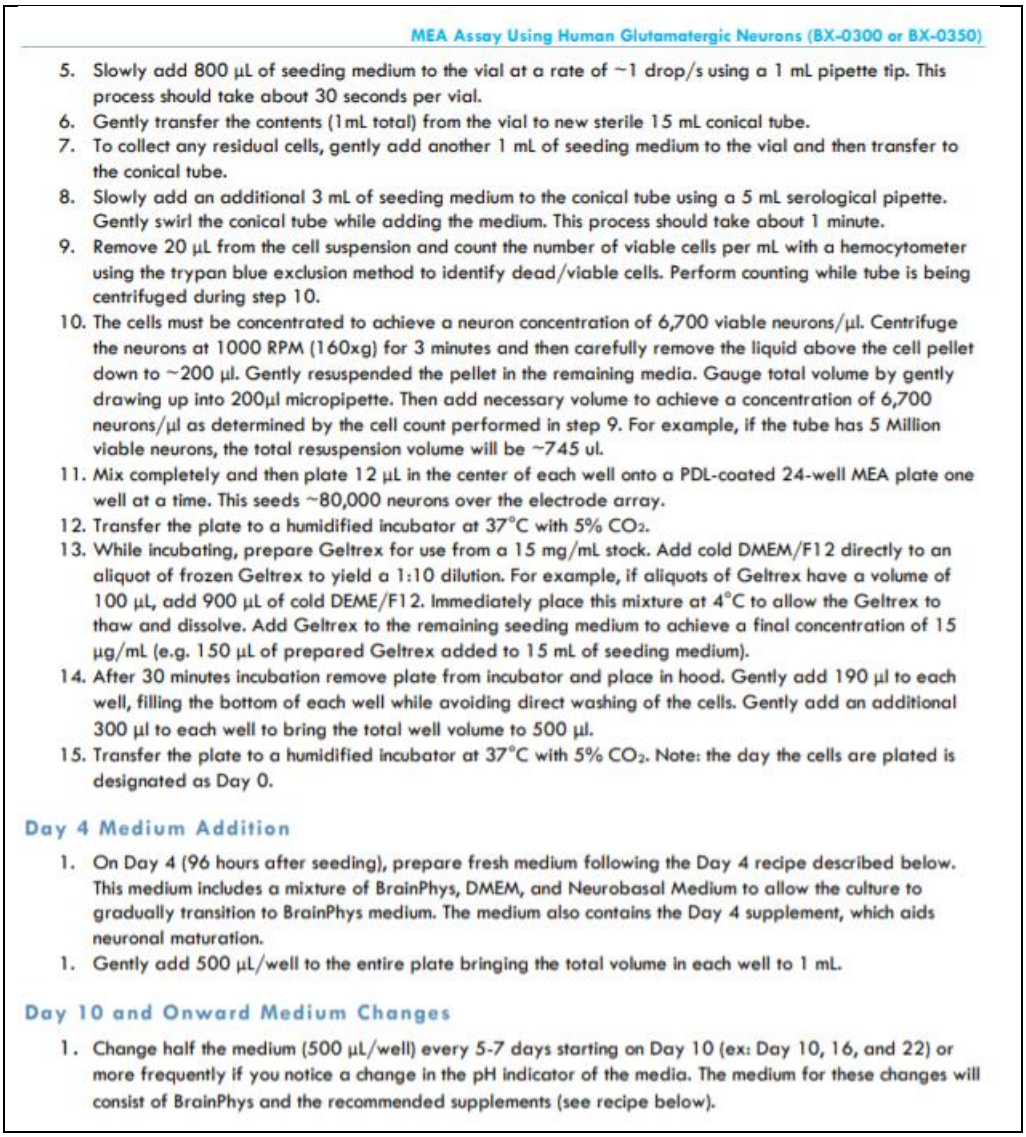

MEA Assay Using Human Glutamatergic Neurons (BX-0300 or BX-0350)

5. Slowly add 800 µL of seeding medium to the vial at a rate of ~1 drop/s using a 1 mL pipette tip. This process should take about 30 seconds per vial.
6. Gently transfer the contents (1mL total) from the vial to new sterile 15 mL conical tube.
7. To collect any residual cells, gently add another 1 mL of seeding medium to the vial and then transfer to the conical tube.
8. Slowly add an additional 3 mL of seeding medium to the conical tube using a 5 mL serological pipette. Gently swirl the conical tube while adding the medium. This process should take about 1 minute.
9. Remove 20 µL from the cell suspension and count the number of viable cells per mL with a hemocytometer using the trypan blue exclusion method to identify dead/viable cells. Perform counting while tube is being centrifuged during step 10.
10. The cells must be concentrated to achieve a neuron concentration of 6,700 viable neurons/µl. Centrifuge the neurons at 1000 RPM (160xg) for 3 minutes and then carefully remove the liquid above the cell pellet down to ~200 µl. Gently resuspended the pellet in the remaining media. Gauge total volume by gently drawing up into 200µl micropipette. Then add necessary volume to achieve a concentration of 6,700 neurons/µl as determined by the cell count performed in step 9. For example, if the tube has 5 Million viable neurons, the total resuspension volume will be ~745 ul.
11. Mix completely and then plate 12 µL in the center of each well onto a PDL-coated 24-well MEA plate one well at a time. This seeds ~80,000 neurons over the electrode array.
12. Transfer the plate to a humidified incubator at 37°C with 5% $CO_2$.
13. While incubating, prepare Geltrex for use from a 15 mg/mL stock. Add cold DMEM/F12 directly to an aliquot of frozen Geltrex to yield a 1:10 dilution. For example, if aliquots of Geltrex have a volume of 100 µL, add 900 µL of cold DEME/F12. Immediately place this mixture at 4°C to allow the Geltrex to thaw and dissolve. Add Geltrex to the remaining seeding medium to achieve a final concentration of 15 µg/mL (e.g. 150 µL of prepared Geltrex added to 15 mL of seeding medium).
14. After 30 minutes incubation remove plate from incubator and place in hood. Gently add 190 µl to each well, filling the bottom of each well while avoiding direct washing of the cells. Gently add an additional 300 µl to each well to bring the total well volume to 500 µl.
15. Transfer the plate to a humidified incubator at 37°C with 5% $CO_2$. Note: the day the cells are plated is designated as Day 0.

### Day 4 Medium Addition

1. On Day 4 (96 hours after seeding), prepare fresh medium following the Day 4 recipe described below. This medium includes a mixture of BrainPhys, DMEM, and Neurobasal Medium to allow the culture to gradually transition to BrainPhys medium. The medium also contains the Day 4 supplement, which aids neuronal maturation.
1. Gently add 500 µL/well to the entire plate bringing the total volume in each well to 1 mL.

### Day 10 and Onward Medium Changes

1. Change half the medium (500 µL/well) every 5-7 days starting on Day 10 (ex: Day 10, 16, and 22) or more frequently if you notice a change in the pH indicator of the media. The medium for these changes will consist of BrainPhys and the recommended supplements (see recipe below).

**Fig C-2:** *Brainxell's protocol for seeding and cell culturing.*

## Staining protocol for 24-well

Materials:

Day 1:

- Goat Serum (GS)
- Primary antibody
- PBS
- Triton-X
- 4 % paraformaldehyde (PFA)

Day 2:

- PBS
- Goat Serum (GS)
- Secondary antibodies
- Tweezers
- Hoescht
- Mounting media (Fluoroshield)
- Kim wipes
- Distilled $H_20$
- Slides

1. Do a quick PBS wash by aspirating off the media and adding 200 µl of PBS to each well.
2. Aspirate off the PBS and add 200 µl of 4% paraformaldehyde to each well. Leave the wells for 15-25 min.
3. Aspirate off the PFA and do a PBS wash 3 times for 10 min each.
4. Add 200 µl of block to each well. The block is made up by diluting GS and Triton-X in PBS. Calculate this by taking 200 µl of PBS for each well (f.ex 200 µl PBS * 24 = 4800 µl or 4.8 ml) then calculating 5 % GS from this (f.ex 4800 * 0.05 = 240 µl of NGS) and 0.3% Triton-X (f.ex 4800 * 0.003 = 14.4 µl. Note: We keep Triton in a 1:10 dilution so the final concentration here is 14.4 * 10 = 144 µl). Add the GS and Triton to the PBS in an Eppendorf or 15 mL tube.
5. After adding the block, leave the wells for 1-2 hours.
6. Remove the block, but do NOT wash.
7. Add 200 µl of primary antibody to each well. The antibody solution is made by diluting the primaries, 1% GS and 0.1% Triton in PBS. Calculate the PBS amount in the same way as the block then calculate the GS and Triton (f.ex 4800 * 0.01 = 48 µl GS). Calculate the primary needed by taking the dilution ratio (f.ex 1:500) and dividing the PBS amount by it (f.ex 4800 / 500 = 9.6 µl). Add the GS and primary to the PBS in a tube. You can make a solution like this with several different antibodies as long as the antibodies are raised in different animals.
8. Leave the primaries in overnight in the fridge.
9. PBS wash the wells 3 times.
10. Add 200 µl of secondaries to each well. Calculate the secondary solution in the same way as the primaries, only the dilution of the secondaries is usually 1:1000. Leave the wells covered in tin foil at room temperature for 2 hours. Add the Hoechst (1:5000 or 1:10000) for 5 min towards the end.
11. PBS wash the wells 3 times for 15 min each.
12. Set up Fluoroshield, slides, Kim wipes and distilled $H_20$
13. Put 4 drops of Fluoroshield on a slide
14. Use tweezers to pick up a coverslip and make sure you know what side is up (side with cells on).
15. Dip the coverslip in the water then touch it gently to the Kim wipe to get the water off.
16. Place the coverslip with the cells facing down on one of the DAPI drops.
17. Once 4 slips have been placed label the slide with the antibodies used, vitamin timeframe, name and date.
18. Once all slides are complete place them in the fridge overnight.

**Fig C-3:** *In-house protocol for ICC staining*

# Appendix D: Supplementary Results

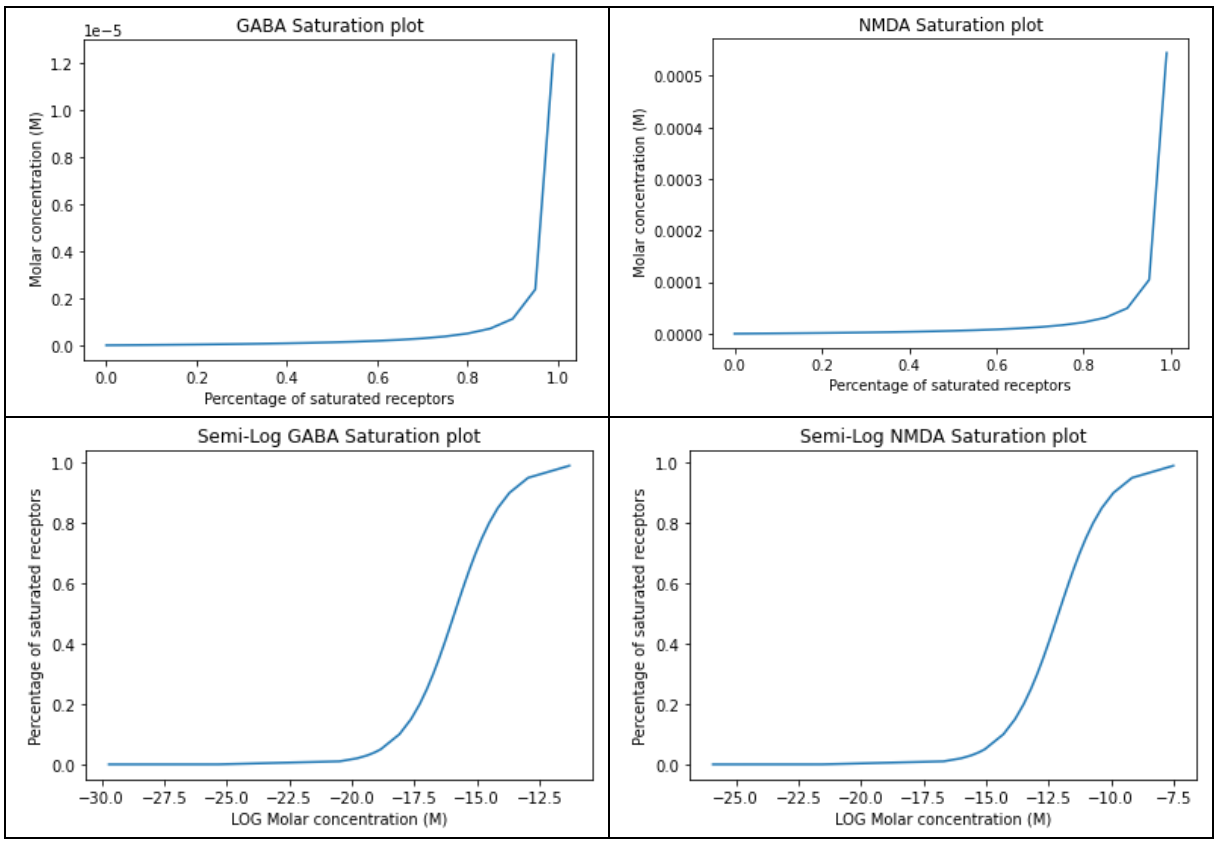


**Fig D-1:** *Saturation curves. Calculated from the Hill–Langmuir equation, Proportion of ligand-bound receptors. Hill constant(n) = 1 (112, 113).*

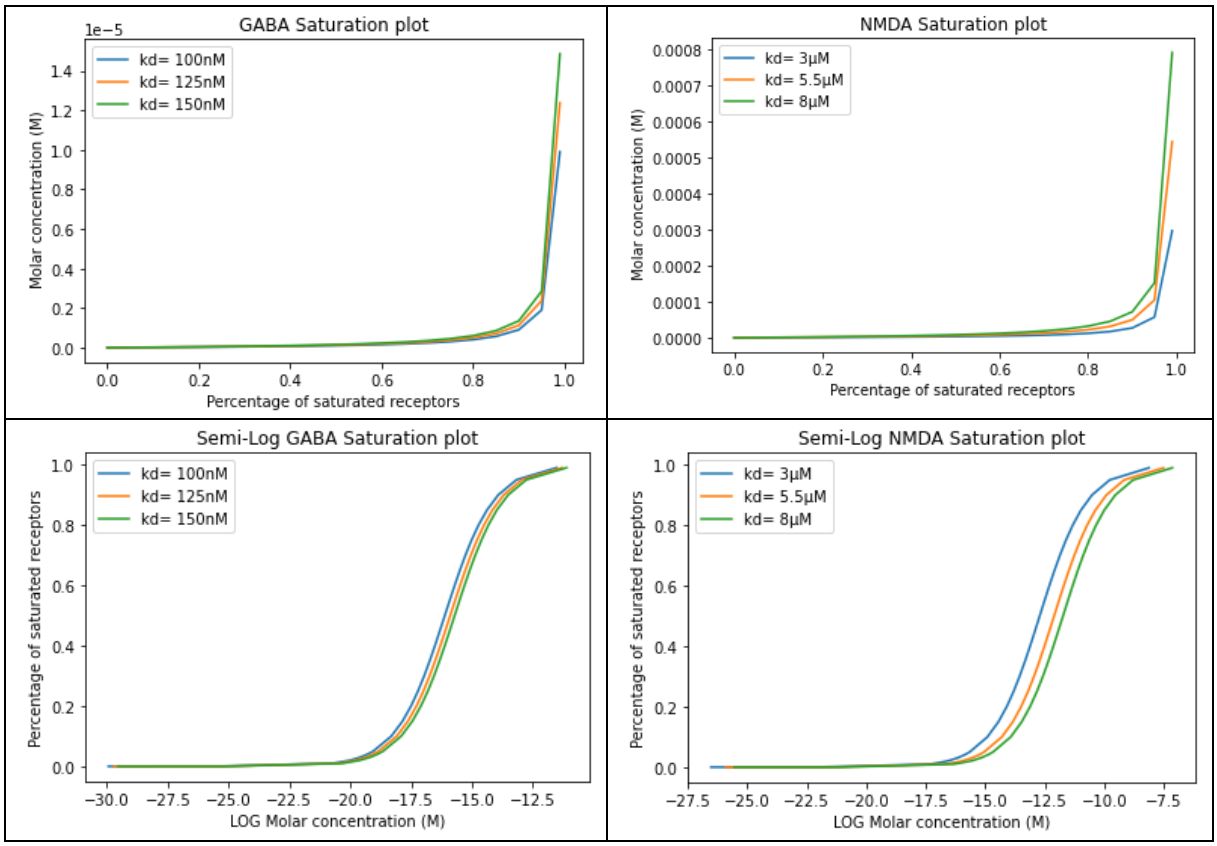


**Fig D-2:** *Different ranges of receptor ligand dissociation coefficient (Kd) for $GABA_A$ and NMDA receptors (112, 113). This figure shows the saturation curve and the semi-log saturation curve of $GABA_A$ receptor with GABA in the upper and lower left respectfully. The saturation curve and the semi-log saturation curve of NMDA receptor with NMDA is shown the upper and lower right respectfully.*

**Table D-3:** *Theis tables shows the excitatory to inhibitory firing ratios at which critical readings emerge in the Izhikevich model. This table also shows the predicted increase and decrease in activity which cause the model to fall out of critical dynamics, and the baseline values of neurotransmitter concentrations used for the calculations.*

| Inhibitory percentage | E/I firing rate | Reduction in firing needed to push E/I passed predicted minimum value | Increase in firing needed to push E/I passed predicted maximum value | Baseline values |
|---|---|---|---|---|
| 8% | 35 ± 2.00 | 449% | 105% | NMDA: 25nM (114)<br><br>GABA: 0.06μM (115) |
| 15% | 15.75 ± 1.25 | 202% | 235% | |
| 24% | 8.28 ± 0.49 | 106% | 445% | |

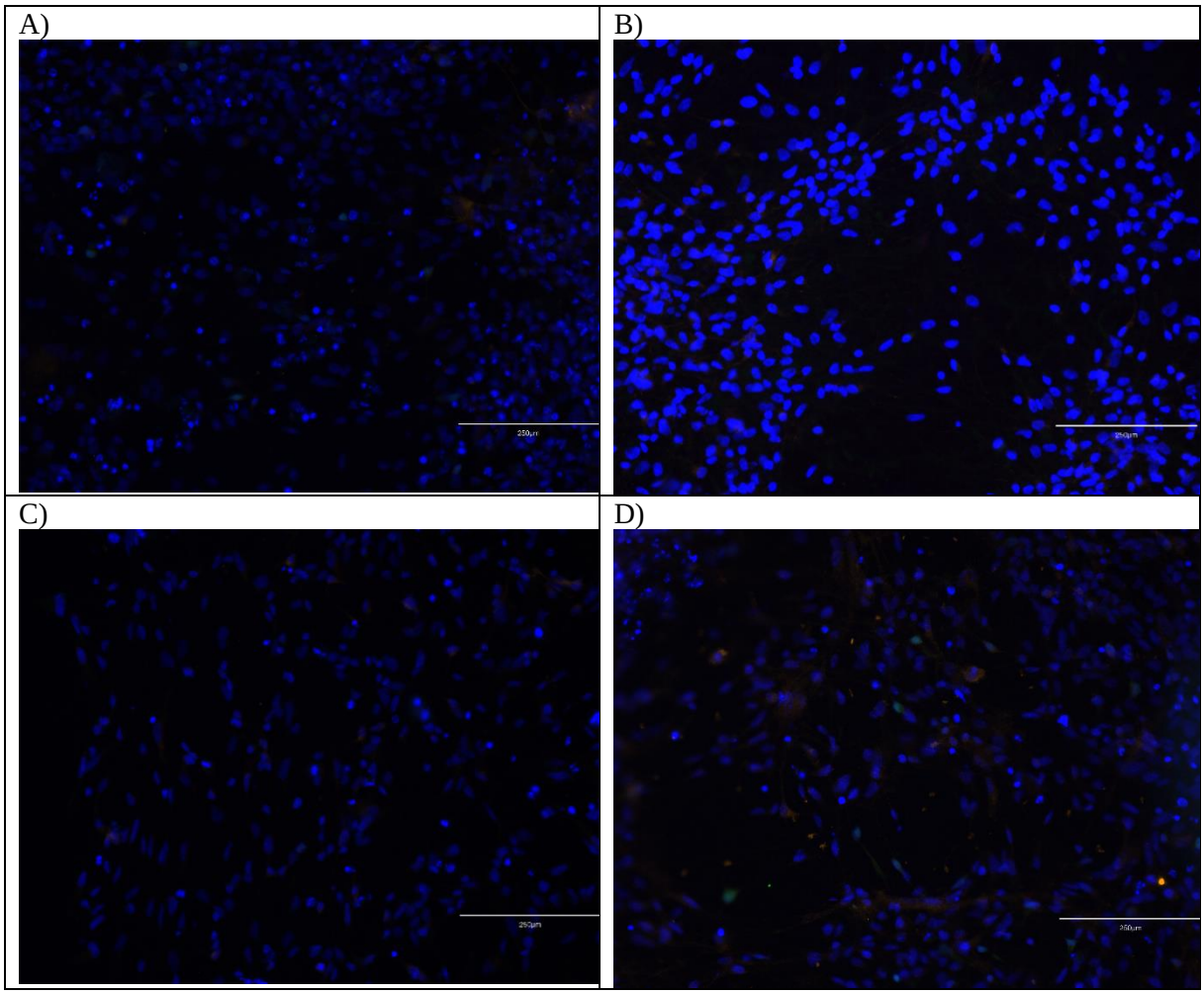


**Fig D-4:** *Negative controls from the immune staining. A) Secondary antibodies and Hoescht only for Glutaminergic neurons, $GABA_B$-R1, AMPA-R1, beta III tubulin staining. B) Secondary antibodies and Hoescht only for Glutaminergic neurons, NeuN, TBR1, βIII-tubulin staining. C) Secondary antibodies and Hoescht only for GABAergic neurons, $GABA_B$-R1, AMPA-R1, beta III tubulin staining. D) Secondary antibodies and Hoescht only for GABAergic neurons, GABA, GFAP, NeuN staining.*

**Table D-5**: *Different E/I population networks effect on electrophysiology. The p-value is found trough testing data on high readings of each electrophysiological measurement against data from day of low recorded electrophysiological values. The mean values of each electrophysiological measurement from 41-55 DIV is also shown along side the standard deviation. Lastly, average mean changed and change in SD between all samples shown, alongside the growth trend for measurement values and SD in percentage over all samples. IN is an abbreviation of inhibitory neurons.*

| Parameter | p-value | Mean values and SD | Mean changes between samples |
|---|---|---|---|
| Firing rate | 0.05 | 8% IN: 22 ± 11<br>15% IN: 34 ± 26<br>24% IN: 41 ± 44 | Increased mean + 9.5<br>Increase SD + 16.5<br>Trend mean: +37%<br>Trend SD: +102% |
| Synchrony | 0.34 | 8% IN: 9.7±5.9<br>15% IN: 8.2±4.1<br>24% IN: 12.0±9.8 | Increased mean + 2.2<br>Increase SD + 3.9<br>Trend mean: +15%<br>Trend SD: +54% |
| Network burst | 0.26 | 8% IN: 0.22±0.09<br>15% IN: 0.24±0.11<br>24% IN: 0.27±0.12 | Increased mean + 0.025<br>Increase SD + 0.0015<br>Trend mean: +10%<br>Trend SD: +15% |
| Bursts/Synchrony | 0.38 | 8% IN: 0.035±0.015<br>15% IN: 0.037±0.016<br>24% IN: 0.043±0.019 | Increased mean + 0.004<br>Increase SD + 0.002<br>Trend mean: +10%<br>Trend SD: +12% |

**Table D-6:** *media changes effect on electrophysiology. The p-value was found by looking at the collective data for all recordings recorded the same day away from last media changes for each electrophysiological measurement. The p-value with data from 44 DIV removed is showed in the parenthesis. The mean values of each measurement from 41-55 DIV is also shown alongside the standard deviation. Lastly, average mean changed and change in SD between all samples shown, alongside the growth trend for measurement values and SD in percentage over all samples. with trend is it meant the average changed counted from one sample to the next over all samples. The number in the Mean section indicates the number of days away from last media change.*

| Parameter | p-value | Mean values and SD | Change between samples |
|---|---|---|---|
| Firing rate | 0.00041<br>(0.0004) | 1 : 34±34<br>2 : 34±45<br>3 : 64±56<br>4 : 32±15<br>5 : 21±39 | Decreased mean – 3.2<br>Increase SD: + 1.25<br>Trend mean: -25%<br>Trend SD: +35% |
| Synchrony | 0.00013<br>(0.0005) | 1 : 10±12<br>2 : 7±3<br>3 : 7±4<br>4 : 5±2<br>5 : 17±15 | Increased mean + 3.0<br>Increase SD: + 4.7<br>Trend mean: +10 %<br>Trend SD: +140% |
| Network burst frequency | 0.092<br>(0.05) | 1 : 0.028±0.027<br>2 : 0.020±0.028<br>3 : 0.034±0.031<br>4 : 0.028±0.023<br>5 : 0.017±0.026 | Decreased mean -0.027<br>Decrease SD -0.003<br>Trend mean: -4%<br>Trend SD: +0.5% |
| Bursts/Synchrony | 0.0088<br>(0.004) | 1 : 0.005±0.006<br>2 : 0.003±0.006<br>3 : 0.008±0.008<br>4 : 0.005±0.005<br>5 : 0.002±0.005 | Decreased mean -0.003<br>Increase SD + 0<br>Trend mean: +7%<br>Trend SD: -1% |

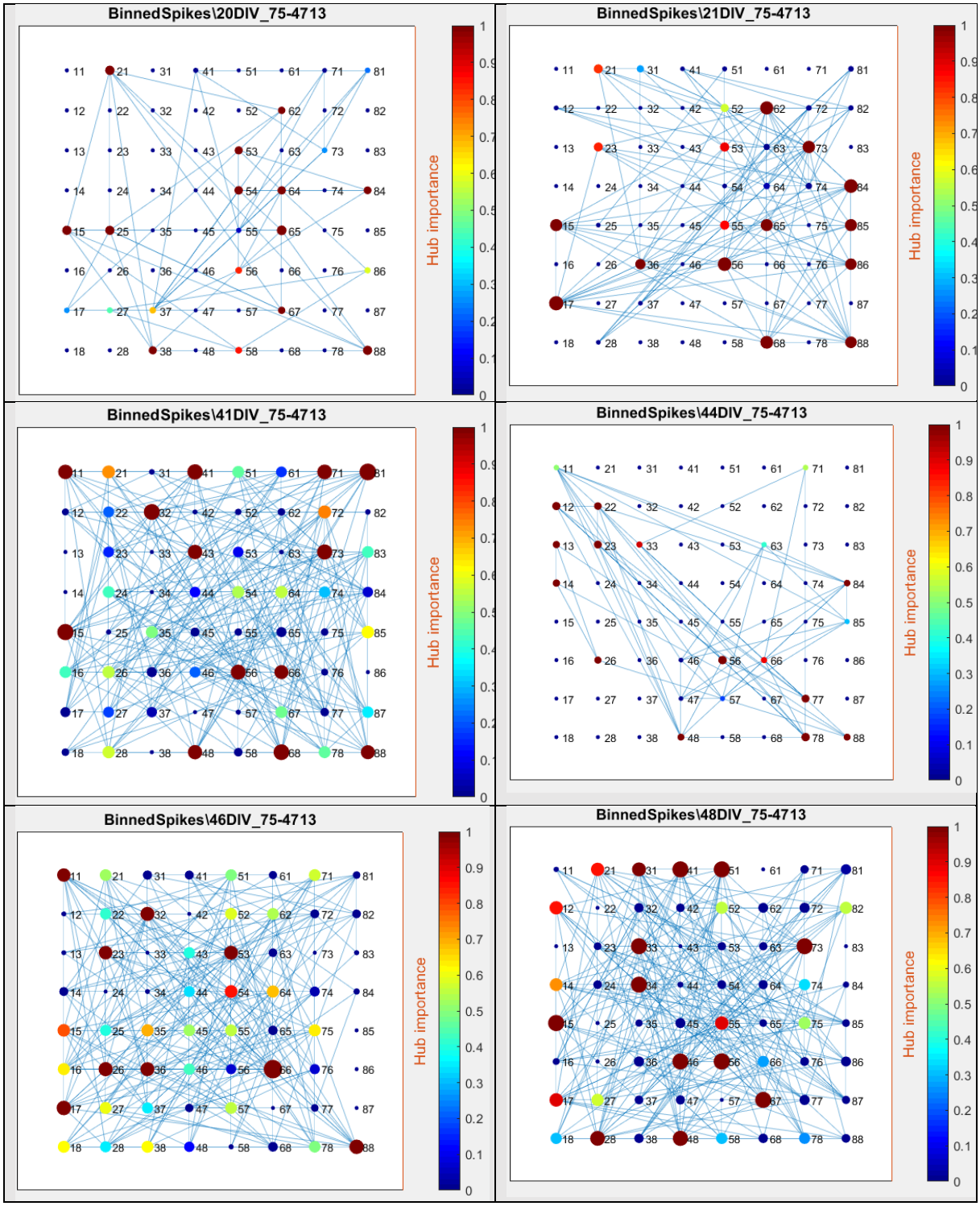


**Fig D-7:** *Maturation of functional topology from 20-48 DIV for network 13-A1. DIV is increasing right to left and from top to bottom.*

**Table D-8:** The mean *topological measurements of all networks. AP is the average pathlength, C is the clustering, SW is the small-world metric ω, and MD is the mean degree distribution. This is shown for all 18 networks. The % category indicates which inhibitory population category the network belonged to. IN is an abbreviation of inhibitory neurons.*

| Network | % | AP | C | SW | MD |
|---|---|---|---|---|---|
| 4708 wA3 | 8% IN | 1.69 | 0.30 | 0.04917 | 16.9 (26 %) |
| 4708 wB1 | 8% IN | 1.72 | 0.38 | 0.01261 | 16.3 (25 %) |
| 4713 wA2 | 8% IN | 1.73 | 0.27 | 0.01633 | 10.0 (15 %) |
| 4713 wB3 | 8% IN | 1.89 | 0.48 | 0.00329 | 11.8 (18 %) |
| 4719 wA1 | 8% IN | 1.84 | 0.41 | 0.01053 | 17.0 (26 %) |
| 4719 wB2 | 8% IN | 1.74 | 0.40 | 0.00647 | 16.1 (25 %) |
| 4708 wA2 | 15% IN | 1.66 | 0.40 | 0.02743 | 18.6 (29 %) |
| 4708 wB3 | 15% IN | 1.62 | 0.41 | 0.02319 | 20.0 (31 %) |
| 4713 wA1 | 15% IN | 1.76 | 0.46 | - 0.0233 | 15.3 (24 %) |
| 4713 wB2 | 15% IN | 1.86 | 0.59 | - 0.12004 | 18.9 (29 %) |
| 4719 wA3 | 15% IN | 1.73 | 0.39 | 0.0291 | 16.4 (25 %) |
| 4719 wB1 | 15% IN | 1.73 | 0.40 | 0.00981 | 16.3 (25 %) |
| 4708 wA1 | 24% IN | 1.63 | 0.53 | - 0.03933 | 23.9 (37 %) |
| 4708 wB2 | 24% IN | 1.61 | 0.64 | - 0.12533 | 26.0 (40 %) |
| 4713 wA3 | 24% IN | 1.73 | 0.31 | 0.0074 | 11.8 (18 %) |
| 4713 wB1 | 24% IN | 1.77 | 0.34 | - 0.01677 | 12.1 (19 %) |
| 4719 wA2 | 24% IN | 2.00 | 0.75 | - 0.37357 | 22.6 (35 %) |
| 4719 wB3 | 24% IN | 1.74 | 0.41 | 0.00443 | 16.4 (25 %) |

**Table D-9:** *topological classification of all networks. The networks were classified binary based on if the value was closest to the highest recoded value or the lowest. AP is the average pathlength, C is the clustering, SW id the small-world metric ω, and MD is the mean degree distribution This is shown for all 18 networks. The % indicates which inhibitory population category the network belonged to.* IN is an abbreviation of inhibitory neurons.

| Network binary classification | | | | | |
|---|---|---|---|---|---|
| **Network** | **%** | **AP** | **C** | **SW** | **MD** |
| 4708 wA3 | 8% IN | 1 | 1 | 2 | 1 |
| 4708 wB1 | 8% IN | 1 | 1 | 2 | 1 |
| 4713 wA2 | 8% IN | 1 | 1 | 2 | 1 |
| 4713 wB3 | 8% IN | 2 | 1 | 2 | 1 |
| 4719 wA1 | 8% IN | 2 | 1 | 2 | 1 |
| 4719 wB2 | 8% IN | 1 | 1 | 2 | 1 |
| 4708 wA2 | 15% IN | 1 | 1 | 2 | 1 |
| 4708 wB3 | 15% IN | 1 | 1 | 2 | 2 |
| 4713 wA1 | 15% IN | 1 | 1 | 1 | 1 |
| 4713 wB2 | 15% IN | 2 | 1 | 1 | 1 |
| 4719 wA3 | 15% IN | 1 | 1 | 2 | 1 |
| 4719 wB1 | 15% IN | 1 | 1 | 2 | 1 |
| 4708 wA1 | 24% IN | 1 | 1 | 1 | 2 |
| 4708 wB2 | 24% IN | 1 | 2 | 1 | 2 |
| 4713 wA3 | 24% IN | 1 | 1 | 2 | 1 |
| 4713 wB1 | 24% IN | 1 | 1 | 1 | 1 |
| 4719 wA2 | 24% IN | 2 | 2 | 1 | 2 |
| 4719 wB3 | 24% IN | 1 | 1 | 2 | 1 |

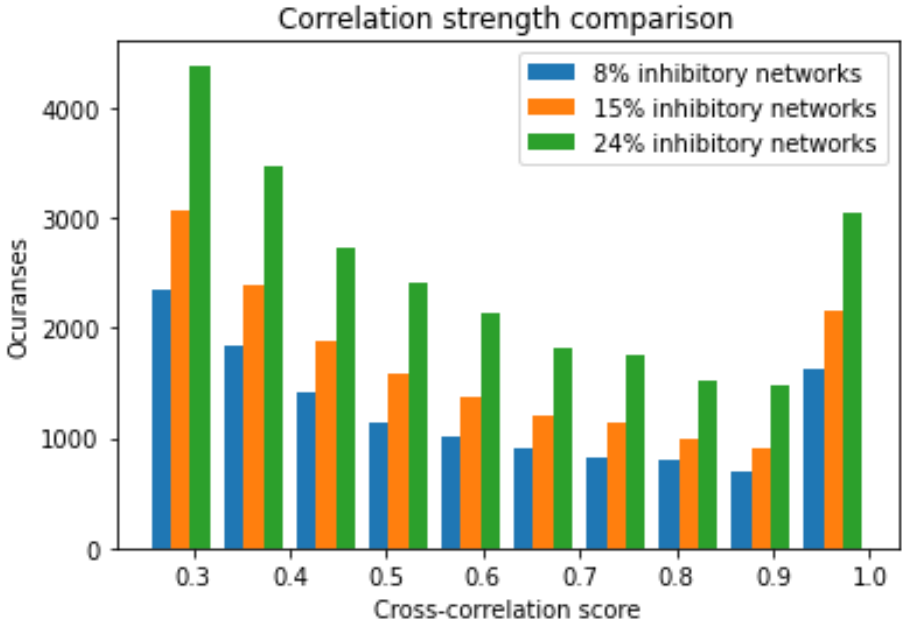


**Fig D-10:** *This figure shows the distribution of cross-correlation strength from the three different inhibitory population networks after filtering with 0.25 cross-correlation hard threshold.*

**Table D-11**: *Total active readings for all different inhibitory population networks.*

| Survivability | | | |
|---|---|---|---|
| Inhibitory ratios | 8% | 15% | 24% |
| Active networks | 70 | 81 | 78 |

**Table D-12:** *Comparison of in vitro data filtered with 25% link-persistence and with a hard threshold of 0.25 in correlations. Here the graph measurements: average clustering, average pathlength, ω, and mean degree are shown.*

| Model | Average clustering | Average Pathlength | Small-world metric ω | Mean Degree |
|---|---|---|---|---|
| *In Vitro* (25% persistence) Collective median | 0.869 | 1.43 | -0.22 | 33(51%) |
| *In Vitro* (MD < active electrodes) Collective median | 0.410 | 1.75 | 0.01 | 16(25%) |

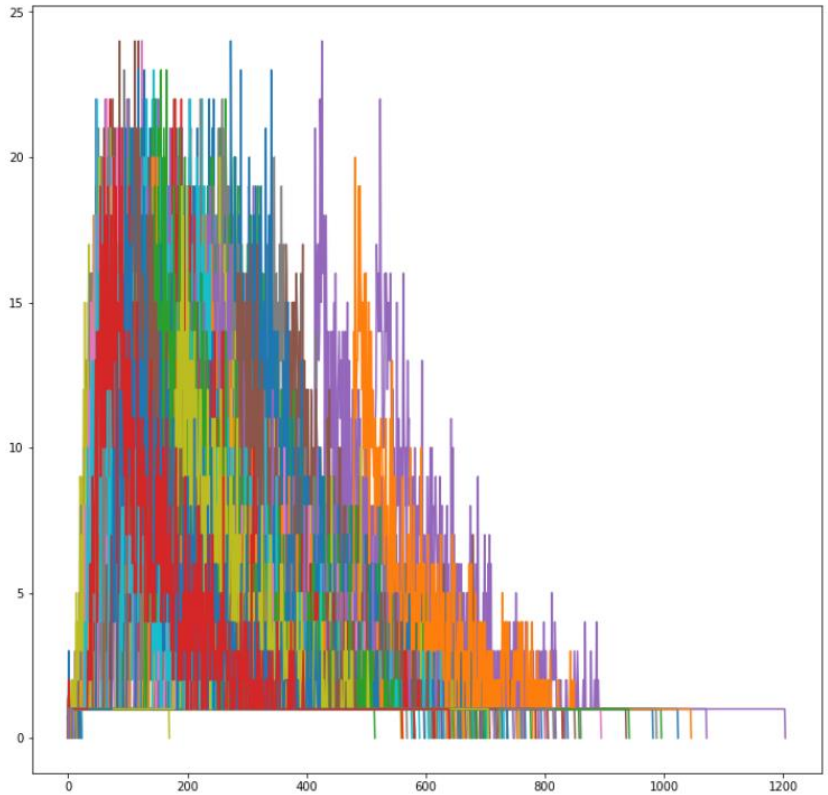


**Fig D-13:** *picture of all avalanches from networks 13-A3, 44 DIV. Avalanches are seen with prolonged single electrode tails.*

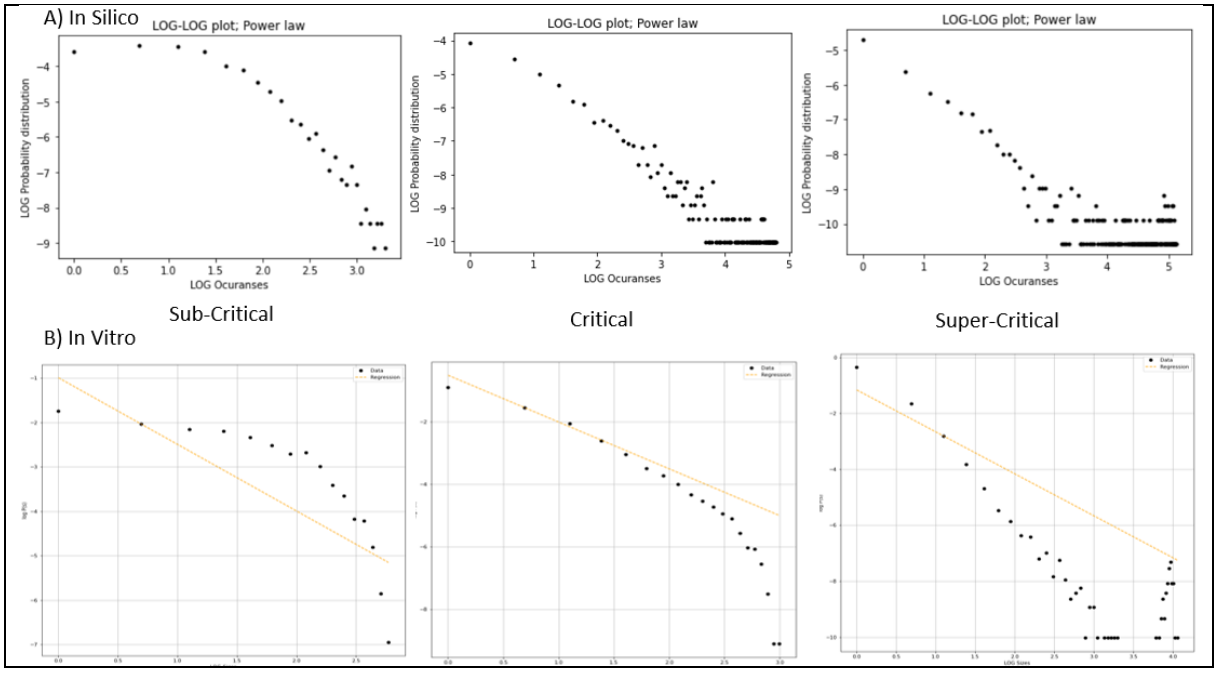


**Fig D-14**: *This figure shows sub-critical, critical and super-critical avalanche size probability distributions from both in silico and in vitro data. A) depicts the sub-critical, critical and super critical avalanche size probability distributions from the in silico model. B) depicts the sub-critical, critical and super critical avalanche size probability distributions from the in vitro data*

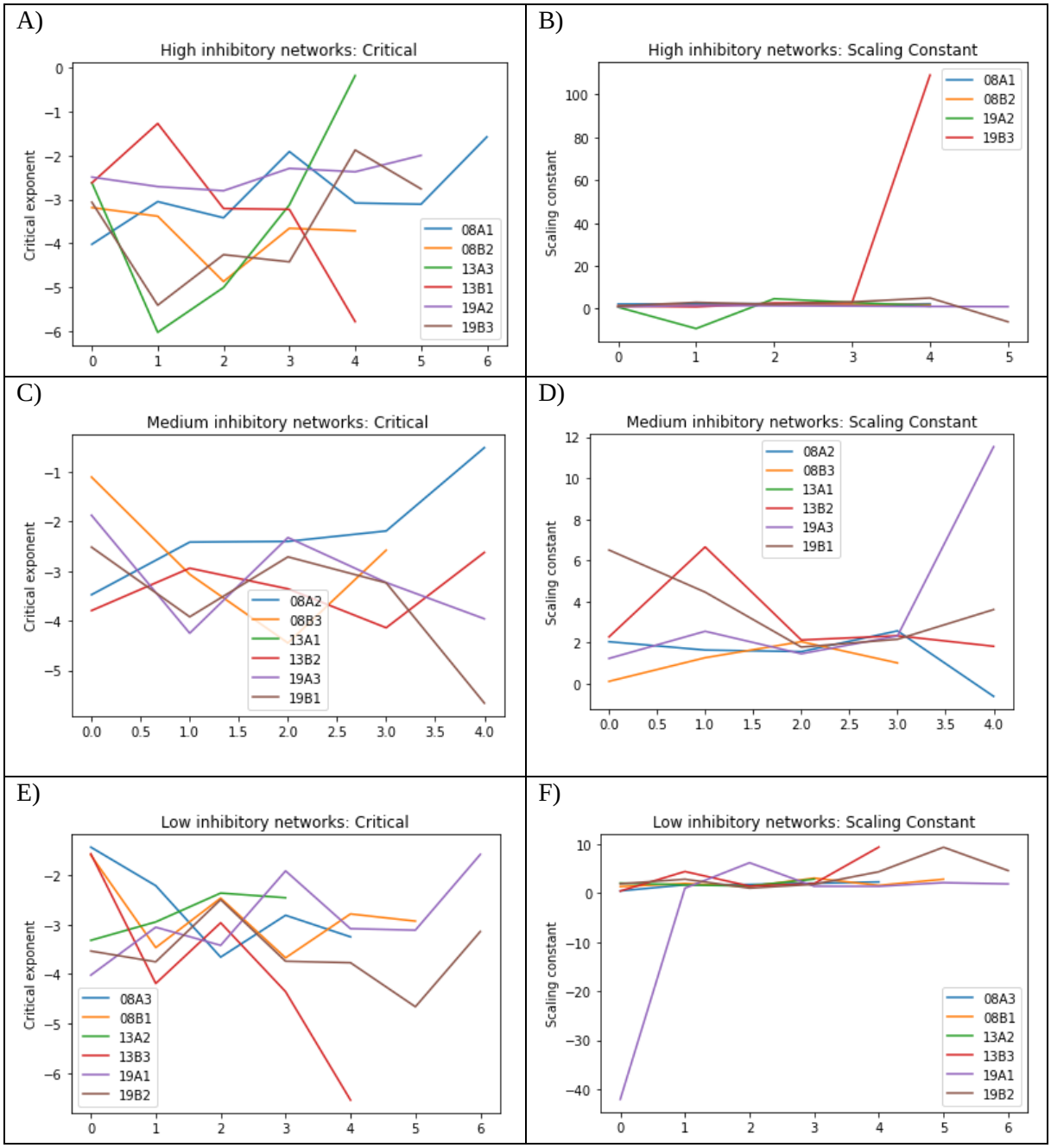


**Fig D-15:** *Critical and scaling constant data from div 41-55 for all different inhibitory ratio networks. A) is the critical exponent of 24% inhibitory networks. B) The scaling constant of 24% inhibitory networks. C) is the critical exponent of 15% inhibitory networks. D) is the scaling constant of 15% inhibitory networks. E) is the critical exponent of 8% inhibitory networks. F) is the scaling constant of 8% inhibitory networks.*

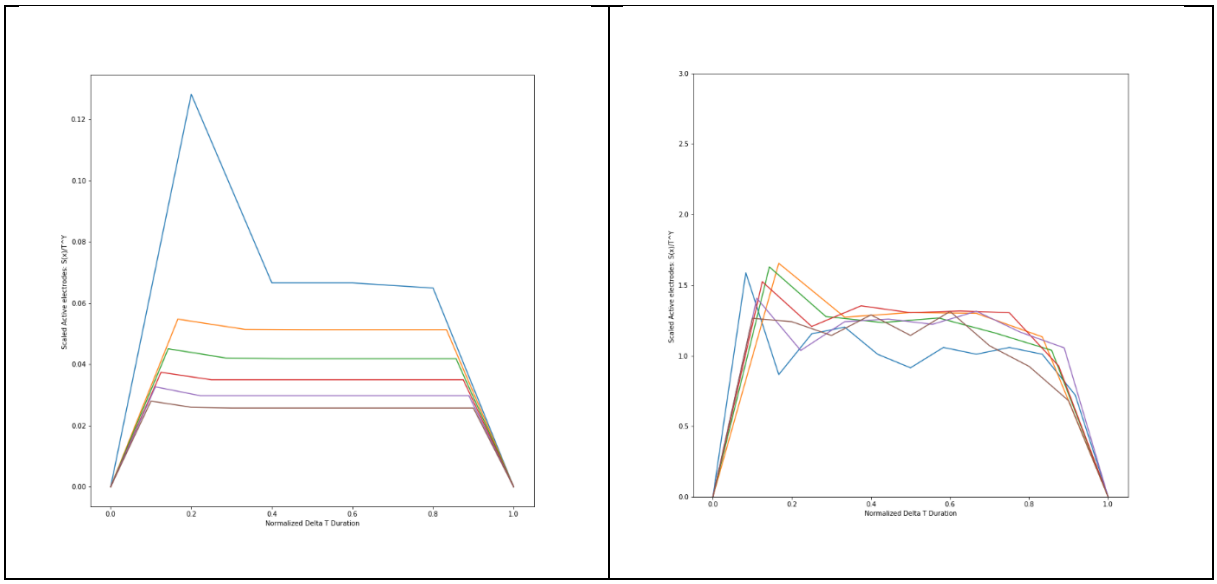


**Fig D-16:** *Non collapsible data (left)( 75-4713_A3 DIV 21) and collapsible none-critical data DIV41 (right).*

**Table D-17:** *Statistical data from different factors effect on critical exponent and scaling constant. The p-value for the electrophysiological measurements was found through comparing the critical exponent and scaling constant values of days with high recorded electrophysiological values against critical exponent and scaling constant data from days of low recorded electrophysiological values of the same measurement with one-way ANOVA. While the p-value for media change was found through looking at the collective critical exponent and scaling constant data from different days away from last media change. The mean and SD is also shown, for the media change is it shown for each day away form last media change, while for the electrophysiological data is it show mean and SD values for days with recorded high and low values.*

| Name | P-Value: Critical exponent | Mean Critical exponent | P-value: scaling constant | Mean Scaling constant |
|---|---|---|---|---|
| Media changes effect on Critical exponent | 0.015 | 1: -2.8 ± 1.3<br>2: -2.6 ± 0.9<br>3: -2.6 ± 1.0<br>4: -3.2 ± 1.2<br>5: -3.2 ± 1.3 | 0.018 | 1: 1.8 ± 1.9<br>2: 0.6 ± 2.5<br>3: 2.0 ± 2.3<br>4: 1.5 ± 3.1<br>5: 2.2 ± 2.8 |
| Bursts effect on Critical exponent | 0.5 | Low : -3.3 ±0.8<br>High : -3.2 ±1.2 | 0.26 | Low : 3.0 ±3.4<br>High: 2.0 ±3.0 |
| Synchrony effect on Critical exponent | 0.012 | Low : -2.5 ± 1.1<br>High : -1.5 ± 0.6 | 0.042 | Low : 2.7 ± 3.2<br>High: 0.6 ± 0.7 |
| Intermediate Burst/synch level effect on Critical exponent | 0.21 | Low : -3.3 ±1.2<br>High : -3.0 ±0.9 | 0.051 | Low : 0.8 ±6.1<br>High: 3.1 ±2.1 |

**Table D-18:** *A table depicting the percental change in firing rates to different volumes of GABA and NMDA in different inhibitory population networks. Additionally, is percental changes in firing from control shown at the bottom of the table*

| Reactant | **Inhibitory Ratio** | **% effect on Firing** |
|---|---|---|
| **GABA** | | |
| 0.1µM | 24% | - 55 % ± 1% |
| 0.15µM | 8% | - 29 % |
| 0.15µM | 24% | - 40 % |
| 0.2µM | 8% | - 74 % |
| 0.2µM | 15% | - 93 % |
| 0.2µM | 24% | - 99 % |
| **NMDA** | | |
| 6µM | 15% | - 50 % |
| 6µM | 24% | - 78 % |
| 18µM | 8% | + 20% ± 170 |
| 18µM | 15% | + 1100% ±2000 |
| 18µM | 24% | - 71 % |
| **Control** | | |
| | 8% | - 38 % |
| | 15% | + 65 % ± 12 |
| | 24% | - 11 % ± 75 |

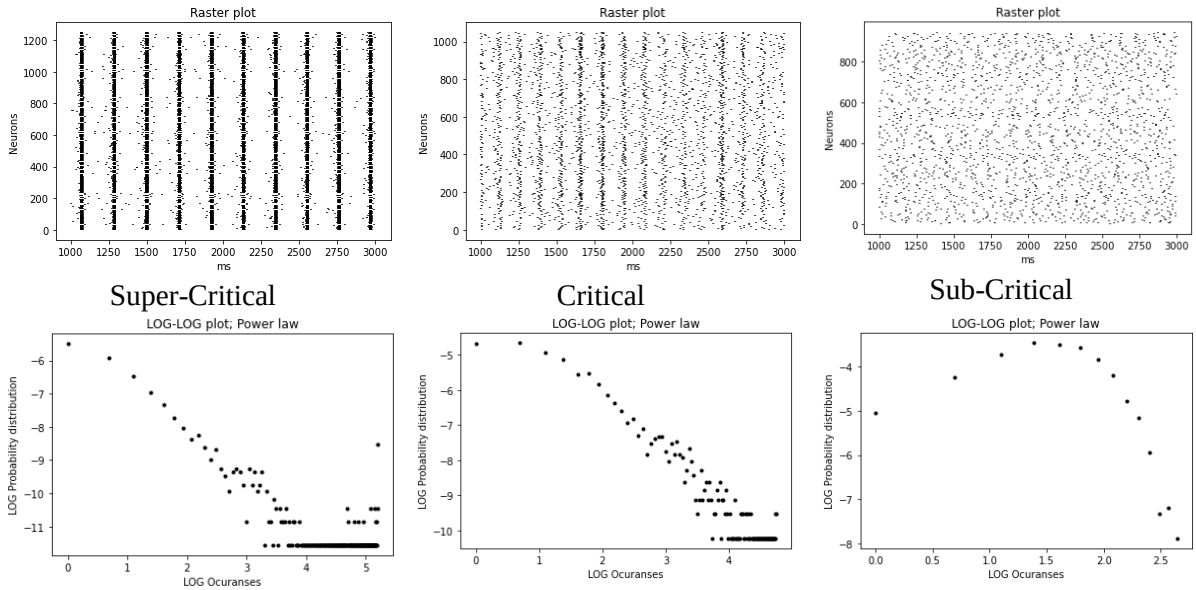


**Fig D-19:** *Figure of the updated model with increased size. Model differs in critical dynamics by size. Over each critical stat is a raster plot showing the firing acticity which varies with synchronys relationshipt to critical stats. The left (super-critical state) picture illustates the updated model with 1250 neurons, the middel (Critical state) show 1100 neuron, and the left (sub-critical) shows the network with 900 neurons. From each state can one see that the synchrony is distinct in different critical phases.*

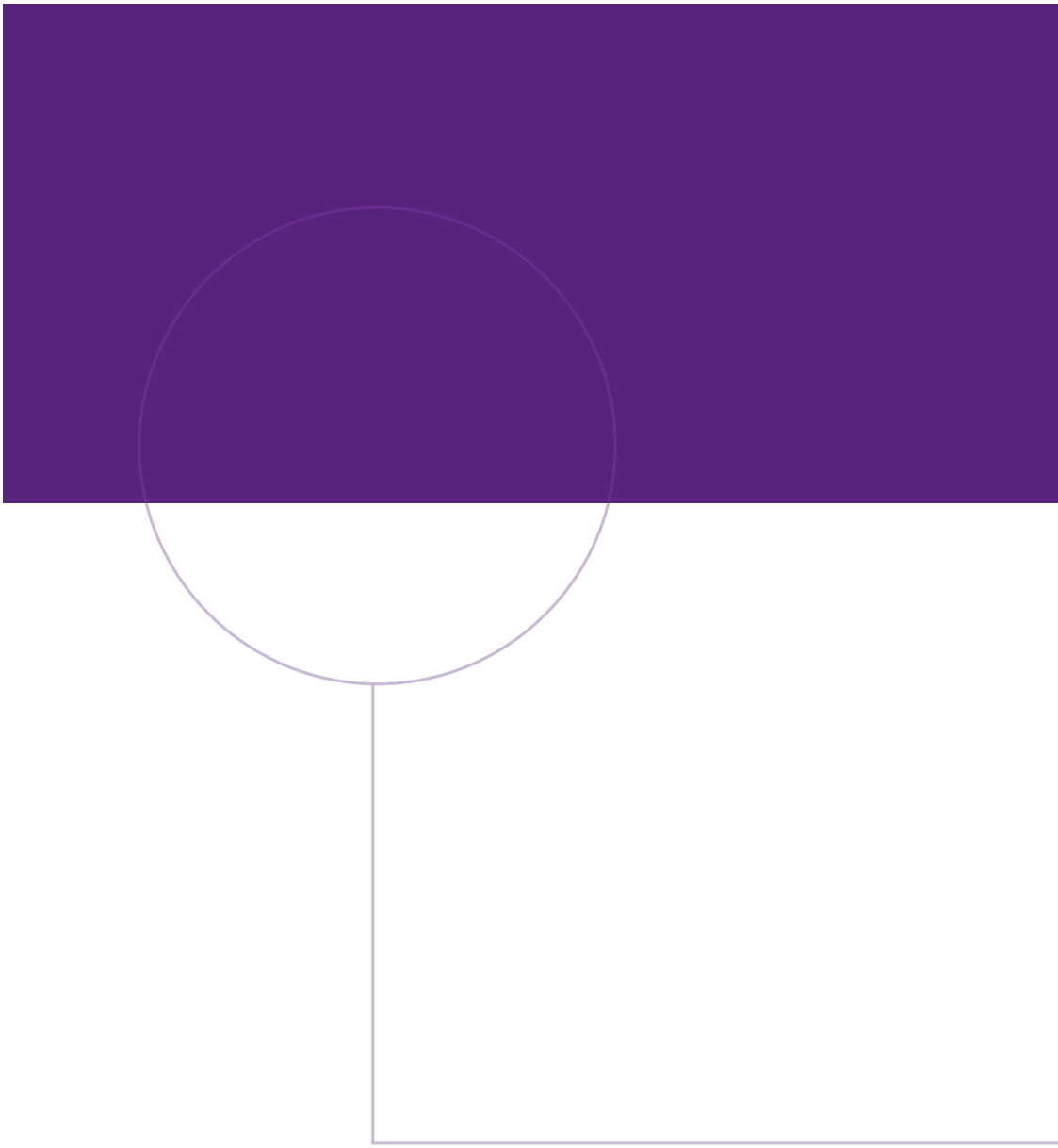

NTNU

Norwegian University of
Science and Technology